

3-10-2010

Consideration of Wear Rates at High Velocities

Stephen P. Meador

Follow this and additional works at: <https://scholar.afit.edu/etd>

 Part of the [Structures and Materials Commons](#)

Recommended Citation

Meador, Stephen P., "Consideration of Wear Rates at High Velocities" (2010). *Theses and Dissertations*. 2047.
<https://scholar.afit.edu/etd/2047>

This Thesis is brought to you for free and open access by the Student Graduate Works at AFIT Scholar. It has been accepted for inclusion in Theses and Dissertations by an authorized administrator of AFIT Scholar. For more information, please contact richard.mansfield@afit.edu.



CONSIDERATION OF WEAR AT HIGH VELOCITIES

THESIS

Stephen P. Meador

AFIT/GAE/ENY/10-M16

DEPARTMENT OF THE AIR FORCE
AIR UNIVERSITY

AIR FORCE INSTITUTE OF TECHNOLOGY

Wright-Patterson Air Force Base, Ohio

APPROVED FOR PUBLIC RELEASE; DISTRIBUTION UNLIMITED.

The views expressed in this thesis are those of the author and do not reflect the official policy or position of the United States Air Force, Department of Defense, or the United States Government. This material is declared a work of the U.S. Government and is not subject to copyright protection in the United States.

AFIT/GAE/ENY/10-M16

CONSIDERATION OF WEAR AT HIGH VELOCITIES

THESIS

Presented to the Faculty
Graduate School of Engineering and Management
Air Force Institute of Technology
Air University
Air Education and Training Command
In Partial Fulfillment of the Requirements for the
Degree of Master of Science in Aeronautical Engineering

Stephen P. Meador, B.S.

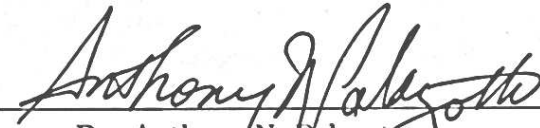
March 2010

APPROVED FOR PUBLIC RELEASE; DISTRIBUTION UNLIMITED.

CONSIDERATION OF WEAR AT HIGH VELOCITIES


Stephen P. Meador, B.S.

Approved:




Dr. Anthony N. Palazotto
(Chairman)

4 Mar 2010
date



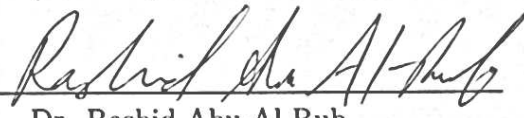
Dr. William P. Baker
(Member)

4 Mar 2010
date



Chad S. Hale, Lt Col, USAF
(Member)

4 Mar 2010
date



Dr. Rashid Abu-Al Rub
(Member)

4 Mar 2010
date

Abstract

The goal of this research is to study sliding contact wear of metals at high velocities. In particular, wear of test sled slippers at the Holloman High Speed Test Track at Holloman AFB, NM is being considered. Experimentation representative of the speeds seen at the test track is infeasible, so numerical studies with appropriate engineering approximations need to be performed. Previous studies have used finite element analysis techniques to characterize the wear phenomenon up to sliding velocities of 1,530 m/s. However, the aim of the test track is to reach sled speeds in excess of 3,000 m/s, and performing analysis at these sliding speeds is beyond the capability of the Lagrangian finite element technique.

The limitations of the Lagrangian technique were overcome by using an Eulerian-Lagrangian hydrocode called CTH. The hydrocode is used to perform plane strain simulations of a test slipper colliding with a hemispherical asperity. Wear involves removal of material through a mechanical process, but the material removal is a phenomenon that is difficult to model numerically. Instead, failure criteria were established that are based on the viscoplastic behavior of the slipper material using the Johnson-Cook constitutive model. The Johnson-Cook constitutive model is used due to its versatility in handling high strains, strain rates, and temperatures. The slipper material used at the test track for high velocity sleds is VascoMax 300, which is a maraging steel. The mechanical wear rates for VascoMax 300 have been evaluated for velocities ranging from 200 to 3,000 m/s, and a method for calculating total wear has been developed and verified using known wear values from a slipper recovered from the test track.

Additionally, the melt wear phenomenon has been evaluated. The thermodynamics of the sliding event have been evaluated by considering the heat conduction in the slipper due to frictional heating. A key parameter that needed to be defined

was the fraction of frictional heat energy entering the slipper. This fraction of heat varies with time, so the analysis was simplified by setting the value as a constant and evaluating it as an average value. Previous studies had used a fraction of 0.5 based on similarity between the track and slipper materials, but it has been found that this value is only reasonable for a steady-state solution, which is not applicable to the test track scenario. It has been found that an average fraction of 0.12 to 0.14 is more reasonable. Based on the mechanical and melt wear analysis, it has been determined that for a typical test track forebody sled velocity profile reaching 3,000 m/s, approximately 3 to 6% of the slipper is worn away.

Acknowledgements

I need to thank many people for making this research possible. First and foremost, I need to thank my advisor Dr. Anthony Palazotto. His contribution to my education is immeasurable, and his expertise has been invaluable as I have completed this research. I also need to thank Lieutenant Colonel Chad Hale for his assistance with this research. His advice has not only helped with the minute details of the research, but he also helped to occasionally step back and “see the forest from the trees.” Additionally, I need to thank the Air Force Office of Scientific Research and Maj. Michelle Ewy for funding this research work. I would also like to thank all of the professors I had at Miami University who prepared me to be able to complete this research work. Finally, I would like to thank all of my family and friends for continuous support as I have worked on my degree and thesis research.

A handwritten signature in black ink, reading "Stephen P. Meador". The signature is written in a cursive style with a large, prominent initial 'S'.

Stephen P. Meador

Table of Contents

	Page
Abstract	iv
Acknowledgements	vi
List of Figures	x
List of Tables	xii
List of Symbols	xiii
List of Abbreviations	xvi
I. Introduction	1
1.1 Research Objective	1
1.2 Holloman High Speed Test Track Background	1
1.3 Summary of Previous Research	4
1.3.1 Mechanical Wear and Friction Research	6
1.3.2 Melt Wear and Thermodynamics Research	11
1.4 Summary of Literature Review and Research Objectives	15
II. Theoretical Background	17
2.1 Wear Mechanisms	17
2.1.1 Adhesive Wear	18
2.1.2 Abrasive Wear	19
2.1.3 Melt Wear	19
2.2 Coefficient of Friction	20
2.3 Sliding Thermodynamics	22
2.3.1 Frictional Heating	22
2.3.2 Flash Heating	23
2.4 Hydrocodes vs. Finite Element Analysis	25
2.4.1 Lagrangian Step and Eulerian Remap	27
2.4.2 Boundary Conditions	28
2.5 Johnson-Cook Viscoplasticity Model	29
2.6 Defining Material Failure	30
2.6.1 Maximum von Mises Criterion (Average Strain Rate)	30
2.6.2 Maximum von Mises Criterion (Pointwise Strain Rate)	34

	Page
2.6.3 Johnson-Cook Plasticity Criterion	35
2.6.4 Plastic Strain Criterion	35
2.7 Summary of Theoretical Background	37
III. Numerical Modeling	39
3.1 Dynamics of the Sled and Slipper	39
3.2 Thermodynamic Analysis	42
3.2.1 Explicit Solution Scheme	42
3.2.2 Implicit Solution Scheme	43
3.2.3 Boundary Conditions and Initial Condition	44
3.2.4 Defining Frictional Heat Flux	45
3.3 Plane Strain Hydrocode Simulation	48
3.3.1 Initial Velocity Vector	51
3.3.2 Initial Temperature	53
3.3.3 Viscoplasticity Model	55
3.3.4 Equation of State	55
3.4 Single Asperity Mechanical Wear Rates	56
3.5 Melt Wear	58
3.6 Total Mechanical Wear Volume Calculation	61
3.7 Summary of Numerical Modeling	62
IV. Results and Discussion	64
4.1 Evaluation of Frictional Heating	64
4.2 Single Asperity Mechanical Wear Rates	69
4.3 Mechanical Wear Criteria Validation	73
4.4 Total Wear	74
V. Summary and Conclusions	78
5.1 Summary of Research	78
5.2 Conclusions	80
5.3 Recommendations for Future Research	81
Appendix A. Heat Transfer Analysis Code	83
A.1 Heat Transfer Code Description	83
A.2 Heat Transfer Matlab [®] Code	83
Appendix B. CTH Input Process	92
B.1 CTH Input Summary	92
B.2 Example CTH Input File	92

	Page
Appendix C. Post Processing of CTH Data	105
C.1 CTH Data Extraction	105
C.2 Post Processing Matlab [®] Code	105
Appendix D. Tabulated Wear Rates	114
Bibliography	115

List of Figures

Figure		Page
1.1	January 2008 Rocket Test Sled	2
1.2	Rocket Sled System at the HHSTT	2
1.3	Slipper Configuration for Low Velocity Sleds	3
1.4	Slipper Configuration for High Velocity Sleds	4
1.5	Basic Dimensions of 1080 Steel Rail and VascoMax 300 Slipper	5
1.6	Coefficient of Friction of Two Steels [15]	7
1.7	Wear Mechanism Map for Steel [26]	9
1.8	Archard Contact Area Model [1]	13
2.1	Wear Mechanism Map for Steel [26]	19
2.2	Graphical Depiction of Friction Mechanisms [4]	21
2.3	μ vs. Pv for Steel on Steel Sliding [16]	22
2.4	Archard Contact Area Model [1]	25
2.5	Finite Element Mesh Used by Chmiel [8]	26
2.6	Finite Element Mesh Used by Hale [16]	27
2.7	Graphical Comparison of Lagrangian and Eulerian Meshes . . .	28
2.8	True Stress-Strain Curves for VascoMax 300 with Johnson-Cook Constitutive Equation [16]	32
2.9	Example Strain Rate Histogram Data, $V = 1,530$ m/s [16] . .	33
2.10	Critical Flow Stress vs. Plastic Strain Rate	35
2.11	Critical Plastic Strain vs. Plastic Strain Rate	36
3.1	DADS Sled Velocity and Slipper Contact Force Profile	41
3.2	One-Dimensional Heat Transfer Schematic	43
3.3	Heat Transfer Boundary Conditions and Initial Condition . . .	45
3.4	Frictional Heat using Hale's Statistical DADS Force [16]	47
3.5	Zoomed-in View of Instantaneous Frictional Heating	47

Figure		Page
3.6	Frictional Heat Accumulation Curve Fit	49
3.7	CTH Materials Illustration	51
3.8	Slipper Vertical Velocity from 2003 Forebody Sled DADS Data	53
3.9	Evaluation of Vertical Velocity Component	54
3.10	Plane Strain vs. Three-dimensional Model	57
3.11	Example Single Asperity Wear Rate Integral	58
4.1	Third Stage Slipper Accumulated Frictional Heating	67
4.2	Surface Temperature Third Stage Slipper, $\lambda_{ave}=0.5$	67
4.3	Melt Depth Example	68
4.4	Evaluation of Frictional Heating Fraction, λ_{ave}	69
4.5	Restricted Range Evaluation of Frictional Heating Fraction, λ_{ave}	70
4.6	One-dimensional Temperature Profile with Respect to Velocity	71
4.7	Temperature Gradient Near Slipper Surface at 1,500 m/s	71
4.8	Single Asperity Mechanical Wear Rates	72
4.9	Sensitivity to Averaged Strain Rate Criteria, Velocity = 1,530 m/s	73
4.10	Wear Criteria Validation	75
4.11	Forebody Sled Slipper Mechanical Wear	76
4.12	Total Forebody Sled Slipper Wear versus Percentage of Total Wear Attributed to Melt Wear	77
4.13	Percentage Forebody Sled Slipper Worn versus Percentage of To- tal Wear Attributed to Melt Wear	77

List of Tables

Table		Page
2.1	VascoMax 300 and 1080 Steel Material Properties [10; 11] . . .	24
2.2	Maximum von Mises Stress vs. Strain Rate	34
2.3	Coefficients for Pointwise Strain Rate Criterion Curve Fit . . .	34
2.4	Coefficients for Plastic Strain Criterion Curve Fit	36
3.1	Coefficients for Frictional Heating Curve Fit	48
3.2	CTH Simulation Times	52
3.3	Plane Strain Simulation Initial Velocity Vectors	54
3.4	Plane Strain Simulation Initial Temperatures	55
3.5	VascoMax 300 and 1080 Steel Johnson-Cook Coefficients [9; 10; 11]	56
3.6	Iron and 1080 Steel Material Properties	56
4.1	Coefficients for Plastic Strain Criterion Curve Fit	66
2.1	VascoMax 300 and 1080 Steel Johnson-Cook Coefficients	92
4.1	Single Asperity Mechanical Wear Rates	114

List of Symbols

Symbol		Page
Pv	Product of Pressure and Sliding Velocity	7
\widetilde{W}	Normalized Wear Rate	18
\widetilde{F}	Normalized Pressure	18
\widetilde{v}	Normalized Velocity	18
W	Wear Rate	18
A_n	Normal Contact Area	18
H_o	Material Hardness	18
v	Sliding Velocity	18
r_o	Pin Radius for Pin-on-Disk Experiment	18
a	Thermal Diffusivity (Used by Lim and Ashby [26])	18
T_{melt}	Melt Temperature	19
μ	Coefficient of Friction	20
F_f	Frictional Force	20
F	Contact Force	20
q_f	Frictional Rate of Heat of Generation	23
q''	Heat Flux	23
$\lambda_{slipper}$	Fraction of Frictional Heat Flux into Slipper	23
α	Material Thermal Diffusivity	23
ρ	Material Density	23
k	Material Thermal Conductivity	23
c_p	Material Specific Heat	23
ν	Poisson's Ratio	24
E	Modulus of Elasticity	24
Pe	Dimensionless Péclet Number	24
ΔT_{flash}	Flash Temperature Increase	24

Symbol		Page
H	Material Hardness	24
W	Flash Temperature Normal Load	24
σ	Flow Stress	30
ε	Equivalent Plastic Strain	30
$\dot{\varepsilon}^*$	Dimensionless Plastic Strain Rate	30
T^*	Homologous Temperature	30
A	Johnson-Cook Material Constant	30
B	Johnson-Cook Material Constant	30
C	Johnson-Cook Material Constant	30
m	Johnson-Cook Material Constant	30
n	Johnson-Cook Material Constant	30
T	Temperature	30
T_0	Ambient Temperature	30
β	Inelastic Heat Fraction	31
ε_f^p	Final Plastic Strain	31
A_{PSR}	Coefficient for Dynamic Strain Rate Failure Criteria	34
B_{PSR}	Coefficient for Dynamic Strain Rate Failure Criteria	34
C_{PSR}	Coefficient for Dynamic Strain Rate Failure Criteria	34
σ_{crit}	Critical Stress	34
A_{PS}	Coefficient for Plastic Strain Failure Criteria	36
B_{PS}	Coefficient for Plastic Strain Failure Criteria	36
C_{PS}	Coefficient for Plastic Strain Failure Criteria	36
Fo	Fourier Number	42
Q_f	Accumulated Frictional Heat	46
A_f	Coefficient for Frictional Heat Curve Fit	48
B_f	Coefficient for Frictional Heat Curve Fit	48
A_f	Coefficient for Frictional Heat Curve Fit	48
B_f	Coefficient for Frictional Heat Curve Fit	48

Symbol		Page
A_d	Damage Area	50
W_{uw}	Wear Rate per Unit Width	50
W_{sa}	Single Asperity Wear Rate	58
T_{surf}	Surface Temperature	59
$T_{friction}$	Frictional Surface Temperature	59
$W_{uw,melt}$	Melt Wear Rate per Unit Width	59
A_{melt}	Melt Area	59
h_{melt}	Melt Depth	59
w_{eff}	Effective Width	60
$W_{sa,melt}$	Melt Single Asperity Wear Rate	60
λ_{ave}	Average Fraction of Frictional Heat Flux into Slipper . . .	61
d_{pc}	Percentage of Sliding Contact	62
W_A	Archard's Wear	62
k_A	Archard's Wear Coefficient	62
W_{tot}	Total Wear	62
E	Internal Energy	64
A_{3S}	Coefficient for Frictional Heat Curve Fit, Third Stage Slipper	66
B_{3S}	Coefficient for Frictional Heat Curve Fit, Third Stage Slipper	66
C_{3S}	Coefficient for Frictional Heat Curve Fit, Third Stage Slipper	66
D_{3S}	Coefficient for Frictional Heat Curve Fit, Third Stage Slipper	66
E_{3S}	Coefficient for Frictional Heat Curve Fit, Third Stage Slipper	66
F_{3S}	Coefficient for Frictional Heat Curve Fit, Third Stage Slipper	66
G_{3S}	Coefficient for Frictional Heat Curve Fit, Third Stage Slipper	66

List of Abbreviations

Abbreviation		Page
AFOSR	Air Force Office of Scientific Research	1
HHSTT	Holloman High Speed Test Track	1
AFB	Air Force Base	1
AISI	American Iron and Steel Institute	1
m	meters	1
s	seconds	1
°C	degrees Celsius	6
DADS	Dynamic Analysis and Design System	10
FEA	Finite Element Analysis	10
Hz	Hertz	12
AFIT	Air Force Institute of Technology	13
K	Kelvin	14
Pa	Pascals	21
W	Watts	48
J	Joules	66

CONSIDERATION OF WEAR AT HIGH VELOCITIES

I. Introduction

The goal of this research, which is funded by the Air Force Office of Scientific Research (AFOSR), is to study sliding contact wear of metals at high velocities. In particular, wear of test sled slippers at the Holloman High Speed Test Track (HHSTT) at Holloman Air Force Base (AFB) is being considered. This chapter will discuss the goals of this thesis research, and provide background information on the HHSTT. The chapter will conclude with a presentation of previous research investigating the wear phenomenon.

1.1 Research Objective

The HHSTT performs a variety of tests at high velocities using a rocket sled system that rides on a set of rails. The sled is attached to the rail using slippers, which are described in greater detail in section 1.2. Currently, the HHSTT uses VascoMax 300, a maraging steel, as the material for slippers that see high velocities. The rail is composed of AISI 1080 steel. The objective of this research is to develop and evaluate numerical methods for quantifying mechanical wear rates of the slipper material in sliding contact with the rail at relative speeds ranging from 750 m/s to 3,000 m/s. These numerical methods are based on the viscoplastic behavior of the VascoMax 300 material being considered. Additionally, the thermodynamics of the sliding event will be examined in detail, and conclusions will be drawn from the analysis.

1.2 Holloman High Speed Test Track Background

The HHSTT is a rocket sled test track located at Holloman AFB in New Mexico. The test track is used for a variety of studies ranging from testing of aircraft munitions and egress systems to hypersonic aerodynamic effects. The use of the test track is advantageous because it is safer, more observable, and more efficient in terms of time

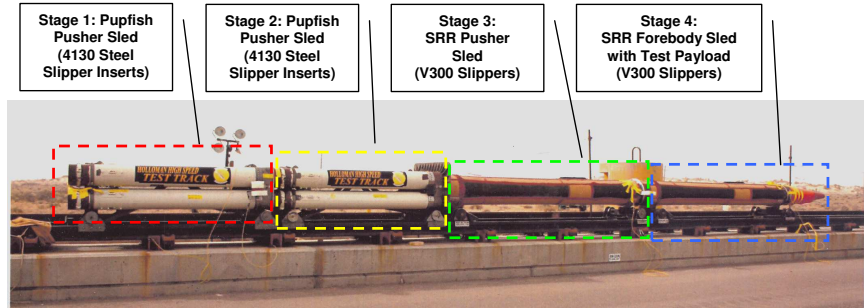


Figure 1.1: January 2008 Rocket Test Sled

and cost spent than flight testing at the velocities seen by payloads at the track. The test track designers set a land speed record of 2,885 m/s (6,453 miles per hour) in April 2003, and customers are interested in performing tests in excess of 3,000 m/s.

The HHSTT achieves these velocities using sleds that ride on a collection of rails laid over a length of approximately 6,000 meters. A typical setup for a configuration used to test munitions and impact phenomena is shown in Figure 1.1. This particular configuration was used for a mission conducted in January 2008 and consists of four rocket-powered sleds. The sleds ride on two parallel rails and are ignited sequentially as they slide down the track. The first three sleds are referred to as “pusher” sleds because they push the “forebody” sled down the track. The forebody sled contains the payload and instrumentation of interest to the HHSTT experimenters.



Figure 1.2: Rocket Sled System at the HHSTT



Figure 1.3: Slipper Configuration for Low Velocity Sleds

Each sled is restrained to the track by four slippers that wrap around the rail as shown in Figure 1.2, which shows the forebody sled used for the record-setting mission in April 2003. Material selection for the slippers is based on the maximum velocity they will experience during a test run. The first two pusher sleds in the January 2008 configuration use AISI 4130 steel inserts that are placed inside slipper housings, as shown in Figure 1.3. The housings are a reusable component while the slipper inserts are discarded and replaced after every run. The third pusher sled and forebody sled use slippers fabricated from VascoMax 300, and are not reusable due to the wear they endure during a test. An example of the VascoMax 300 slippers is shown in Figure 1.4. As shown in Figure 1.5, the VascoMax 300 slippers are nominally 20.32 cm long by 10.16 cm wide, and have a thickness of 1.47 cm.

The HHSTT designers need to consider several variables when they design a sled system. The sleds experience considerable drag forces at high velocity, and the track designers circumvent this by using helium-filled tunnels. The tunnels are constructed of plastic film draped over selected intervals of the track. The helium exerts less air resistance on the sled and also has desirable heat transfer characteristics for maintaining acceptable operating conditions for the payload and slippers. The designers



Figure 1.4: Slipper Configuration for High Velocity Sleds

are also aware of the gouging phenomenon, which occurs as slipper and rail materials mix upon impact at high velocities, and is marked by a tear drop shaped removal of material on the rail. The HHSTT mitigates the gouging effect by using epoxy coatings on the rail in areas that are prone to gouging based on the sled velocity profile for a given mission. The sled designers are also concerned with wear of the slippers. In order to increase their peak velocity capability safely and effectively, the designers need to estimate whether the slippers will wear to a critical thickness before the end of a test run.

1.3 Summary of Previous Research

Researchers have been interested in the wear phenomenon for decades, and efforts have been made to define the mechanisms that result in the wear of materials. The various mechanisms are discussed in Section 2.1. Models have been developed that define the rate at which volume is removed from one material as it slides against another material, and these evaluations were performed for different velocity ranges depending on the interest of the individual researcher. As a result, an inconsistency

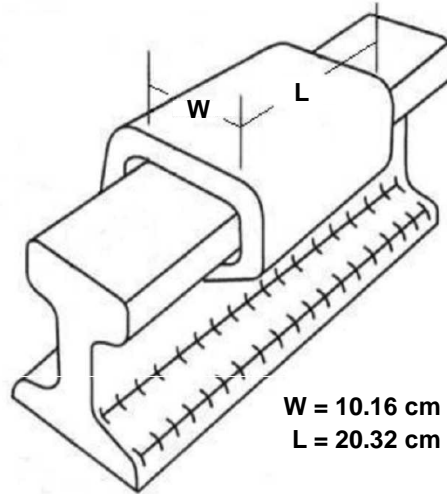


Figure 1.5: Basic Dimensions of 1080 Steel Rail and VascoMax 300 Slipper

in nomenclature developed with respect to the term “high velocity.” Much of the early literature considered velocities on the order of 10 m/s as high velocities, but obviously within the context of the HHSTT environment this is a very low velocity. For consistency in this thesis, low velocities will be considered as those that are less than 750 m/s, while velocities exceeding 750 m/s will be regarded as high velocities.

In addition to wear, the HHSTT is concerned with other phenomena that occur during the sliding event, as mentioned in the previous section. As anyone who has rubbed their hands together on a cold day knows, two objects rubbing together will produce heat. The slipper-rail interaction being studied is no different. The amount of heat generated is a function of the frictional force and the relative velocity of the two materials, as discussed in Section 2.3. The next sub-section will discuss previous mechanical wear studies, followed by a discussion on previous research studying the temperature and melt of two sliding objects.

Previous research by Hale [16] has investigated the wear rates of the third pusher sled for the January 2008 mission, which reached a peak velocity of 1,530 m/s. Sections 1.7-1.9 of Hale’s dissertation provide a thorough synopsis of research relevant to this research work, and supplements the discussion provided below.

1.3.1 Mechanical Wear and Friction Research. In 1956, Archard and Hirst [2] published a study of the wear of metals under unlubricated conditions. The experimental study utilized a pin and ring wear machine to make measurements. The ring was 2.38 cm in diameter and mounted to a shaft, which rotated the ring at linear speeds ranging from 2 to 660 cm/s. The pin was a 0.635 cm in diameter and applied with a load varying from 0.05 to 10 kg. Under the test conditions, the metals exhibited both mild and severe wear. The mild wear was observed at lighter loads, while the severe wear occurred at higher loads. The severe wear was several orders of magnitude greater than the mild wear. Archard and Hirst observed that the wear rate was initially dependent on time, until the surface layers reached an equilibrium point and the wear rate became constant.

In 1970, Farrell and Eyre [15] studied friction and wear characteristics of two steels using a pin and disc wear test machine. A discussion of the transition from mild wear to severe wear is provided and is dependent on both load and sliding speed. Mild wear “involves the relatively slow removal of the tops of the highest contacting asperities with little substrate distortion,” while severe wear shows a greater scale of surface damage and “the wear rate increases by some two orders of magnitude from that of mild wear and the maximum size of the wear particles increases suddenly at the transition load.”

The pin and disc experiments were conducted with the pin loaded with as much as 10 kg, and the sliding speed of the disc was 100 cm/s. The tests showed that the sliding distance required for the onset of mild wear increased with increasing load for both steels tested. The authors calculated a flash temperature based on Archard’s model, discussed in Section 1.3.2, in the range of 700 to 1,100 °C. The calculations of the flash temperature were made assuming the coefficient of friction was constant. However, the authors indicated that the coefficient of friction is dependent on the applied load and the sliding velocity, as shown in Figure 1.6.

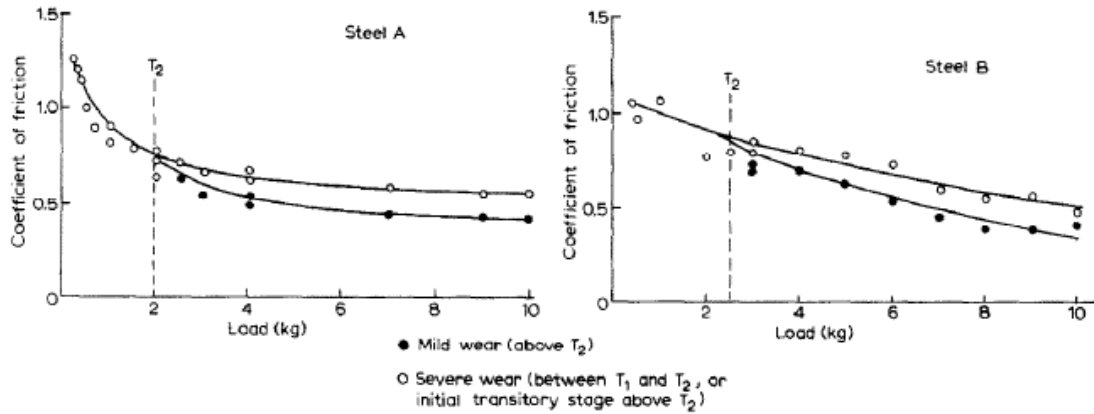


Figure 1.6: Coefficient of Friction of Two Steels [15]

In 1976, Montgomery [29] studied friction and wear of metals within the context of high muzzle velocity weapons. A pin and disc experimental setup was used to take measurements. The pins were 0.080 inches in diameter and the load was applied to the pin using air pressure. The bearing pressure on the pins ranged from 760 to 26,200 psi, and the sliding velocity ranged from 3 to 550 m/s. The pins were moved radially during the test so that the paths did not overlap on successive revolutions of the disc. The frictional and normal forces were measured continuously by attaching strain gages to the specimen holders. The amplified signals were analyzed and the data tabulated.

Similar to Farrell and Eyre, Montgomery showed that the coefficient of friction was a function of the bearing pressure and the sliding velocity. Montgomery plotted the coefficient of friction as a function of the product of the pressure and velocity, referred to as the “ Pv ” term. At lower levels of Pv , higher friction coefficients were measured and oscillations were observed. As the Pv values increased, the coefficient of friction was lower and more stable. The decrease in coefficient of friction as Pv increased was attributed to the raising of the surface temperature. This effect was more evident when the coefficient of friction is plotted as a function of the rate of heat input. Below some critical level of heat input, the coefficient of friction data is sporadic, but above the critical level the coefficient of friction is very stable and is indicative of melting occurring at the surface, according to Montgomery.

In 1977, Saka et al. [31] studied the sliding wear of 1020 steel, 304 stainless steel, and 75A titanium at sliding speeds ranging from 0.5 to 10 m/s and a load of 49 N. The experimental setup consisted of a steel ring 0.2 m in diameter mounted to a variable speed lathe. A normal load was applied to the test specimen, which was machined to conform to the surface of the rotating ring, using a dead weight and the tractive force was measured using a dynamometer. The tests were run for 1800 seconds, and the specimen was removed and weighed afterward. Select specimens were cut, polished, and etched and observed using a scanning electron microscope.

They reported coefficient of friction results similar to the results of the studies by Montgomery and Farrell and Eyre. As the sliding speed increased, the coefficient of friction decreased. Also, the coefficient of friction fluctuated at lower sliding speeds, but reached a steady state condition at higher sliding speeds. The 304 stainless steel wear rate increased monotonically with sliding speed. However, the 1020 steel and 75A titanium wear rates decreased from 0.5 to 1.0 m/s and then increased from 1.0 m/s until approximately 5.0 m/s and then decreased again from 5.0 to 10.0 m/s. Metallurgical analysis showed that the surface of the specimen was significantly rougher than the virgin specimens examined prior to testing, and evidence of plastic deformation at the surface was evident. Micrographs of the subsurface indicate that the sliding event caused large scale subsurface deformation.

In 1987, Lim and Ashby [26] developed a method of classifying dominant wear mechanisms for steel based on the loading and sliding scenario. Two approaches were used. An empirical method built mechanism maps by plotting experimental data for wear rates on “suitable axes” and identifying the dominant mechanism at each point by observation. A physical modeling method numerically combined equations describing the wear rate caused by each mechanism to generate a map showing the total wear rate and the contribution of the various mechanisms. The wear rate is defined to be a function of the normal force, sliding velocity, initial temperature, and the thermal, mechanical, and chemical properties of the material. If the mechanisms

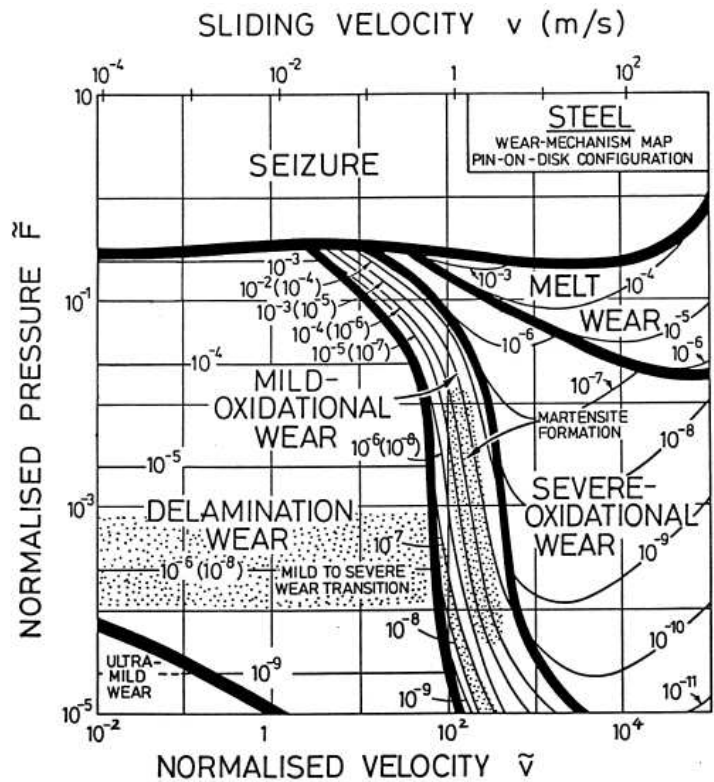


Figure 1.7: Wear Mechanism Map for Steel [26]

do not interact, the dominant mechanism is defined as the one which provides the highest wear rate.

To correlate specimens from different sources and of varying sizes and shapes, the wear rate, normal force, and sliding velocity are normalized. The normalization equations are presented in greater detail in Section 2.1. Figure 1.7 shows the wear rate mechanism map developed for steel. Contours of normalized wear rates are superimposed on the fields showing the regions indicating dominance of differing wear mechanisms. Discontinuities in the contours exist at the transition into the severe-oxidational wear region. The wear rate values in parentheses indicate wear rates when mild wear occurs and. The transition between mild and severe wear is indicated by the shaded regions.

In 2007, Cameron [7] analyzed the wear of the HHSTT slipper for the 2003 test run based on the equations developed by Archard and by Lim and Ashby. Code was

written to utilize data characterizing the dynamics of the sled and slipper to calculate mechanical and melt wear depths for a specific sled test run based on equations for mechanical and melt wear developed by Lim and Ashby. The dynamics data was generated by the HHSTT using a program called Dynamic Analysis and Design System (DADS). The DADS sled data is discussed in greater detail in Section 3.1. The DADS data used by Cameron was a simulation of a forebody sled accelerating from 0 to 3,030 m/s at constant acceleration over a span of 2.5 seconds. For the entire sled run, Cameron’s analysis calculated a total melt wear depth of 0.08 cm and total mechanical wear depth of 0.27 cm. Superimposing the melt and mechanical wear gives a total wear depth of 0.35 cm. This value was considered acceptable as an initial approximation for high speed slipper wear because slippers used at the test track, which are 1.47 cm in thickness, have not been shown to wear completely through their thickness during a test run.

In 2008, Chmiel [8] studied the feasibility of predicting slipper wear using the finite element analysis (FEA) technique. Two methods were investigated. One method was a macro-scale, incremental method utilizing the wear equations developed by Archard. The other method was a micro-scale, material property method that used failure criteria to determine wear. The study was performed at lower velocities so that comparisons could be made with results in literature. The incremental approach produced accurate results, but the method had many numerical problems. The material property method was found to be a feasible solution.

In 2009, Hale [16; 17; 18] used the micro-scale FEA technique to model mechanical wear rates for the third stage pusher sled used during the 2008 HHSTT test run. While wear is a three-dimensional phenomenon, the analysis was simplified using a plane strain modeling approach, which collided a VascoMax 300 test slipper with a semicircular asperity having a radius of 6 μm . A material damage criterion, based on the viscoplastic behavior of the slipper material, was developed to determine if an element in the finite element analysis had “worn.” The viscoplastic model used was the Johnson-Cook [22] model, which is presented in Section 2.5. The total damage

area accumulated during the simulation was divided by the distance slid during the simulation to calculate a plane strain wear rate.

It should be noted that this wear rate has units of area per distance, and Hale used units of mm^2/mm . Since the wear event is three-dimensional, a method to convert the plane strain wear rates to a volume per distance slid needed to be developed. This was accomplished by running additional simulations with semicircular asperities of radius $4\ \mu\text{m}$ and $2\ \mu\text{m}$, and integrating the plane strain wear rates for each across the width of the asperity. This approximates the volume removal that would be experienced if the slipper were to collide with a single hemispherical asperity of $6\ \mu\text{m}$. This process was repeated for several velocities of interest ranging from 0 to 1,530 m/s, the peak velocity of the third stage pusher sled used during the 2008 test mission. The wear rates were integrated through the sliding distance and multiplied by the percentage of rail contact experienced by the slipper and a scaling factor (based on Archard's work) to determine a total mechanical wear removal.

1.3.2 Melt Wear and Thermodynamics Research. In 1954, Bowden and Thomas [5] investigated the surface temperature increase resulting from rubbing contact of two solids. The surface temperatures were determined experimentally by rubbing a metal against a transparent solid and measuring the infra-red radiation transmitted through the transparent solid. The measurements showed that high, fluctuating temperatures occurred. These hot spots were shown to be a transient phenomenon and the formation and decay times were measured.

The apparatus used to make the measurements consisted of a metallic cylinder 1 mm in diameter being pressed against a rotating glass disk about 0.2 cm thick. The glass disk was rotated using a motor that provided linear speeds ranging from 100 to 700 cm/s at the metallic cylinder. A photosensitive cell, enclosed in a brass holder, was placed below the glass disk. In the top of the holder, a narrow slit was placed in line with the direction of motion and the signal from the cell was amplified for

viewing using an oscillograph. The load on the metallic cylinder was increased up to 0.45 kg until hot spots formed.

The photographic plate was exposed for a relatively long period of time (in the range of 8 seconds) and data was collected at approximately 200 Hz. The data collected showed the short formation and then decay of hot spots, and indicated a dependence of load on the temperature increase at the hot spot. Also, the authors note that while the surface temperatures reached a very high temperature near the melting point of the metal, if only for a short period of time, the bulk temperature of the two solids remained cool. Thus, the temperature increases are a very localized phenomenon at the sliding velocities used during the tests.

In 1959, Archard [1] formulated methods to calculate the “flash temperatures” that form at the surface of two rubbing solids. The assumption is made that the heat generated is formed at the true contact area and is dissipated into the bulk of the solid via heat conduction. Figure 1.8 depicts the true contact area, which is labeled “A,” and the bulk solid, which is labeled “B.” The equations for the flow of heat into each body are developed, and the derived surface temperatures are expressed in terms of the heat flow rate, the size and speed of the heat source, and the thermal properties of the material. The proportion of the heat flow into each body is determined by assuming that the heat flow equations for each body will give the same average temperature across the contact area.

The heat flow equations differ based on the relative sliding speed. A dimensionless speed criterion is used to differentiate between slow sliding speeds and fast sliding speeds, and the heat flow equations are also different if the contact area is formed by a load causing elastic or plastic deformation. Equations for the maximum attainable flash temperature are also developed. The equations developed by Archard are discussed in greater in detail in Section 2.3.

In 1968, Korkegi and Briggs [24] studied the hypersonic convection and fluid frictional heating effects on the HHSTT slipper setup. The flow between the slipper

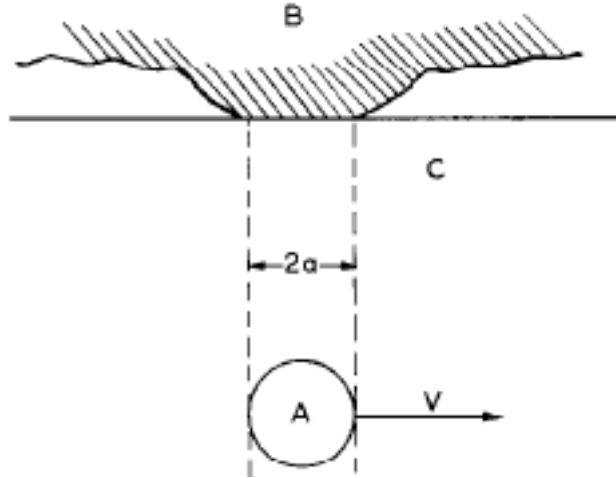


Figure 1.8: Archard Contact Area Model [1]

and rail was modeled as an inlet with decreasing area. As such, the flow between the slipper and rail would accelerate to, at most, sonic speeds. The flow at the stagnation point is considered to be uniform sonic flow, which transitions to laminar flow and then turbulent flow. As the flow continues down the length of the slipper, the slipper and rail boundary layers grow until they eventually merge. Past this merge point, the flow is considered to approach a Couette flow. Korkegi and Briggs find that at higher speeds, a free stream Mach number of four or higher, the aerodynamic heating rates due to fluid friction are comparable to sliding friction with realistic bearing loads.

In 2006, Szmerekovsky [33; 34] studied the temperature changes between the slipper and rail during hypervelocity impact in the context of gouging. While previous research at the Air Force Institute of Technology (AFIT) had studied the effect of temperature on hypervelocity impacts, those studies did so using an isothermal environment. Szmerekovsky used a hydrocode called CTH, which is developed by Sandia National Laboratories, to study gouging when heat is allowed to flow within the solution domain. This study considered 4 cases: a vertical impact on a “clean” rail with a horizontal velocity of 3,000 m/s and a vertical velocity of 1 m/s into the rail, a vertical impact into a “coated” rail with the same 3,000 m/s horizontal and 1 m/s vertical velocity vector as the clean rail, a tangential velocity impact of 3,000

m/s into a clean rail with “roughness,” and a 3,000 m/s tangential velocity impact into a coated rail with roughness.

The coating that Szmerekovsky refers to is the epoxy coating used by the HHSTT to mitigate gouging. The thickness of the coating in the simulations was the minimum allowable thickness of approximately 0.15 mm set by the HHSTT standards. The clean rail refers to the bare 1080 steel rail. The rail with roughness simulates discontinuities in the rail profile, which are common at the seams where rail pieces are joined. The simulations modeled the rail as iron because tabular equation of state models for 1080 steel are not available in CTH. Iron was chosen because it has material properties that are similar to 1080 steel. To model the heat conduction, the conductivity of the materials was defined as a function of temperature.

The study found that the temperatures at the surface rose to approximately 1,300 K for the clean, smooth rail case. For a clean rail with roughness, the surface temperatures in the rail and slipper were approximately 1,500 K, and the boundary layer showed temperatures ranging from 500 to 1,000 K. When modeling the rail with the epoxy coating the temperatures were lower, as expected. For the smooth epoxy-coated rail, the slipper boundary layer was approximately 625 K, which was similar to the clean rail, but the surface temperature was lower by about half the magnitude reached without the coating. Likewise, while the surface temperature of the clean rail with roughness reached 950 K, the epoxy-coated rail with roughness only reached 625 K at the surface.

In 2007, Cameron [7] calculated melt wear of the HHSTT slipper based on the developments of Lim and Ashby [26]. The model is an unsteady finite difference heat transfer analysis based on a heat flux in to a sliding element. The assumption is that a portion of the heat flux into the sliding element goes towards heating the element, while the remainder of the flux goes towards melting the element. The heat transfer was modeled using heat diffusion with a heat flux boundary. The heat flux was defined as a function of the heat generated due to friction, which is the product of the

frictional force and sliding velocity. The heat flux into the slipper was taken to be half of the total heat generation because the slipper and rail have similar conductivities. The solution also required a second boundary condition and an initial condition. For the second boundary condition, the temperature at the top of the slipper was held at ambient conditions. The initial condition defined the temperature at every point through the thickness of the slipper to initially be at ambient conditions. The results of this analysis gave values that were reasonable in the opinion of the author.

In 2009, Hale [16; 17; 18] studied the melt wear of the third stage of the rocket sled used for the 2008 HHSTT test mission by considering the effects of frictional heating and flash temperature rise. Hale's overall wear modeling method calculated single asperity wear rates at target velocities along the velocity profile of the sled, and the total wear accumulation was calculated by integrating the wear rates.

The frictional heating was analyzed using the same finite difference method as Cameron with the same boundary conditions for the entire sled run. This frictional heating provided the surface temperature of the slipper as a function of time and sliding distance. A finite element model was built using a program called ABAQUS® to calculate impact pressure in the slipper so that the flash temperature could be calculated. The flash temperature was then added to the frictional temperature to determine the surface temperature, and a one-dimensional heat diffusion analysis was performed for a length of time equal to the asperity collision time for each respective velocity of interest. The depth of material above the melting point of the slipper, which is 1,685 K, was considered to be the melt depth and thus provided a melt wear rate at that velocity.

1.4 Summary of Literature Review and Research Objectives

A goal of this research is to calculate mechanical wear of the HHSTT VascoMax 300 slipper resulting from sliding down the 1080 steel track. This will be accomplished by using the micro-scale damage method initially developed by Chmiel and later utilized by Hale. However, rather than using the finite element technique, a

hydrocode simulation will be used. This will be discussed later in Sections 2.4 and 3.3. An important parameter to define for the hydrocode simulations is the material temperature. The temperature will be determined using a numerical finite difference approach, which is described in Section 3.2, and the sliding coefficient of friction will be critical for determining the heat generated by the sliding event. The coefficient of friction testing by Montgomery will be used to define the coefficient of friction for the slipper and rail, as discussed in Section 2.2.

The hydrocode simulations will be used to calculate plane strain wear rates for a single semicircular asperity collision. The plane strain wear rates will then be integrated across the width of the asperity to simulate the effect of a collision with a single hemispherical asperity. Since the slipper actually collides with multiple asperities of varying sizes on the rail, a scaling factor will need to be developed to account for this aspect of the sliding event. This scaling factor will be determined by comparing the calculated single asperity wear rates with the wear rate models developed by Archard. This is important because it makes a connection between the single asperity collision wear rates and experimental wear rates that account for the three-dimensional nature of the wear phenomenon.

Additionally, the finite difference thermal analysis will be used to analyze the melt wear phenomenon. Currently, models are not available that can appropriately define the amount of frictional heating absorbed by the VascoMax 300 slipper. This research will evaluate the total melt wear, as a function of the frictional heating, with respect to experimental wear results so that appropriate levels of frictional heating can be defined. This is discussed in detail in Sections 3.5 and 4.1

II. Theoretical Background

This chapter will present the theoretical background that is the foundation of the numerical modeling and results presented in Chapters III and IV, respectively. First, the various wear mechanisms will be addressed, followed by a discussion of the coefficient of friction between two metals sliding against each other. The concepts relating to friction will feed directly into a discussion on the thermodynamics of the sliding event. Following the thermodynamic discussion, two different numerical modeling techniques will be introduced.

The simulation techniques, which are finite element analysis and hydrocodes, will be discussed with respect to modeling high velocity wear phenomena. The discussion on hydrocodes will address the Eulerian-Lagrangian simulation process in addition to implementation of boundary conditions. The Johnson-Cook [22] viscoplastic model will then be introduced. Finally, the chapter will conclude with a discussion of the various material failure criteria considered for this research.

2.1 Wear Mechanisms

In order to properly analyze wear, a precise definition must be established to avoid ambiguity. The simplest definition is the removal of material volume through some mechanical process between two surfaces [30]. The material is progressively lost as the wear event occurs, and the mechanical process can take many forms. Sliding motion, the most severe process due to the tangential relative motion of the surfaces, is the process being considered in this research. Wear can also result from rolling of two surfaces, impact between materials, and from abrasive materials causing cutting, plastic deformation, and fracture.

Additionally, perhaps the most important consideration to make is that wear is not a material property, but rather a system response. While the material properties of the contacting materials do influence the wear process, the geometry and topography of the materials, the relative motion and contact, the loading scenario, and any environmental conditions including lubrication have an impact on wear [3]. A

product of the systematic nature of the wear event is that the mechanisms resulting in wear can vary.

As discussed in Section 1.3.1, Lim and Ashby [26] developed a method for mapping these mechanisms for sliding wear based on the loading scenario and the material properties, as shown in Figure 2.1. The wear rates were normalized, \widetilde{W} , using Equation 2.1 and plotted against the normalized pressure, \widetilde{F} , and normalized velocity, \widetilde{v} , which are represented by Equations 2.2 and 2.3, respectively. In these equations, W represents the wear rate, A_n represents the normal contact area, H_o represents the material hardness, v represents the sliding velocity, r_o represents the radius of the pin used for experimentation, and a represents the thermal diffusivity of the material. These normalized equations are used so that experiments using the same material can be correlated even if the experimental setup varies or the material is obtained from a different source.

$$\widetilde{W} = \frac{W}{A_n} \quad (2.1)$$

$$\widetilde{F} = \frac{F}{A_n H_o} \quad (2.2)$$

$$\widetilde{v} = \frac{v r_o}{a} \quad (2.3)$$

Lim and Ashby provide detailed descriptions of the wear mechanisms. Additionally, the texts by Bayer [3; 4], Rabinowicz [30], and Stachowiak [32] thoroughly cover the topic of wear mechanisms. A summary of the material is presented here, and this research will focus on mechanical wear caused by adhesive and abrasion wear in addition to melt wear.

2.1.1 Adhesive Wear. Adhesive wear results when contact is made between materials at discrete locations, or asperities, and bonding occurs. If the bond is

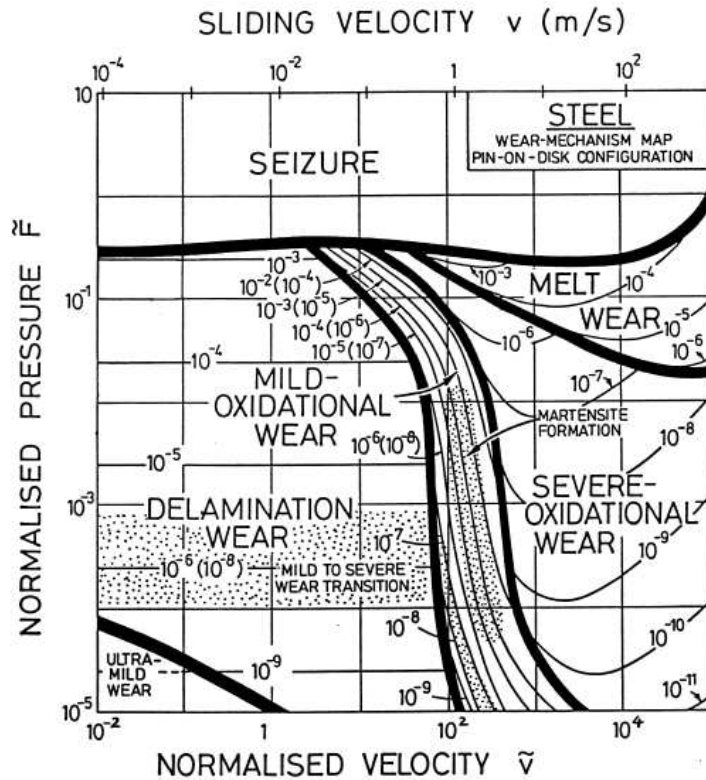


Figure 2.1: Wear Mechanism Map for Steel [26]

strong enough, as the surfaces move relative to each other, fracture will occur within the weaker asperity. The mechanism requires a large amount of plastic deformation, and the removed material is typically in the form of highly deformed fragments.

2.1.2 Abrasive Wear. Abrasive wear occurs when a hard asperity slides along a surface with sufficient tangential force to cause plastic deformation. This mechanism is analagous to a machining cutting tool, although on a micro-level scale.

2.1.3 Melt Wear. Melt wear occurs when the thermal environment at the surface of the contacting materials is severe enough to reach the melting temperature, T_{melt} , of the material. As discussed in Section 1.3.2, the melting occurs locally at points of contact where flash temperatures resulting from impact cause the material to reach the point of melting, while the bulk of the material remains relatively cool.

For metals in sliding contact, as the velocity increases a film of molten metal forms at the interface and acts as a lubricant reducing the coefficient of friction.

2.2 Coefficient of Friction

Friction is a phenomenon resulting from tangential motion between two bodies, and conventionally is thought of as the force required to initiate or sustain the tangential motion. This phenomenon is an important aspect in the context of wear because the wear process is heavily influenced by the deformation mechanisms resulting at the sliding interface. Additionally, wear is affected by the temperature increase in the material caused by frictional heating.

Three mechanisms are attributed to frictional force: adhesion, abrasion, and hysteresis [3; 4]. These mechanisms are represented graphically in Figure 2.2. Adhesion involves the shearing of the bonds formed by contact between two surfaces, and abrasion involves the deformation, which can be elastic or plastic, of the materials at the motion interface. Hysteresis is related to the time-dependent response of a material to an applied force. This component of the friction mechanisms is only significant for viscoelastic materials, such as rubbers. However, this research is concerned with wear of metals, so the only mechanisms which will be considered are adhesion and abrasion.

The simplified engineering approach to friction is to establish a coefficient of friction term, μ , which relates the frictional force to the normal force between the two sliding bodies. The coefficient is assumed to be proportional to the normal load, and is independent of the contact area as expressed in Equation 2.4, where F_f is the frictional force and F is the normal contact force.

$$\mu = \frac{F_f}{F} \tag{2.4}$$

While assuming the coefficient of friction is independent of area is generally appropriate for mild sliding; as the sliding velocity increases and the loading intensifies,

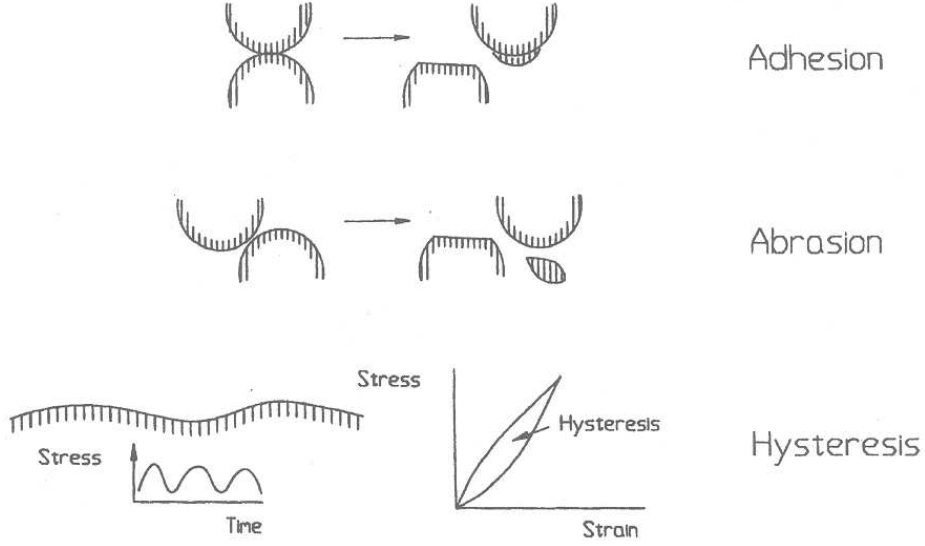


Figure 2.2: Graphical Depiction of Friction Mechanisms [4]

the contact area begins to make a significant contribution. As discussed in the literature review in Section 1.3.1, the coefficient of friction for sliding between two steels has been studied, and experimental results show that as Pv increases the coefficient of friction decays exponentially until reaching an asymptotic value. Hale [16] used the data published by Montgomery [29] for steel on steel sliding to represent the coefficient of friction for the VascoMax 300 slipper sliding against the 1080 steel rail as a function of the Pv term. Figure 2.3 shows the data and curve fit, and the exponential curve fit is given below as Equation 2.5. When the curve fit was generated, Pv was in units of $\text{MPa} \cdot \text{mm/s}$, so any subsequent use of the equation requires the same units. This is the definition for coefficient of friction that is used for this research and is a vital element for the analysis of the thermodynamics of the sliding event.

$$\mu(Pv) = \begin{cases} 0.2696e^{-3.409 \times 10^{-7} \cdot Pv} + 0.3074e^{-6.08 \times 10^{-9} \cdot Pv} & : 0 < Pv < 4.45 \times 10^8 \\ 0.02 & : Pv > 4.45 \times 10^8 \end{cases} \quad (2.5)$$

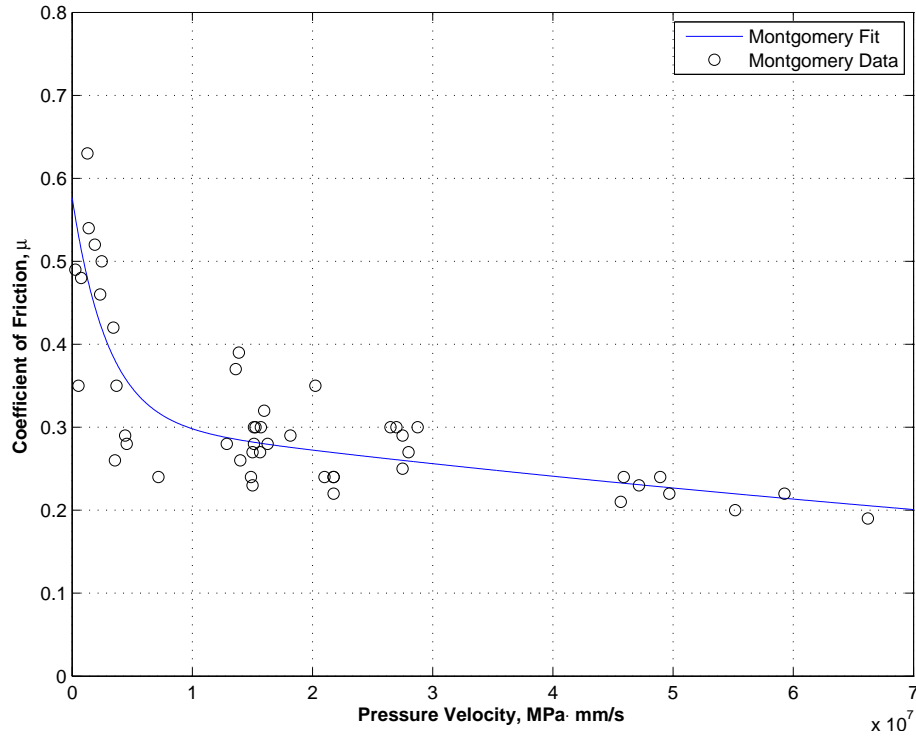


Figure 2.3: μ vs. Pv for Steel on Steel Sliding [16]

2.3 Sliding Thermodynamics

A result of the frictional energy dissipated through adhesion and abrasion is the formation of heat, and the thermal environment of the HHSTT slipper is one in which the heating may be severe enough to induce melting. As the slipper slides on the track, this frictional energy is continually fluxed into the bottom of the slipper. While the frictional energy dominates the bulk heating of the slipper, melting is a local phenomenon. As the slipper impacts asperities on the rail, the local temperature increases considerably for a brief period of time. The following two sections will discuss the frictional heating and flash heating experienced by the test track slipper.

2.3.1 Frictional Heating. Previous research has found that the rate of energy produced by friction can be expressed as the product of the frictional force and the sliding velocity. Equation 2.6 expresses the rate of frictional heat energy as a function

of time, where q_f is the rate of frictional heat energy generation, F_f is the contact force, as defined in Equation 2.4, and v is the sliding velocity.

$$q_f(t) = F_f(t)v(t) = \mu(t)F(t)v(t) \quad (2.6)$$

This is the total thermal energy generated by the friction, which is split between the rail and the slipper. This heat flux into the rail, q'' , is defined as shown in Equation 2.7, where $\lambda_{slipper}$ is the fraction of the total frictional heat energy that enters the slipper, and A_n is the slipper contact area of 20,600 mm².

$$q''(t) = \frac{\lambda_{slipper}(t)q_f(t)}{A_n} \quad (2.7)$$

Methodologies for defining the heat flux as a function of time are discussed in Section 3.2.4. The heat flux function is used as a boundary condition for solving the heat transfer equations to determine the temperature gradient of the slipper, which is governed by the heat conduction equation defined as

$$\frac{\partial T}{\partial t} = \alpha \nabla^2 T \quad (2.8)$$

where α is the thermal diffusivity. The thermal diffusivity is a function of the density, ρ , thermal conductivity, k , and the specific heat, c_p , defined as

$$\alpha = \frac{k}{\rho c_p} \quad (2.9)$$

Methods for solving these heat equations are discussed in Section 3.2 in the chapter on numerical modeling.

2.3.2 Flash Heating. In 1959, Archard [1] developed models for flash temperature increase based on the local deformation, whether elastic or plastic, of the contact point or asperity illustrated in Figure 2.4. Based on metallurgical studies

Table 2.1: VascoMax 300 and 1080 Steel Material Properties [10; 11]

Property	VascoMax 300	1080 Steel
Melt Temperature, T_{melt} (K)	1,685	1,670
Density, ρ (kg/m ³)	8,000	7,800
Poisson's Ratio, ν	0.283	0.27
Modulus of Elasticity, E (GPa)	180.7	202.8
Hardness, H (GPa)	200	—

performed by Hale [16], only the plastic deformation models are considered for the HHSTT slipper. The model also considers ranges of sliding velocity (high and low). The speed of the collision is evaluated using the dimensionless Péclet number, Pe , defined as

$$Pe = \frac{\rho c_p v L_c}{k} = \frac{v L_c}{\alpha} \quad (2.10)$$

where L_c is a characteristic length and v is the sliding velocity. The flash temperature increase, ΔT_{flash} , is defined at low speeds ($Pe < 0.2$) for plastic deformation as

$$\Delta T_{flash} = \mu \frac{\sqrt{\pi H}}{8k} W^{0.5} v \quad (2.11)$$

and at high speeds ($Pe > 200$) for plastic deformation as

$$\Delta T_{flash} = \frac{\mu(\pi H)^{0.5} W^{0.25}}{3.25} \sqrt{\frac{v}{k \rho c}} \quad (2.12)$$

where H is the material hardness, and W is the normal load. Hale evaluated the Péclet number for the 2008 HHSTT test mission. Using the 6 μm asperity radius for the characteristic length, the velocity at which $Pe = 200$ is at 307 m/s. During the 2008 mission, this velocity was achieved at a sliding distance of 230 meters, which is 4% of the total sliding distance. Since most of the sled run was at high velocity with respect to Pe , the plastic deformation model for high velocity was used by Hale. Table 2.1 provides numerical values for VascoMax 300 and 1080 steel for the constants presented in this section.

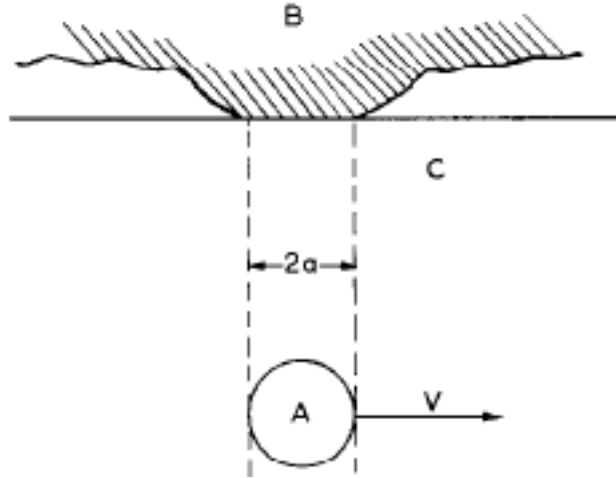


Figure 2.4: Archard Contact Area Model [1]

2.4 Hydrocodes vs. Finite Element Analysis

Previous studies at AFIT used the Lagrangian finite element analysis technique to evaluate damage to the slipper due to asperity collisions. Chmiel [8] conducted a proof of concept study to determine if the Lagrangian technique was appropriate for wear prediction in the context of the HHSTT slipper-rail interaction. Chmiel's study used a code called ABAQUS[®] to model the slipper using 4-node plane strain elements and the rail using 3-node plane strain elements, as shown in Figure 2.5. The results were promising as the simulations did show small levels of damage due to asperity collisions. However, running simulations where the slipper runs the whole length of the rail while evaluating the damage on a micro-level scale would be infeasible with the available computing capacity. Chmiel recommended simulating localized asperity collisions on the micro-level at various velocities to determine wear rates, and to then calculate the total wear using appropriate models.

Later research by Hale [16] utilized ABAQUS[®] to implement Chmiel's recommendation. While the asperity collision event is a three-dimensional phenomenon, a three-dimensional simulation presented complications so plane strain simulations were used, and the results were integrated across the width of the asperity to approximate the three-dimensional effect of a single asperity and expanded to multiple asperities

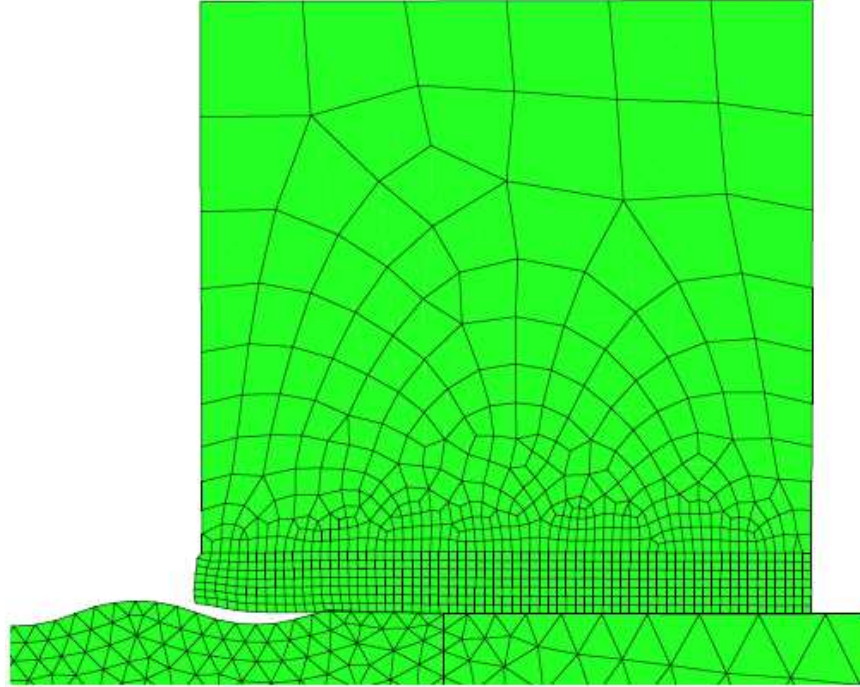


Figure 2.5: Finite Element Mesh Used by Chmiel [8]

using wear rate equations developed by Archard [2]. This process is discussed later in Section 3.6. The slipper and rail were modeled using a combination of 3-node linear plane strain triangular elements and 4-node bilinear reduced integration elements, as shown in Figure 2.6. A total simulation time was established such that the slipper would slide 110% of the asperity radius, and the simulation time was divided into 100 time steps. However, due to numerical convergence and mesh distortion issues at higher sliding velocities, the entire simulation time could not be evaluated. The total sliding distance that could be evaluated using the Lagrangian technique was approximately 55% of the asperity radius.

In order to evaluate the full asperity collision at higher velocities, an alternative to the Lagrangian technique needs to be utilized. This research evaluates the asperity collision using an Eulerian-Lagrangian hydrocode. In Lagrangian codes, the mesh is embedded within the material so the mesh grid and the material deform together. This technique can be desirable because the equations are conceptually straightforward and simple to solve. However, as previously mentioned, issues can arise if the mesh

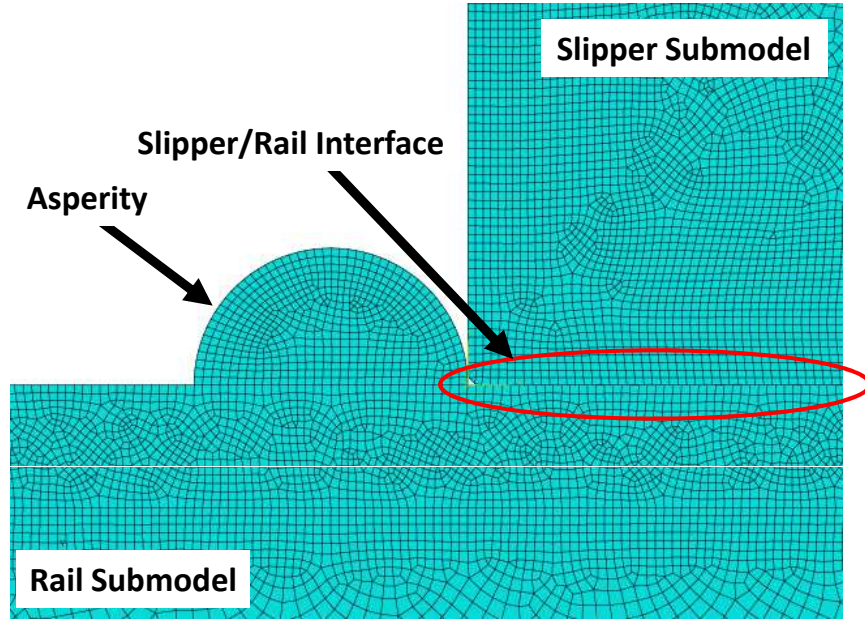


Figure 2.6: Finite Element Mesh Used by Hale [16]

becomes excessively distorted. Eulerian codes differ from Lagrangian codes in the way that the mesh is defined. While the Lagrangian mesh is attached to the material, an Eulerian mesh is fixed in space and the material flows through the mesh. The difference between the two mesh types is depicted in Figure 2.7, which shows a crudely simplified slipper-rail scenario where the red area represents the slipper and the blue area represents the rail and single asperity. The Lagrangian-Eulerian code used for this research is called CTH and is developed by Sandia National Laboratories. The following two sections will explain the key elements of the code. More thorough descriptions of hydrocodes have been published by Sandia National Laboratories [12; 27] and by researchers in archived journals [6]. Additionally, Zukas [35] published a book detailing the hydrocode simulation technique. The information presented here is taken from these sources.

2.4.1 Lagrangian Step and Eulerian Remap. CTH uses a two-step process to solve the conservation of mass, momentum, and energy equations. The first step is the Lagrangian step in which the equations are evaluated across the time step, and the mesh deforms with the material. No mass flow occurs across cell boundaries, so

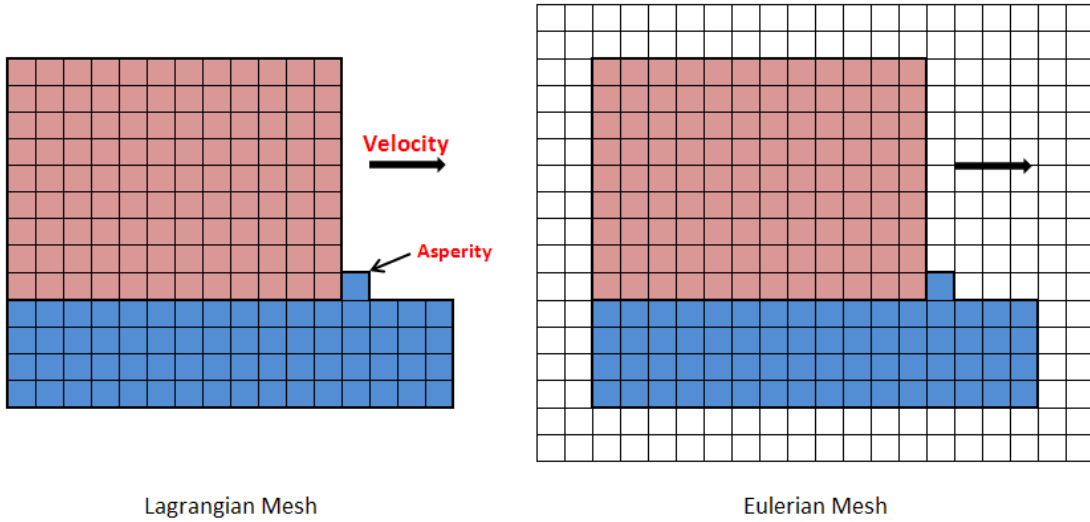


Figure 2.7: Graphical Comparison of Lagrangian and Eulerian Meshes

the conservation of mass is satisfied trivially. The momentum and energy integrals are solved using their explicit finite volume representations. The stress deviators are then updated using the cell velocities, and the internal energy equation is used to update the cell pressure, density and temperature via the equation of state. The constitutive equation is also implemented at this point, and this research utilizes the Johnson-Cook model discussed in the next section.

Following the Lagrangian step is the Eulerian remap step, which maps the distorted cells back to the fixed mesh. The volume flux between the deformed and fixed mesh is calculated from geometry of the cell face due to motion, and an interface tracking algorithm is used to track the location of material interfaces within mixed cells that contain multiple materials. The mass and internal energy of each material are then mapped to the fixed mesh. Finally, the interface tracking algorithm results are used to map the momentum and kinetic energies of the materials to the Eulerian mesh, and the equation of state is used to update the cell state variables.

2.4.2 Boundary Conditions. Finite volume approximations are used to determine the conditions of each cell based on the conditions of the surrounding cells, but cells that are at a boundary of the mesh have at least one side without an adjacent

cell. In order to solve the finite volume approximations, a boundary condition must be established to control mass, momentum, and energy fluxes across the boundary. CTH allows four possible boundary conditions: a symmetry boundary condition (type 0), a sound speed based absorbing boundary condition (type 1), an outflow boundary condition (type 2), and an extrapolation boundary condition (type 3).

The type 0 boundary condition sets the values of all cell-centered parameters to the values of the adjacent cell in the mesh interior. The velocity between the boundary cell and the mesh interior is set to zero and any kinetic energy is converted to internal energy. Additionally, no mass flux is allowed across the boundary. The type 1 boundary condition allows mass to flow in and out of the mesh, and is used to approximate semi-infinite bodies. The type 2 boundary condition places an empty cell at the boundary and the boundary pressure is set to a user-specified void pressure. Mass is allowed to leave the mesh with the type 2 boundary condition, but it cannot enter the mesh. The type 3 boundary condition linearly extrapolates the boundary pressure from the interior mesh. This type of boundary condition allows mass to flow in and out of the mesh.

2.5 Johnson-Cook Viscoplasticity Model

In 1983, Johnson and Cook [22] developed a constitutive model for metals that are subjected to large strains, high strain rates, and high temperatures. The model is intended to be used for computations, so it is defined using variables that are common to most simulation codes. Test data for the model was obtained using torsion tests, with strain rates ranging from quasi-static to 400 s^{-1} , and dynamic Hopkinson bar tensile tests over a range of temperatures. The elevated temperatures were obtained by surrounding the specimen with an oven for several minutes. The strains evaluated were limited by necking of the material which complicated the analysis. Additionally, adiabatic heating resulting from high strains complicated the results because elevated temperatures showed a softening of the material strength.

Based on the experimentation, Johnson and Cook proposed a flow stress, σ , of the form

$$\sigma = [A + B\varepsilon^n][1 + C\ln\dot{\varepsilon}^*][1 - T^{*m}] \quad (2.13)$$

where ε is the equivalent plastic strain, $\dot{\varepsilon}^* = \dot{\varepsilon}/\dot{\varepsilon}_0$ is the dimensionless plastic strain rate for $\dot{\varepsilon}_0 = 1.0 \text{ s}^{-1}$, and T^* is the homologous temperature. A , B , C , m , and n are material constants. The homologous temperature is defined by Equation 2.14, where T is the material temperature and T_0 is the ambient temperature.

$$T^* = \frac{T - T_0}{T_{melt} - T_0} \quad (2.14)$$

2.6 Defining Material Failure

In order to determine wear, criteria need to be established to determine if a material has been damaged. This is done using the Johnson-Cook constitutive equation. The first method uses Equation 2.13 to generate true stress-strain curves for discrete strain rates. Simulations are then run with strain rate for each cell as the output. An average strain rate is determined and the maximum stress for that strain rate is defined to be the failure criteria. The second method is similar to the first with one exception. Rather than averaging the strain rates, the strain rate for each sampling point at each point in time is evaluated to determine the maximum flow stress for that location at the current time step. The third method is a direct application of the Johnson-Cook viscoplastic model, and it evaluates the strain, strain rate, and temperature at each sampling point for each time step. The fourth method is similar to the second; however, rather than evaluating the maximum flow stress, the strain at the maximum flow stress is used as the failure criterion.

2.6.1 Maximum von Mises Criterion (Average Strain Rate). This method to evaluate material failure from an asperity collision uses stress-strain curves based on the Johnson-Cook constitutive equation. To generate the curves, the strain rate and homologous temperature need to be determined. Meyers [28] defined the adiabatic

temperature rise in a material under high plastic strain rate due to plastic strain energy as

$$\Delta T = \frac{\beta}{\rho c_p} \int_0^{\varepsilon_f^p} \sigma \, d\varepsilon \quad (2.15)$$

where β is the inelastic heat fraction and ε_f^p is the final plastic strain. The inelastic heat fraction is defined to be 0.9 in this analysis based on typical results for ductile metals [28]. Substituting the Johnson-Cook constitutive equation (Equation 2.13) for the stress term in Equation 2.15 and assuming the strain rate is constant yields

$$\int_{T_0^*}^{T_f^*} \frac{dT^*}{1 - T^{*m}} = \frac{\beta(1 + C \ln(\dot{\varepsilon}^{p*}))}{\rho c_p (T_{melt} - T_{ref})} \int_0^{\varepsilon_f^p} (A + B(\varepsilon^p)^n) d\varepsilon^p \quad (2.16)$$

where T_0^* is the initial homologous temperature and T_f^* is the final homologous temperature. Evaluation of the integral on the left hand side of Equation 2.16 for $m \neq 1$ requires a numerical technique. Meyers simplifies the integral by making the approximation that $m \cong 1$. In actuality, $m = 0.8$ for VascoMax 300; although, studies by Hale using the finite element technique indicate that the approximation is reasonable. Utilizing this simplification, the homologous temperature reduces to

$$T^* = 1 - \exp \left[-\frac{\beta(1 + C \ln(\dot{\varepsilon}^{p*}))}{\rho c_p (T_{melt} - T_{ref})} \left(A\varepsilon^p + \frac{B(\varepsilon^p)^{n+1}}{n+1} \right) \right] \quad (2.17)$$

which is expressed in terms of the material properties, the strain, and the strain rate. The flow stress for a constant strain rate can now be calculated by substituting Equation 2.17 for the homologous temperature in Equation 2.13. The stress-strain curves for a range of discrete strain rates are shown in Figure 2.8.

To determine the dominant strain rate for a velocity of interest, the strain rates for each cell at the final frame of a single asperity collision simulation are evaluated. A histogram of the strain rate data is generated using contour groups that cover an order of magnitude: $1 \times 10^2 - 1 \times 10^3 \text{ s}^{-1}$, $1 \times 10^3 - 1 \times 10^4 \text{ s}^{-1}$, $1 \times 10^4 - 1 \times 10^5 \text{ s}^{-1}$, etc. The histogram data is used to determine the percentage of area that

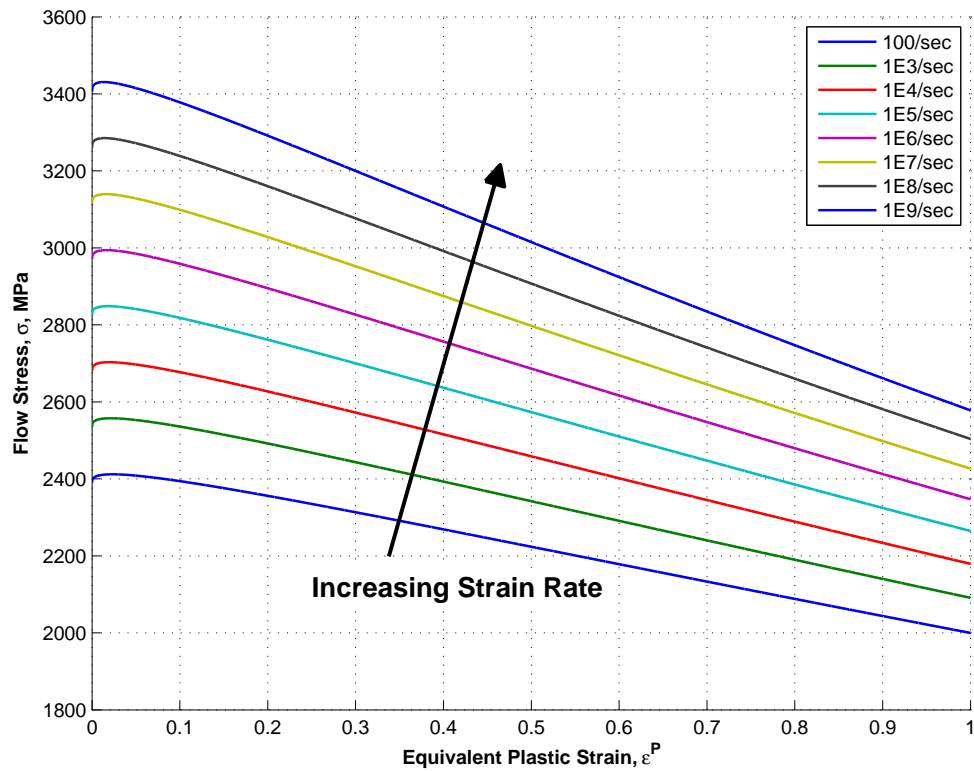


Figure 2.8: True Stress-Strain Curves for VascoMax 300 with Johnson-Cook Constitutive Equation [16]

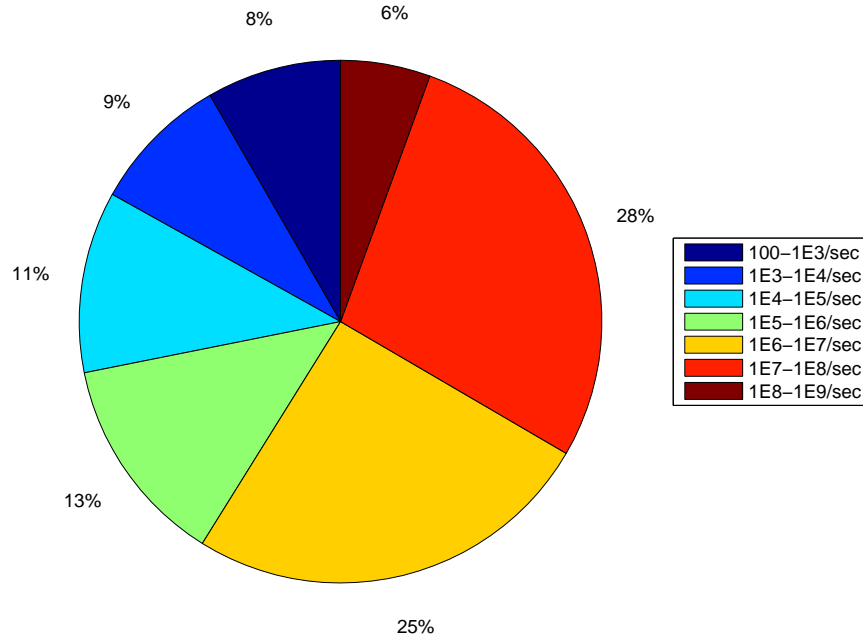


Figure 2.9: Example Strain Rate Histogram Data, $V = 1,530$ m/s [16]

each contour grouping contribute to the slipper strain rate map. An example of this histogram area percentage data is depicted in Figure 2.9.

The histogram percentages are then used as weights to compute a weighted average. The center of the contour groups ($5.5 \times 10^2 \text{ s}^{-1}$, $5.5 \times 10^3 \text{ s}^{-1}$, etc.) are used as the data points corresponding to the respective weights. For example, using the data in Figure 2.9, the average strain rate is calculated by summing $(0.06)(5.5 \times 10^8) + (0.28)(5.5 \times 10^7) + (0.25)(5.5 \times 10^6) + (0.13)(5.5 \times 10^5) + (0.11)(5.5 \times 10^4) + (0.09)(5.5 \times 10^3) + (0.08)(5.5 \times 10^2)$ to give a weighted average of $4.985 \times 10^7 \text{ s}^{-1}$. Since the weighted average strain rate is closer to the low end of the $1 \times 10^7 - 1 \times 10^8 \text{ s}^{-1}$ range, the dominate strain rate is said to be 1×10^7 .

Table 2.2 shows a tabulation of the maximum von Mises flow stress versus strain rate. Studies show that the dominant strain rate for a slipper colliding with a $6 \mu\text{m}$ plane strain asperity at velocities greater than 750 m/s is $1 \times 10^7 \text{ sec}^{-1}$, so this research will use a critical stress value of 3139.7 MPa when implementing this criterion.

Table 2.2: Maximum von Mises Stress vs. Strain Rate

Strain Rate (sec ⁻¹)	Maximum Stress (MPa)
1×10^2	2,411.9
1×10^3	2,557.5
1×10^4	2,703.1
1×10^5	2,848.6
1×10^6	2,994.2
1×10^7	3,139.7
1×10^8	3,285.2
1×10^9	3,430.7

Table 2.3: Coefficients for Pointwise Strain Rate Criterion Curve Fit

Coefficient	Value	(Units)
A_{PSR}	-1.820×10^6	(MPa)
B_{PSR}	-3.474×10^{-5}	(unitless)
C_{PSR}	1.822×10^6	(MPa)

2.6.2 Maximum von Mises Criterion (Pointwise Strain Rate). This method is very similar to the method described in the previous section, but a notable difference is the treatment of the strain rate. Rather than calculating a dominant strain rate, the strain rate is evaluated at every sampling point, (x,y) , for every time step, t , of the simulation. This is because the method of calculating the weighted average strain rate inherently favors higher strain rates due to the wide range in orders of magnitude of the strain rates seen during the simulations.

Plotting the critical stress, σ_{crit} , against the strain rate and applying a curve fit produces a closed form function for the critical stress and it takes the form shown in Equation 2.18, where the constants for VascoMax 300 are given in Table 2.3. The “PSR” in the subscripts is used to indicate that they pertain to the pointwise strain rate critical stress function. The curve fit for VascoMax 300 is shown in Figure 2.10.

$$\sigma_{crit}(x, y, t) = A_{PSR}\dot{\epsilon}(x, y, t)^{B_{PSR}} + C_{PSR} \quad (2.18)$$

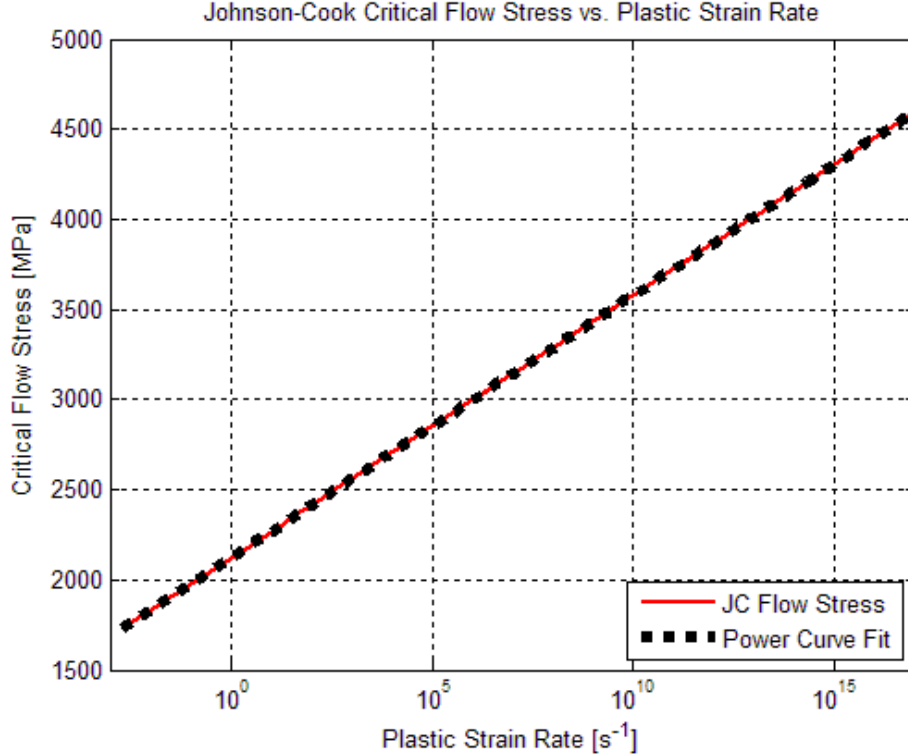


Figure 2.10: Critical Flow Stress vs. Plastic Strain Rate

2.6.3 Johnson-Cook Plasticity Criterion. The Johnson-Cook plasticity criterion is similar to the previous dynamic strain rate maximum von Mises criterion. This criteria is different in that it directly applies the Johnson-Cook flow stress equation, Equation 2.13, and calculates the critical stress as a function of the strain, strain rate, and temperature at each sampling location for each point in time as shown in Equation 2.19.

$$\sigma_{crit}(x, y, t) = [A + B\varepsilon(x, y, t)^n][1 + C \ln \dot{\varepsilon}^*(x, y, t)][1 - T^*(x, y, t)^m] \quad (2.19)$$

2.6.4 Plastic Strain Criterion. This criterion is very similar to the von Mises criterion using the pointwise strain rate. However, rather than evaluating the maximum stress as a function of strain rate, the strain at maximum stress is defined as the failure mode. Similar to the previous failure criterion, the critical strain is

Table 2.4: Coefficients for Plastic Strain Criterion Curve Fit

Coefficient	Value	(Units)
A_{PS}	2.259×10^{-2}	(MPa)
B_{PS}	-5.029×10^{-2}	(unitless)
C_{PS}	5.344×10^{-3}	(MPa)

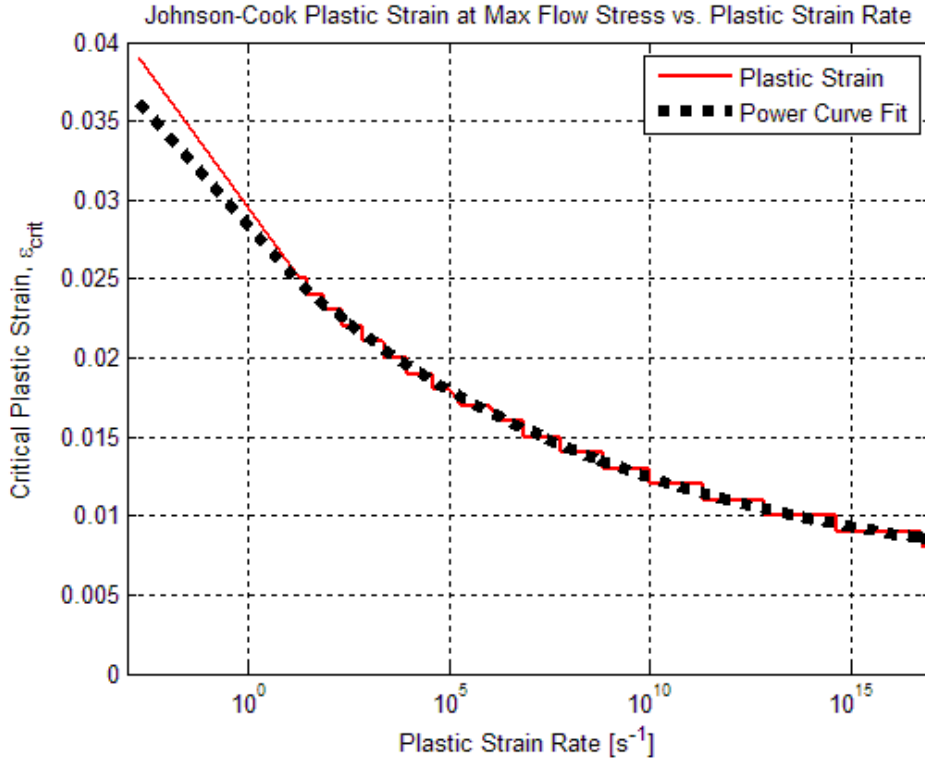


Figure 2.11: Critical Plastic Strain vs. Plastic Strain Rate

determined as a function of the strain rate, and assumes the form

$$\varepsilon_{crit}(x, y, t) = A_{PS}\dot{\varepsilon}(x, y, t)^{B_{PS}} + C_{PS} \quad (2.20)$$

where the constants for VascoMax 300 are given in Table 2.4. The “PS” subscript is used to indicate the coefficients pertain to the curve fit relating plastic strain rate to critical plastic strain. Figure 2.11 shows the curve fit for VascoMax 300.

2.7 Summary of Theoretical Background

This chapter has presented the theoretical background information that is critical to this research work, and the information will be used to develop numerical tools to evaluate the mechanical and melt wear phenomena, which are discussed in the next chapter. First, important definitions pertaining to wear and wear rates were defined, and the systematic nature of wear was discussed. Also, the various mechanisms resulting in wear were discussed from a tribological perspective. These mechanisms are also important in the discussion of the frictional force at the sliding interface of the HHSTT slipper and rail. The Pv term, introduced by Montgomery [29] and mentioned in Section 1.3.1, was discussed in greater detail. The data collected by Montgomery, which represents sliding friction at velocities as high as 550 m/s, was evaluated by Hale [16] and an exponential curve fit was applied. This curve fit is given by Equation 2.5.

Within the context of this research, the coefficient of friction plays a major role in the analysis of sliding thermodynamics. Two separate modes of heating were discussed here: a macro-level heating and a micro-level heating. The macro-level heating, which is defined as either the frictional heating or the bulk heating, evaluates the frictional energy at the slipper-rail interface. The micro-level heating, or “flash” heating, is the result of plasticity due to a single asperity collision. Archard [1] developed analytical models to define the flash heating, and those models have been presented here.

This research will also utilize the micro-level material property method developed by Chmiel [8], and utilized by Hale [16; 18], to evaluate mechanical wear rates. However, the sliding velocities being considered are too high for the Lagrangian finite element technique to evaluate because numerical issues arise as a result of mesh distortion. The Eulerian-Lagrangian hydrocode technique is introduced as an alternative to the finite element technique. This solution utilizes a fixed mesh that the slipper and rail materials flow through, rather than attaching a mesh to the slipper and rail

materials. The use of a fixed mesh means that element distortion does not result, so any sliding velocity can be evaluated. A discussion of the hydrocode solution process and the applicable boundary conditions has been provided here.

Since metallurgical studies by Hale [16] show that mechanical wear results from plastic deformation and the micro-level simulation is a time-dependent process, a viscoplastic constitutive model needed to be chosen. The Johnson-Cook [22] model was chosen because it is tailored for metals subjected to large strains, high strain rates, and high temperatures. This constitutive equation was used to develop criteria for evaluating mechanical wear. While wear, in actuality, involves the removal of material, simulating the material removal would be very complicated. Instead, criteria have been developed to estimate material removal from a “damage” perspective. This means that the criteria will evaluate the stress and strain in the material and determine if the material has “worn” based on the failure criteria. While this does not completely represent the physics of the micro-level asperity collisions, models developed by Archard [2] will be used to relate the damage criteria to experimental data that does account for the three-dimensional wear effect. This is discussed in detail in Chapter III.

III. Numerical Modeling

To conduct an experimental wear study replicating the conditions seen by the slipper at the HHSTT would be economically infeasible from the perspective of both monetary cost and time spent. However, the wear phenomena can still be evaluated by carefully implementing models verified for slower sliding velocities. This chapter will first discuss the generation of slipper dynamics data, which is the foundation for much of the numerical modeling techniques used. The plane strain simulation method is then described, and the choices for initial velocity, initial temperature, the viscoplasticity model, and equation of state are justified. Included is a discussion of the post-processing methods used to evaluate the data from the plane strain simulation. These plane strain simulations will be used to calculate plane strain mechanical wear rates, which are geometrically expanded to three-dimensional, single asperity mechanical wear rates. The single asperity wear rates are integrated with respect to sliding distance, and scaling factors accounting for percentage of rail contact and multiple asperities are applied, to calculate a total mechanical wear volume. Additionally, methods for evaluating melt wear are introduced.

3.1 Dynamics of the Sled and Slipper

The dynamics of the slipper is integral to the numerical analysis of the slipper wear event. Dynamics data is supplied by the HHSTT and is generated using a program called Dynamic Analysis of Design System (DADS). The DADS data is a tabulation of the sled position and velocity with respect to time for all three orientation axes. Additionally, the vertical velocity of the slipper and contact forces on every face of the slipper are provided. The mathematical model is developed as a complicated system of masses, springs, and dampers, while the sled forward velocity and rail undulations are supplied as inputs to the system [19]. The HHSTT engineers have validated the dynamics data using test sleds instrumented with accelerometers [20], and due to its complexity, the data extracted from the model is assumed to be valid for the requirements of this research.

While the goal of this research is to make wear predictions for the slippers attached to the forebody sled of the January 2008 HHSTT test mission, complete dynamics data is currently not available that exhibits the behavior of the forebody sled for that particular mission. Dynamics data is available for a simulation of a forebody sled starting from rest and accelerating at a constant rate to 3,030 m/s over a 2.5 second time span; however, this data is inadequate for assessing history-dependent behavior, such as the thermal analysis presented in Section 3.2, due to the short simulation time. Data for the third stage pusher sled used for the 2008 test mission is available, but the sliding velocity of that sled peaks at 1,530 m/s, which is significantly lower than the 3,000 m/s that needs to be analyzed. However, the data does offer the capability to represent a more realistic time history of the event.

For the purpose of this research a compromise must be made between accuracy of slipper dynamics and the ability to effectively represent the time history. As will be discussed later, the thermal history plays an important role in the calculation of both mechanical and melt wear rates. For this reason, the 2008 third stage pusher sled data is used until the sled reaches a velocity of 1,530 m/s. After that point, the data representing the forebody sled at constant acceleration is used beginning at 1,530 m/s and ending at 3,030 m/s. It is recognized that the dynamics of the third stage pusher sled and the forebody sled may differ due to mass changes from expended propellant, aerodynamics, etc. However, the dynamics are characteristically similar, so it is assumed that the approximation is adequate to be used as a proof of concept. Additionally, using this combined data set provides the time history representative of an actual test track mission. Figure 3.1 shows the velocity profile and contact force as a function of time for this combined data set, and any subsequent references to “combined dynamics data” are referring to this data set.

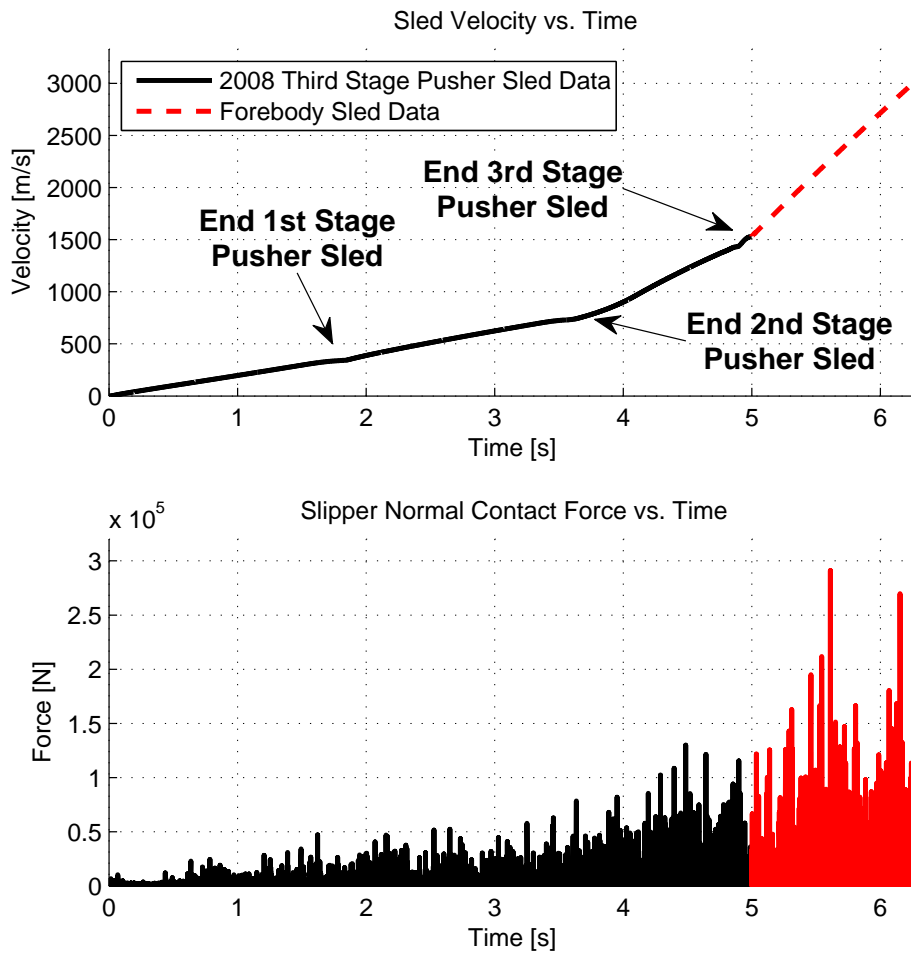


Figure 3.1: DADS Sled Velocity and Slipper Contact Force Profile

3.2 Thermodynamic Analysis

As mentioned previously in Section 2.3.1, the thermal gradient of the slipper is defined by the heat conduction equation given as

$$\frac{\partial T}{\partial t} = \alpha \nabla^2 T \quad (3.1)$$

which can be expanded and simplified to one dimension by assuming that the temperature gradient is constant in one direction, giving Equation 3.2.

$$\frac{\partial T}{\partial t} = \alpha \left(\frac{\partial^2 T}{\partial y^2} \right) \quad (3.2)$$

This equation can be solved numerically, using either an explicit or implicit solution scheme.

3.2.1 Explicit Solution Scheme. The advantage of the explicit scheme, which utilizes a forward difference on time and a central difference in space, is that the implementation is straightforward as the temperature for each node at a given time step is a function of the surrounding nodes at the previous time step as shown in Equation 3.3, where the n superscript refers to the previous time step and $n + 1$ refers to the current time step, and the i subscript refers to the node location.

$$T_i^{n+1} = T_i^n + \alpha \frac{\Delta t}{\Delta y^2} (T_{i+1}^n - 2T_i^n + T_{i-1}^n) \quad (3.3)$$

By definition, the temperature at a node for the current time step is denoted as T_i^{n+1} , and Figure 3.2 shows a schematic of the one-dimensional layout. The drawback to the explicit scheme is that it is *conditionally stable*. The coefficient attached to the second term in the right hand side of Equation 3.3 is known as the Fourier number, Fo , and defined as

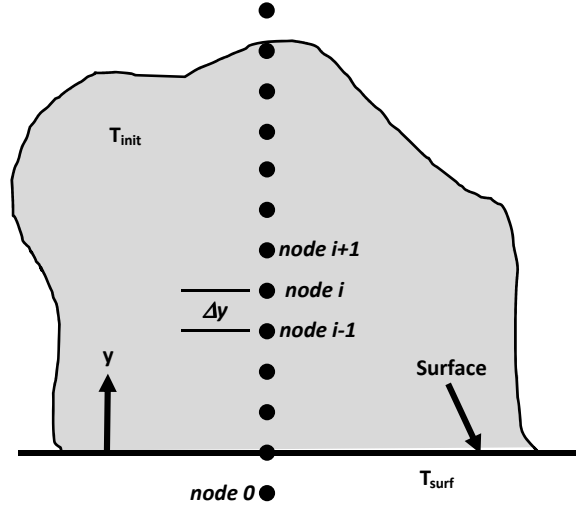


Figure 3.2: One-Dimensional Heat Transfer Schematic

$$Fo = \alpha \frac{\Delta t}{\Delta y^2} \quad (3.4)$$

The stability criterion for the explicit scheme requires that the coefficient associated with the temperature at the node of interest at the previous time step, T_i^n , be greater than or equal to zero, or $(1 - 2Fo) \geq 0$. This requires a Fourier number such that $Fo \leq 0.5$ [21]. This limits the range of available time and space intervals, Δt and Δy , respectively. If a fine resolution of the temperature gradient is desired near the surface of the slipper, the node spacing needs to be small, but to maintain stability the time step must be small as well. This presents potential issues with computer memory allocation on machines available for this research work if the resolution requirements are too fine. This drawback can be circumvented by using an implicit scheme to solve the heat conduction equation.

3.2.2 Implicit Solution Scheme. The implicit scheme differs from the explicit scheme in that it uses a backward difference on time and a central difference in space, and most importantly is *unconditionally stable* because it requires the temperatures be solved simultaneously, as discussed below. This means that no restrictions are

placed on Δt and Δy . The heat conduction equation using implicit method is defined as follows

$$\frac{T_i^{n+1} - T_i^n}{\Delta t} = \alpha \left[\frac{T_{i+1}^{n+1} - 2T_i^{n+1} + T_{i-1}^{n+1}}{(\Delta y)^2} \right] \quad (3.5)$$

The most notable difference is that the “new” temperature for any node at time $n + 1$ is a function of the “new” temperatures at the surrounding nodes. Thus, to solve the equations, the temperatures must be determined simultaneously. This complicates the programming slightly, but the relaxation of the time and space intervals allows for a fine resolution of the temperature gradient without encountering memory allocation errors due to an equally fine time step interval. For this reason, this research will utilize the implicit scheme. The Matlab[®] code used is provided as Appendix A.

3.2.3 Boundary Conditions and Initial Condition. Solving the one-dimensional finite difference heat equation approximations requires the implementation of two boundary conditions and an initial condition, which are depicted in Figure 3.3. The initial condition used for this analysis is that the slipper is at the ambient temperature of 293 K through the entire thickness. The boundary condition at the top of the slipper holds the temperature at the ambient condition of 293 K for the entirety of the simulation. A convective flux boundary condition would more closely approximate the true physics of the problem; however, this adds unnecessary complexity to the solution. The region where high resolution of the temperature gradient is desired is at the slipper-rail interface, so setting the top node to ambient temperature is a reasonable approximation.

The second boundary condition is the frictional heat flux condition applied at the bottom edge of the slipper defined as

$$q''(t) = -k \frac{\partial T}{\partial y} \Big|_{y=0} \quad (3.6)$$

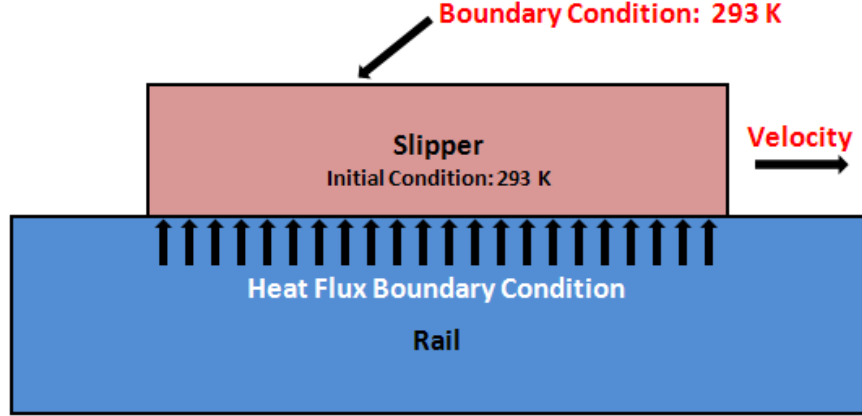


Figure 3.3: Heat Transfer Boundary Conditions and Initial Condition

which can be represented for each time increment using a second-order approximation as

$$T_0 = T_2 + \frac{2\Delta y q''(t)}{k} \quad (3.7)$$

where T_0 is the temperature at an imaginary node outside the slipper boundary, as indicated in Figure 3.2, which is used to represent the T_{i-1}^{n+1} variable when calculating the surface boundary temperature.

3.2.4 Defining Frictional Heat Flux. The most important boundary condition for this heat conduction analysis is the heat flux due to friction. As discussed in Section 2.3.1, the frictional heat flux is defined as a function of the coefficient of friction, the normal load, the sliding velocity, the normal contact area, and the thermal properties of the contacting materials as defined in Equation 3.8.

$$q''(t) = \frac{\lambda_{slipper}(t)\mu(t)F(t)v(t)}{A_n} = \frac{\lambda_{slipper}(t)q_f(t)}{A_n} \quad (3.8)$$

If full contact of the slipper is assumed, the slipper contact area and the velocity profile are known entities. Conversely, the normal forces needs to be defined, so that subsequently the coefficient of friction can be evaluated using Equation 2.5. Hale [16] performed a statistical analysis of the sled and slipper dynamics to determine a pres-

sure function that assumed the normal load was distributed evenly across the entire slipper area. A moving window technique was used for this analysis. A histogram of the contact force data within each window was generated, and a gamma distribution was fit to the histogram. By definition, the gamma distribution has an area of one underneath its curve, so an upper limit force for each window was determined by integrating the gamma distribution against force intensity until the integral reached a critical value of 0.95. The force at which this occurs is greater than or equal to 95% of all the forces occurring during the given window and is defined as the upper limit force for that window. A closed form curve fit of the upper limit forces for each window was created using a Fourier curve fit. Since full slipper contact is assumed, the upper limit force function is converted to an upper limit pressure function.

Hale used this upper limit pressure function as a boundary condition for FEA simulations in addition to heat transfer analysis. While the upper limit pressure may be effective for mechanical simulations, it produces a frictional heat accumulation, Q_f , with respect to time, as defined in Equation 3.9, that is higher than what is seen using the dynamics data, as shown in Figure 3.4. The upper plot in this figure shows the instantaneous frictional heating rate. The dashed black line indicates the heating rate if Hale’s upper limit pressure function is used in Equation 2.6. The solid red line indicates the heating rate obtained using the DADS data. The lower plot shows the accumulated frictional heat energy, calculated using a trapezoidal rule numerical integration technique. Based on the upper plot, it would appear that the statistical analysis should produce an accumulated frictional heat lower than that produced by the dynamics data. However, as shown in Figure 3.5, the frictional heating has time gaps between the peaks where heat is not accumulated.

$$Q_f = \int_0^t q_f(t)dt \quad (3.9)$$

In order to better represent the heat flux input to the slipper for this research, a curve fit was applied to the frictional heat energy accumulation, Q_f , that was

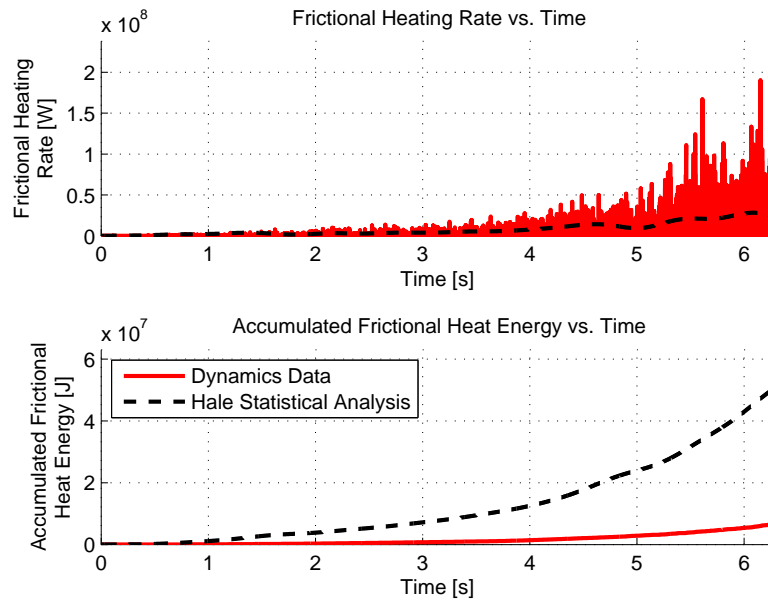


Figure 3.4: Frictional Heat using Hale's Statistical DADS Force [16]

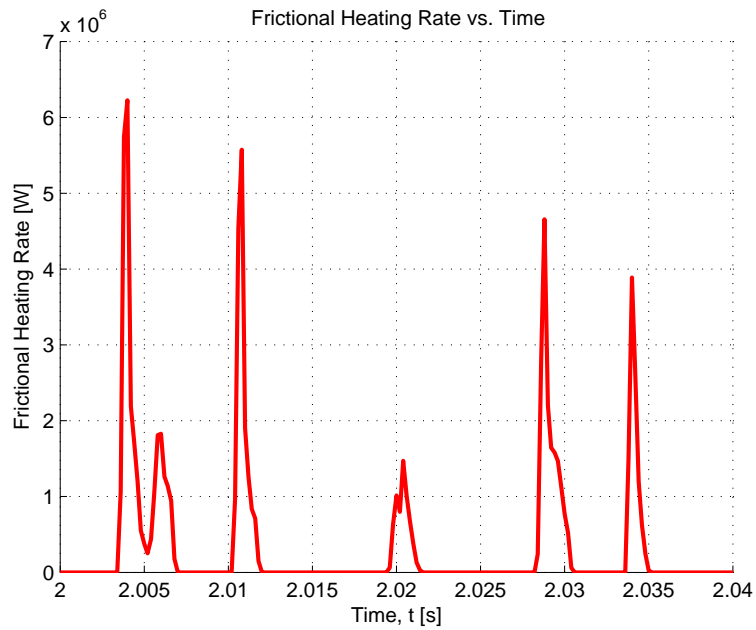


Figure 3.5: Zoomed-in View of Instantaneous Frictional Heating

Table 3.1: Coefficients for Frictional Heating Curve Fit

Coefficient	Value	(Units)
A_f	6.4969×10^4	(W)
B_f	0.6720	(unitless)

calculated using the combined dynamics data set, and the derivative was taken to provide the frictional heat generation as a function of time as shown in Figure 3.6. The curve fit is an exponential function, such that

$$q_f(t) = A_f e^{B_f t} \quad (3.10)$$

where A_f and B_f are curve fitting coefficients, and are defined in Table 3.1. Substituting Equation 3.10 into Equation 3.8 provides a frictional heat flux as a function of time, normal contact area, and the fraction of heat frictional energy entering the slipper as shown in Equation 3.11. The only unknown in this equation is the fraction of frictional energy imparted on the slipper. This will be discussed later in Section 3.5.

$$\dot{q}''(t) = \frac{\lambda_{slipper}(t) A_f e^{B_f t}}{A_n} \quad (3.11)$$

This heat flux function will be used to define the bulk temperature of the slipper, which is used as an initial condition for hydrocode simulations and is also an important component of the melt wear model. Both of these aspects will be discussed in subsequent sections.

3.3 Plane Strain Hydrocode Simulation

Running a two-dimensional plane strain CTH simulation requires several user inputs including mesh and window size, material characteristics and geometries, initial conditions, and boundary conditions. A rectilinear mesh was used to simulate the asperity collision, and the window containing the slipper and rail materials were

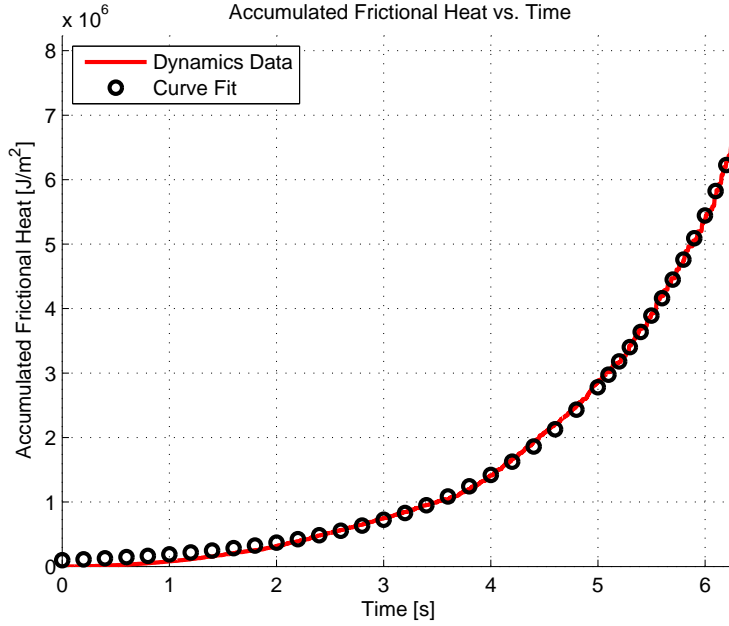


Figure 3.6: Frictional Heat Accumulation Curve Fit

sized appropriately so that wave interactions did not occur at the boundaries of the mesh. The slipper used for this analysis is $125 \mu\text{m}$ by $125 \mu\text{m}$, which is large enough that the waves cannot propagate to the edges during the duration of a simulation. A $2 \mu\text{m}$ radius fillet is included at the leading edge of the slipper. The fillet was added by Hale to his finite element models to reduce numerical errors during finite element simulations. Additionally, Cameron [7] and Cinnamon [9] used a filleted leading edge for CTH simulations. A fillet is included here to maintain some level of consistency with previous research. The type 1, or sound speed-based absorbing boundary condition is used on all boundaries of the mesh because it is appropriate for approximating semi-infinite bodies. However, the choice of boundary condition was not critical due to the selection of window size. The mesh size used is $1 \mu\text{m} \times 1 \mu\text{m}$ throughout. In addition to window and mesh sizing, the initial velocity and temperature of the materials, the equations of state, and the viscoplastic model of the materials must be specified. These components of the simulation are discussed in subsequent sections.

The simulations consist of a VascoMax 300 slipper colliding with a semi-circular asperity on a 1080 steel rail, as shown in Figure 3.7. Asperity sizes of $2 \mu\text{m}$, $4 \mu\text{m}$, and $6 \mu\text{m}$ are simulated and used to approximate the three-dimensional effects of wear for a single asperity which is discussed in Section 3.4. Stress, strain, and strain rate data of the materials need to be exported for post-processing, and the data can be exported from CTH using either the mesh locations or tracer points for sampling. This research opts to use tracer points because they travel with the material rather than remaining attached to the fixed mesh. This is important because as the stress wave propagates through the material, points of the material are tagged as damaged. If the fixed mesh points are used for sampling, a particular cell may be tagged as damaged during a previous time step while, in fact, new material has entered the cell. Consequentially, this new material will not be tagged as damaged because the associated cell at that point in time is already tagged as damaged. This results in wear predictions that are too low.

The data extracted from the tracer points is post-processed to determine total damage area accrued during a simulation, and the post-processing methodology along with the code used is provided in Appendix C for reference. The tracers are initially placed at the center of the mesh cells, so the area associated with a tracer is the same as the cell area. The damage area, A_d , divided by the sliding distance is defined as the wear rate per unit width, W_{uw} . This is expressed as Equation 3.12 where the distance slid is a function of the velocity, v , and the simulation time, t_{sim} .

$$W_{uw} = \frac{A_d}{vt_{sim}} \quad (3.12)$$

Evaluating this equation results in units of L^2/L , which could be reduced to L , where L is some unit of length. However, they are left as L^2/L here to denote that they represent a damaged area per distance slid, and units of mm^2/mm will be used. The simulation times used are a function of the horizontal sliding velocity and the hemispherical asperity radius. The sliding distance was chosen to be 110% of the 6

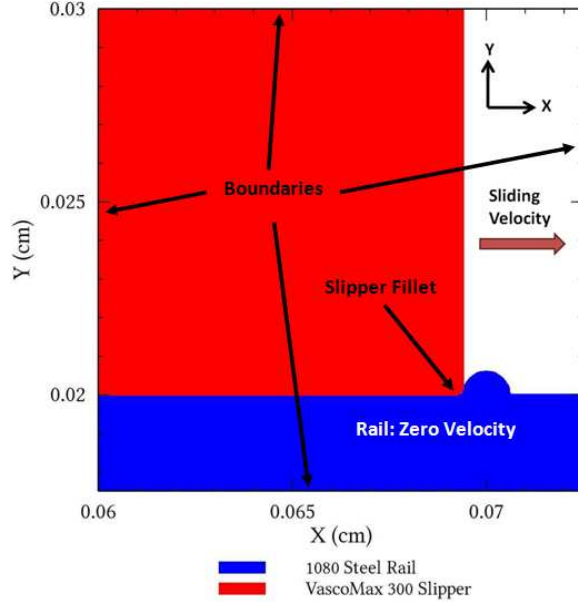


Figure 3.7: CTH Materials Illustration

μm asperity radius, so the simulation time for a given velocity defined by Equation 3.13. Based on this, the simulation times used are shown in Table 3.2. The unit width wear rates are integrated across the width of the asperity using the method which will be described in Section 3.4 to calculate a wear rate resulting from a collision with a single hemispherical asperity. The actual wear event is the result of several asperity collisions, and the single asperity wear rates will be scaled to account for this phenomenon using the method provided in Section 3.6

$$t_{sim} = \frac{(1.1)(6\mu\text{m})}{v} \quad (3.13)$$

3.3.1 Initial Velocity Vector. The CTH plane strain simulations are evaluated in two dimensions, so a two-dimensional initial velocity vector must be defined. The vector is broken into two components: horizontal and vertical. The horizontal component is straightforward to define because arbitrary sliding velocities are chosen to reasonably represent the range of velocities achieved by the slipper during a test run. The vertical velocity needs to be determined using the DADS data. DADS and

Table 3.2: CTH Simulation Times

Horizontal Velocity (m/s)	Simulation Time (s)
750	8.80×10^{-9}
1,000	6.60×10^{-9}
1,250	5.28×10^{-9}
1,500	4.40×10^{-9}
2,000	3.30×10^{-9}
2,500	2.64×10^{-9}
3,000	2.20×10^{-9}

CTH define a positive vertical velocity as being in the upward direction, as shown by the axes in Figure 3.7, so the negative vertical velocities shown here indicate the slipper is traveling towards the rail. While previous rail gouging analysis at AFIT was dependent on vertical velocity, the vertical velocity component is not critical to the study of the mechanical wear phenomenon.

The insensitivity to the vertical velocity component is due to the relatively small contribution of the vertical velocity to the total velocity vector. The peak vertical velocity extracted from the DADS data is on the order of 7 m/s into the rail, as shown in Figure 3.8, which shows the vertical velocity for each slipper from the forebody sled data, while the slowest horizontal velocity considered for this research is 750 m/s. The initial vertical velocity used for CTH simulations was determined by averaging the slipper vertical velocities in a window centered on the horizontal velocity of interest. The lower limit window was defined as 25 m/s slower than the horizontal velocity of interest, and the upper limit was defined as being 25 m/s faster than the horizontal velocity of interest. Figure 3.9 shows the vertical velocity data for each slipper within the window for a horizontal velocity of 3,000 m/s, and the x-axis ranges from 2,075 to 3,025 m/s. The red curves indicate velocities in to the rail, and conversely, the black curves indicate velocities away from the rail.

The velocities into the rail are of interest for this research, and an average of the data is taken for each slipper to determine the average vertical velocities of the slippers. The average velocities are indicated by the dashed lines in Figure 3.9. The

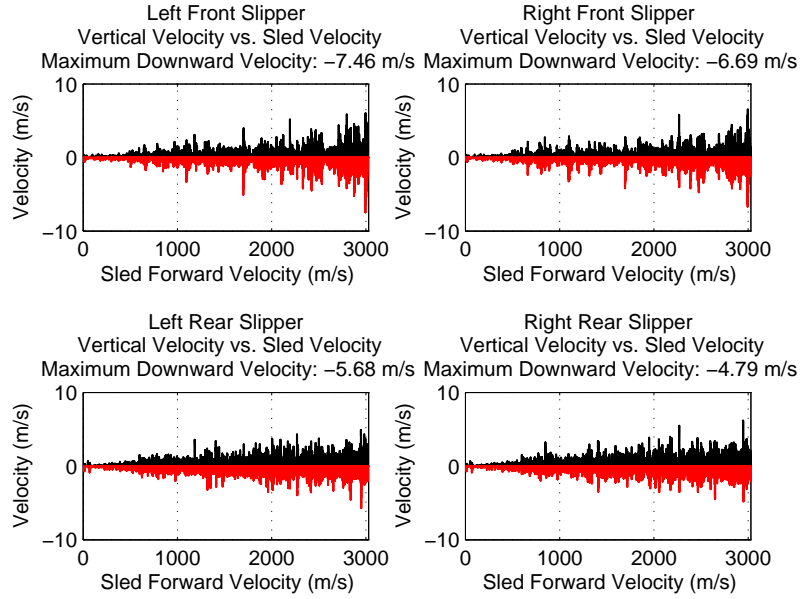


Figure 3.8: Slipper Vertical Velocity from 2003 Forebody Sled DADS Data

largest average vertical velocity is used as the initial condition for the CTH simulation, and for simplicity, the vertical velocity is rounded to the nearest 0.25 m/s. In the case presented in Figure 3.9, the maximum average vertical velocity is 1.78 m/s, which is rounded to 1.75 m/s. Table 3.3 shows the velocity vectors considered for the CTH simulations. The initial velocity of the rail is a zero vector since the rail is stationary for this analysis.

3.3.2 Initial Temperature. The possibility of defining a one-dimensional initial temperature gradient was considered, and the temperature profile for the combined velocity profile, generated using the implicit solution scheme discussed previously, is shown in Figure 4.6. This temperature profile assumed a λ_{ave} value of 0.1265 for reasons discussed in Section 4.2. Temperature gradients for target velocities were generated and an example gradient is shown in Figure 4.7, which shows the temperature profile from the lower surface of the slipper through 400 μm of the thickness when the sled has reached a velocity of $1,500$ m/s.

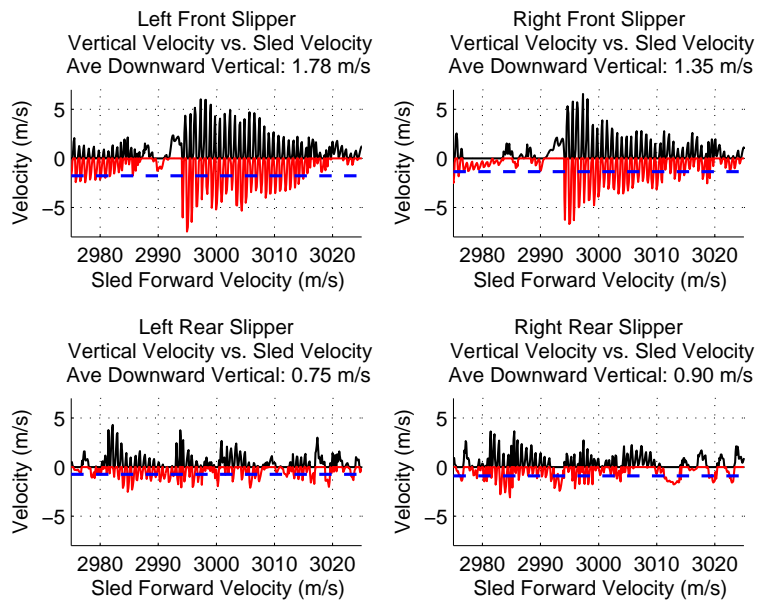


Figure 3.9: Evaluation of Vertical Velocity Component

Table 3.3: Plane Strain Simulation Initial Velocity Vectors

Horizontal Velocity (m/s)	Vertical Velocity (m/s)
200	-0.50
300	-0.50
500	-0.50
750	-0.50
1,000	-0.50
1,250	-0.50
1,500	-0.50
2,000	-1.00
2,500	-1.25
3,000	-1.75

Table 3.4: Plane Strain Simulation Initial Temperatures

Slipper Velocity (m/s)	400 μm Depth Temperature (K)
200	356
300	393
500	500
750	784
1,000	981
1,250	1,194
1,500	1,479
2,000	1,541
2,500	1,541
3,000	1,541

Since the temperature profile is nearly constant in proximity to the surface, a bulk temperature is defined as the initial temperature of the slipper for the CTH simulations. This eliminates unnecessary complexity from the model. The temperature at a depth of 400 μm into the slipper is chosen to be the initial temperature. This depth is based on metallurgical studies that show the heat affected zone of the slipper to be approximately 400 μm deep [16]. The temperatures at the velocities considered are provided in Table 3.4.

3.3.3 Viscoplasticity Model. The Johnson-Cook viscoplasticity model is utilized because of its ability to handle materials at elevated temperatures and strain rates. To implement the Johnson-Cook constitutive model in CTH, material constants needed to be obtained for the slipper and rail materials, VascoMax 300 and 1080 steel, respectively. Cinnamon et al. [9; 10; 11] performed flyer plate experiments to determine these constants, which are shown in Table 3.5.

3.3.4 Equation of State. An equation of state is necessary for hydrocode simulations because an additional equation is required to solve for all of the cell parameters. A tabular equation of state is used for CTH simulations, and this particular equation of state is used because it

Table 3.5: VascoMax 300 and 1080 Steel Johnson-Cook Coefficients [9; 10; 11]

Coefficient	VascoMax 300	1080 Steel
A (GPa)	2.1	0.7
B (GPa)	0.124	3.6
C	0.03	0.17
m	0.8	0.25
n	0.3737	0.6

Table 3.6: Iron and 1080 Steel Material Properties

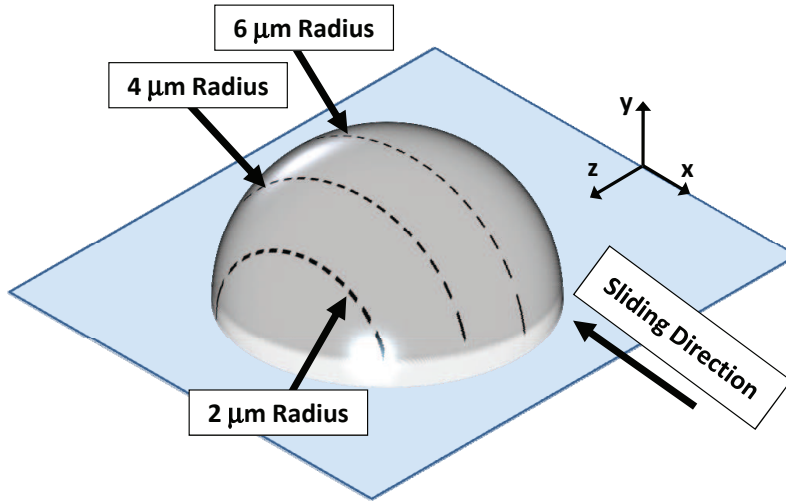
Property	Iron	1080 Steel
Density (g/cm ³)	7.28	7.85
Yield Stress (MPa)	50	585
Modulus of Elasticity (GPa)	200	205
Melt Temperature (K)	1,811	1,836
Poisson's Ratio	0.28	0.25

is the most general way to represent an equation of state. It allows for the use of sophisticated models that are too complicated to be incorporated into analytic formulas. A good tabular equation of state gives valid results over a much wider density-temperature-pressure range than analytic models. [14]

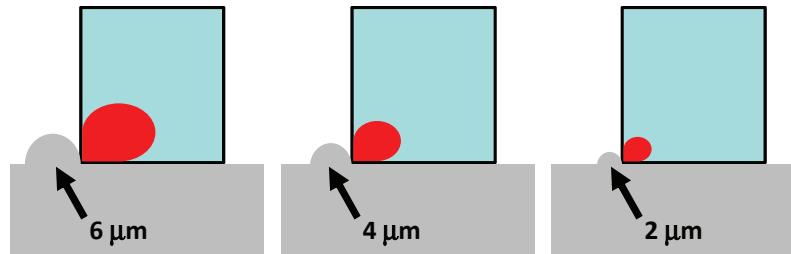
A tabular equation of state for VascoMax 300 is used to represent the slipper, while tables for iron are used to represent the rail. Iron is used because equation of state tables are not available for 1080 steel in CTH, but iron and 1080 steel exhibit similar material properties, as shown in Table 3.6.

3.4 *Single Asperity Mechanical Wear Rates*

Wear is a three-dimensional phenomenon, and it should be evaluated as such. The wear rates per unit width, as defined by Equation 3.12, that are determined from the CTH plane strain simulations of 2 μm , 4 μm , and 6 μm semi-circular asperities are integrated across the width of the asperity to determine a volume of damaged material per distance slid. Figure 3.10 illustrates how the plane strain models are related to the 3-dimensional analysis. The red areas in Figure 3.10(b) illustrate the



(a) Hemispherical Asperity



(b) Plane Strain Analyses Illustration

Figure 3.10: Plane Strain vs. Three-dimensional Model

damage area resulting from a collision with the various semi-circular asperities. For a given velocity, the damage area will decrease as the asperity size decreases.

To determine the location of the 2 μm and 4 μm asperities along the z-axis, as indicated in Figure 3.10(a), the circular geometry in the YZ-plane is evaluated as

$$z = \sqrt{r^2 - y^2} \quad (3.14)$$

where r is the asperity radius of 6 μm . This places the 2 μm and 4 μm asperities at z-locations of 4.47 μm and 5.66 μm , respectively. The points are indicated by the dashed lines in Figure 3.11, which represents the integral in Equation 3.15. The wear rate per unit width values are integrated with respect to z to obtain the single

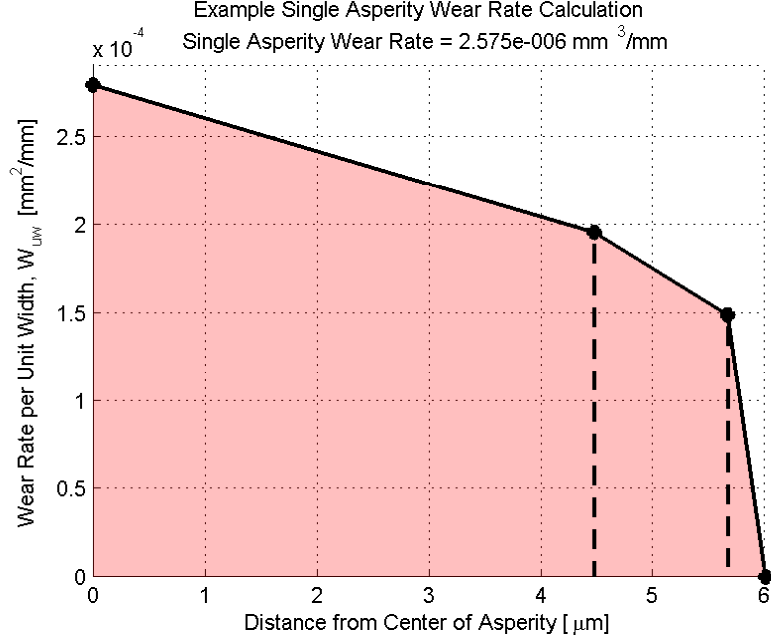


Figure 3.11: Example Single Asperity Wear Rate Integral

asperity wear rate, W_{sa} , for that velocity. The integral is multiplied by two to account for symmetry of the asperity.

$$W_{sa} = 2 \int_0^r W_{ww}(z) dz \quad (3.15)$$

3.5 Melt Wear

It has already been discussed that the heating of the slipper is evaluated in to two parts: frictional bulk heating and flash localized heating. Hale [16] developed a method for evaluating the melt wear rates using these two components. The frictional heating was evaluated using the explicit finite difference numerical scheme discussed previously. The flash temperature was evaluated at various target velocities using Equation 3.16 below.

$$\Delta T_{flash} = \frac{\mu(\pi H)^{0.5} W^{0.25}}{3.25} \sqrt{\frac{V}{k\rho c}} \quad (3.16)$$

Hale defined the load, W , in Equation 3.16 using a global finite element model to simulate the bounce effect of the slipper traveling down the rail. A downward velocity was imparted on the slipper and allowed to collide with the rail. The pressure along the surface of the slipper was measured during the collision. The load was defined as the maximum pressure on the slipper surface multiplied by the contact area of the asperity. The surface temperature, T_{surf} , is then defined as

$$T_{\text{surf}} = T_{\text{friction}} + \Delta T_{\text{flash}} \quad (3.17)$$

where T_{friction} is the surface temperature due to the bulk frictional heating, and ΔT_{flash} is the flash temperature increase. By definition, the wear rate per unit width has units of area per distance, and the wear rate per unit width for melt, $W_{\text{uw,melt}}$, is the same. However, the thermal analysis is one-dimensional so the melt area, A_{melt} , cannot be explicitly calculated. A simplifying assumption can be made that the melt area is equal to the product of the melt depth, h_{melt} , multiplied by the sliding distance. This reduces the unit width wear rate to the melt depth, as shown in Equation 3.18.

$$W_{\text{uw,melt}} = \frac{A_{\text{melt}}}{d} = \frac{h_{\text{melt}}d}{d} = h_{\text{melt}} \quad (3.18)$$

If the slipper is approximated as a semi-infinite body near an asperity impact, then analytic solutions are available to approximate the transfer of heat energy during the short duration of a transient when the interior temperature has not yet been affected by a change in the surface temperature [25]. If a sudden thermal change is imposed at the surface of the slipper, then a one-dimensional temperature wave will propagate by conduction in the solid. If a constant surface temperature is assumed based on the short asperity impact duration, a semi-infinite transient conduction analysis can be used to evaluate the melt depth. For any time, $t > 0$, the temperature at a depth from the lower boundary surface, y , in the semi-infinite slipper is given as

$$T(y, t) = T_{\text{surf}} + (T_{\text{init}} - T_{\text{surf}})\text{erf}\left(\frac{y}{2\sqrt{\alpha t}}\right) \quad (3.19)$$

where the Gaussian error function is defined as

$$\operatorname{erf}(w) = \frac{2}{\sqrt{\pi}} \int_0^w e^{-v^2} dv \quad (3.20)$$

Hale defined the initial temperature, T_{init} , as the temperature at the 400 μm depth, $T_{400\mu\text{m}}$, based on the metallurgical studies mentioned previously. The melt depth is defined as the depth, y , that is equal to the melt temperature of the material at the end of the collision time. If the material does not reach the melt temperature then the melt wear rate per unit width is defined to be zero. To convert the melt wear rate per unit width to single asperity melt wear rates an effective width, w_{eff} , needs to be determined. Hale determined this effective width by selecting a sampling of single asperity mechanical wear rates and dividing them by their respective plane strain 6 μm asperity wear rates per unit width. For each of the sampled velocities, the effective width was approximately the same, and the average of the effective widths was calculated as 8.29 μm . This defines the melt single asperity wear rate, $W_{sa,melt}$, as

$$W_{sa,melt} = w_{eff} W_{sa,melt} = (8.29\mu\text{m}) h_{melt} \quad (3.21)$$

The equations as they are presented here presume a predetermined surface temperature due to frictional heating. However, as mentioned in Section 3.2.4, the fraction of frictional heat imparted upon the slipper is an unknown value, which is actually a function of the temperature of the slipper and the rail and the relative sliding velocity. Hale assumed that the frictional heating was split evenly between the slipper and rail with 50% of the frictional heating entering the slipper and 50% entering the rail. This assumption was based on previous research [7; 26] and similar conductivity of the slipper and rail materials.

While this assumption is appropriate for steady-state solutions, it is inadequate for a transient analysis. The sliding velocity of the slipper reaches high speeds and

achieves thermal levels much higher than the rail. Under these conditions, the slipper will acquire less of the frictional heating. This fact is made apparent when the heat transfer solution is run with the 50% heat split. Under this scenario, the surface temperature of the slipper achieves levels on the order of 5,000 to 10,000 K. Hale accounted for this by adding an artificial boundary condition to the analysis that restricts the surface temperature to be less than or equal to the melt temperature.

This artificial boundary condition does not accurately reflect the physics of the phenomenon. The goal of this research is to evaluate the frictional heat fraction without this boundary condition. Since an exact value is indeterminable without experimentation, an average slipper fraction of frictional heat, λ_{ave} , is determined based on experimental wear measurements made by Hale on the third stage pusher sled used for the 2008 HHSTT mission.

From the experimental results, a maximum possible wear value is known, so a maximum λ_{ave} can be determined. To perform this analysis, the total melt wear calculation is simplified. Rather than evaluate the frictional heating and the local effect of flash heating, only the frictional energy is considered because it makes a significantly higher contribution to melt. The numerical heat transfer solution is run, and the thermal profile is evaluated at the point in which the melt depth penetrates furthest. The melt depth is defined as the depth of material which exceeds the melt temperature. Since the numerical solution is one-dimensional, the melt depth is converted to a volume by multiplying by the slipper normal area. The results of this analysis are presented in Section 4.1.

3.6 Total Mechanical Wear Volume Calculation

To evaluate total wear removal, the single asperity wear rates need to be integrated with respect to sliding distance. The single asperity wear rates assume that the slipper is in contact with the rail for the duration of the wear event and only accounts for wear due to one asperity collision. For this reason, two scaling factors need to be included in the model. The first scaling factor accounts for the bouncing

of the slipper as it travels down the rail. This is derived from the DADS force data. The data is evaluated for an entire test mission, and if a force is non-zero the slipper is said to be in contact with the rail. The ratio of the number of non-zero forces to zero forces is defined as the percentage of contact, d_{pc} . The percentage of sliding contact for the forebody sled was calculated to be 24%.

The second scaling factor accounts for the multiple asperity collisions experienced by the slipper, and is derived by relating the wear rates to Archard's wear rate model at lower velocities [2]. Equation 3.22 shows the relationship between Archard's wear, W_A , and the single asperity wear rates.

$$W_A = \frac{k_A F}{H} = N W_{sa} \quad (3.22)$$

In this equation, k_A represents Archard's wear coefficient, F is the loading, H is the material hardness, and N is the desired scaling factor. Rearranging the equation, the scaling factor can be defined as

$$N = \frac{k_A F}{W_{sa} H} \quad (3.23)$$

Hale [16] evaluated N for a sliding velocity of 10 m/s. Assuming a k_A value 4.4×10^{-5} and using the DADS upper limit force curve discussed in Section 3.5, N was calculated to be 11.77. Knowing these scaling factors, the total wear, W_{tot} , can be calculated using Equation 3.24, where d_{max} is the total sliding distance.

$$W_{tot} = N d_{pc} \int_0^{d_{max}} W_{sa}(s) ds \quad (3.24)$$

3.7 Summary of Numerical Modeling

Models for evaluating both mechanical and melt wear have been developed in this chapter. The next chapter will provide the results of the implementation of these models. The results of the thermodynamic and melt wear models that were

described in Sections 3.2 and 3.5, respectively, will be shown in Section 4.1. Based on these results, mechanical wear rates will be evaluated and presented in Section 4.2. The mechanical wear rate calculations will be validated using experimental wear volume data obtained from a third stage slipper recovered during the 2008 HHSTT test mission. The validation results are shown in Section 4.3. Finally, Section 4.4 will present the total calculated wear for a forebody sled slipper for a typical HHSTT mission profile.

IV. Results and Discussion

This chapter will present the results of the numerical modeling techniques discussed in the previous chapter. First the average fraction of frictional heat absorbed by the slipper, λ_{ave} , will be evaluated. The results of this analysis will be used to calculate a temperature profile of the slipper with respect to time using the implicit heat transfer technique described previously. This temperature profile is used to define initial temperatures for hydrocode simulations, which are used to calculate single asperity wear rates based on the failure criteria developed in Section 2.6. These mechanical wear rates are validated by using Equation 3.24 to calculate a total wear volume for the 2008 third stage slipper velocity profile, and comparing the result with an experimental wear volume. Finally, given the validated mechanical wear rates, a total wear volume is calculated using the velocity profile for the forebody slippers.

4.1 Evaluation of Frictional Heating

Since the increase in internal energy, E , is proportional to the increase in temperature, the slipper thermal profile only needs to be evaluated for a single average frictional heat fraction, λ_{ave} . The change in internal energy per unit volume is defined as

$$\Delta E = \int_{T_0}^{T_f} \rho c_p dT \quad (4.1)$$

where ρ is the material density and c_p is the specific heat of the material. Evaluating this integral produces

$$\Delta E = \rho c_p (T_f - T_0) = \rho c_p \Delta T \quad (4.2)$$

The only energy flux being evaluated is the frictional energy flux into the slipper, so the change in internal energy can also be represented as

$$\Delta E = \int_0^t \lambda_{ave} q_f(t) dt = \lambda_{ave} Q_f \quad (4.3)$$

where Q_f is the accumulated frictional energy absorbed by the slipper, as defined previously as Equation 3.9. Combining Equations 4.2 and 4.3 and rearranging gives

a change in temperature defined as

$$\Delta T = \frac{\lambda_{ave} Q_f}{\rho c_p} \quad (4.4)$$

This equation can be evaluated for a single λ_{ave} to determine a ΔT . Equation 4.5 shows this change in temperature, where the "0" subscripts indicate the measurements were taken at a single specific slipper heat fraction.

$$\Delta T_0 = \frac{\lambda_{0,ave} Q_f}{\rho c_p} \quad (4.5)$$

Since Q_f , ρ , and c_p are constants, this equation can be combined with Equation 4.4 and rearranged so, the change in temperature for any slipper frictional heat fraction can be defined as

$$\Delta T = \frac{\lambda_{ave}}{\lambda_{0,ave}} \Delta T_0 \quad (4.6)$$

This change in temperature can be used to define the temperature profile for any slipper frictional heating fraction. The temperature profile at the final time step of a sled run, t_{final} , is defined by Equation 4.7

$$T(y, t_{final}) = \frac{\lambda_{ave}}{\lambda_{0,ave}} [T_0(y, t_{final}) - T_{init}] + T_{init} \quad (4.7)$$

In order to evaluate the average frictional heating fraction, an experimental wear value must be used for comparison. The only wear data available for the HHSTT slippers is a third stage slipper from the 2008 test mission. However, this experimental data only represents the total wear resulting from both mechanical and melt wear. The mechanical and melt wear cannot be decoupled during the experimental measurements, so the frictional heating fraction is evaluated as a fraction of total wear. Evaluation of the implicit heat transfer equations requires a frictional heating equa-

Table 4.1: Coefficients for Plastic Strain Criterion Curve Fit

Coefficient	Value	(Units)
A_{3S}	1.047×10^5	(J)
B_{3S}	0.6627	(unitless)
C_{3S}	-1.433×10^5	(J)
D_{3S}	-0.3251	(unitless)
E_{3S}	-6.069×10^4	(J/s ²)
F_{3S}	1.074×10^6	(J/s)
G_{3S}	-1.05×10^6	(J)

tion, $q_f(t)$. This is defined for the third stage slipper using the same method outlined in Section 3.2.4.

The nature of the third stage slipper dynamics means that a discontinuity in the frictional heating energy exists at the point where the third stage rocket is extinguished and the sled begins to decelerate. This requires a two-stage curve fit. The curve fit for the accumulated frictional heating prior to the discontinuity is an exponential fit, and the curve fit after the discontinuity is a quadratic fit, as defined in Equation 4.8 where the “3S” subscript indicates the coefficient applies to data from the third stage slippers. The coefficients for this equation are given in Table 4.1. The derivative of the curve fit for the accumulated frictional heat energy was taken to define the frictional heating as a function of time.

$$Q_{f,3S} = \begin{cases} A_{3S}e^{B_{3S}t} + C_{3S}e^{D_{3S}t} & : 0 < t < 5.0 \\ E_{3S}t^2 + F_{3S}t + G_{3S} & : t > 5.0 \end{cases} \quad (4.8)$$

From this, a single point temperature profile needed to be generated. As seen in Figure 4.2, which shows the surface temperature of the third stage slipper for $\lambda_{ave} = 0.5$, the magnitude of the temperature profile for the third stage slipper peaks when the discontinuity in the frictional heating is reached. The temperature profile was evaluated at this peak location, and the temperature profiles for λ_{ave} ranging from 0 to 0.5 were calculated using Equation 4.7. The melt depth was then determined as

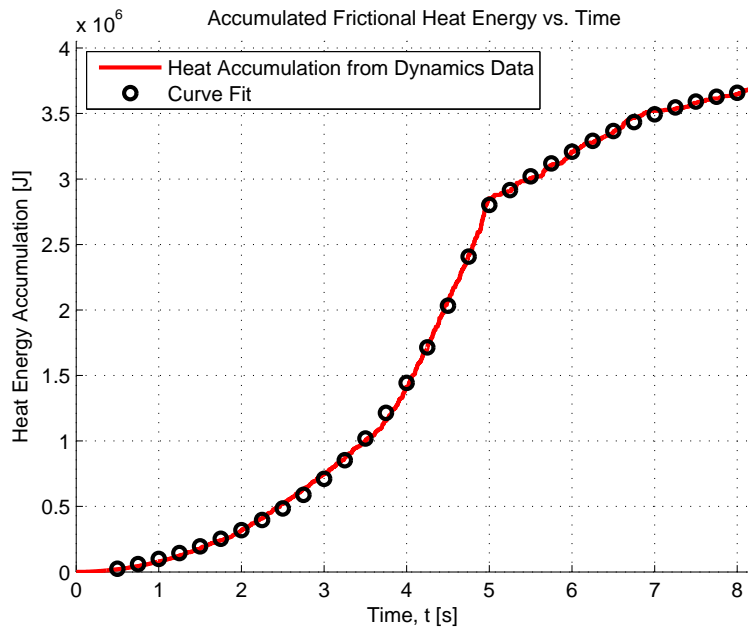


Figure 4.1: Third Stage Slipper Accumulated Frictional Heating

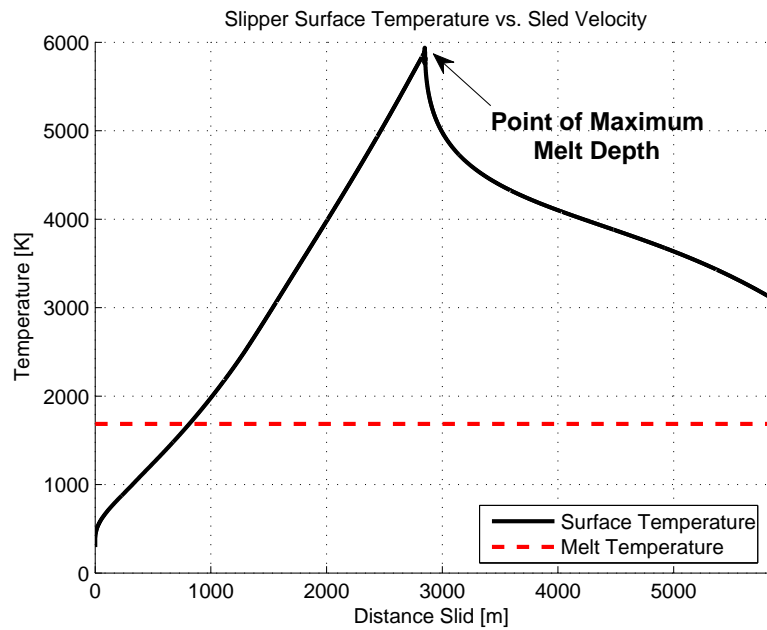


Figure 4.2: Surface Temperature Third Stage Slipper, $\lambda_{ave}=0.5$

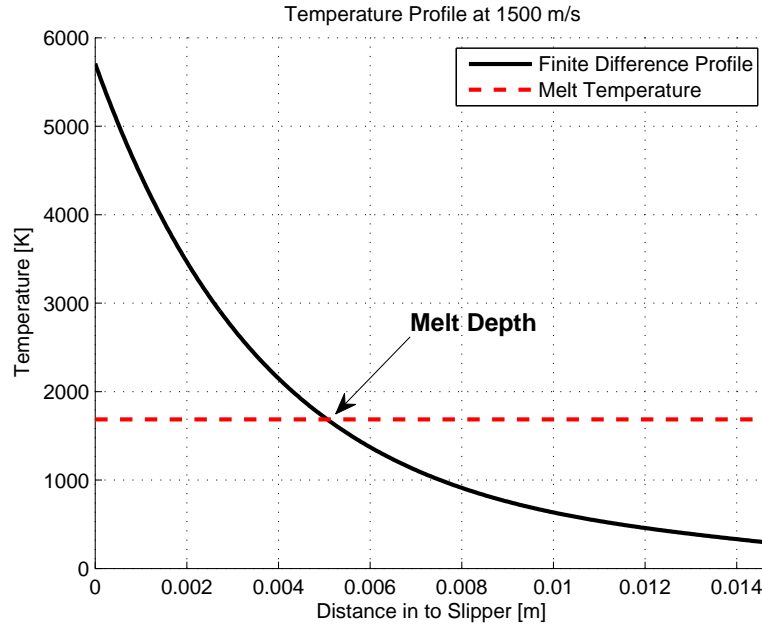


Figure 4.3: Melt Depth Example

the depth into the slipper which exceeds the melt temperature, shown in Figure 4.3. The results of this analysis are plotted in Figure 4.4. The x-axis of this plot represents the slipper frictional heating fraction, and the y-axis represents the relative melt wear volume compared to the experimental wear volume of $10,516 \text{ mm}^3$, which is expressed as a percentage. The black circles represent single point calculations at λ_{ave} values of 0.1, 0.2, 0.3, 0.4, and 0.5, and are used to verify that the model correctly evaluates the melt depth. The close fit indicates that Equation 4.7 accurately scales the single point temperature profile.

The results are not unexpected. A slipper frictional heating fraction of 0.5 results in a melt wear percentage on the order of 1,000%, which is not surprising given that the surface temperature reaches 6,000 K. However, it is not physically possible for the melt wear to represent more than 100% of the total wear volume, so Figure 4.5 shows the same results, except the y-axis is restricted between 0% and 100%. This figure shows that if melt wear occurs, the average slipper frictional heating fraction would be between approximately 0.123 and 0.140. However, these values should not be taken as absolutes. The model used here to define melting does

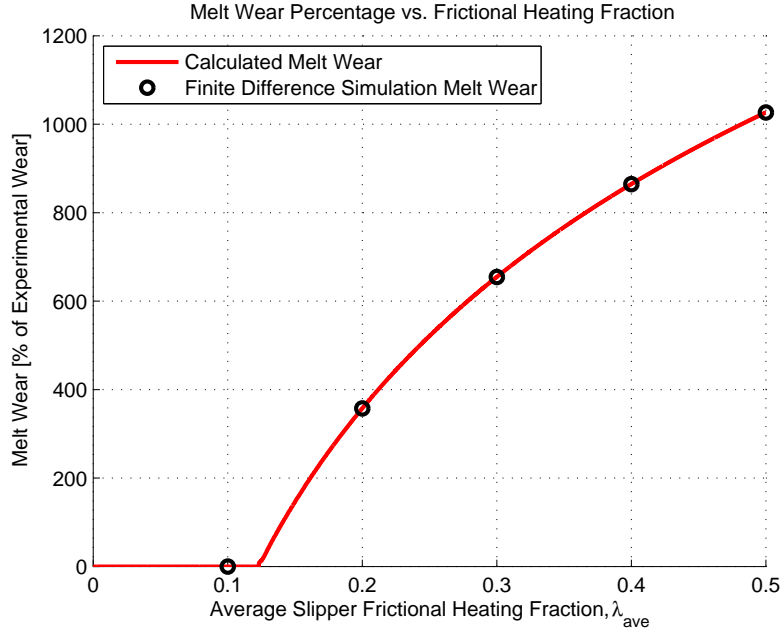


Figure 4.4: Evaluation of Frictional Heating Fraction, λ_{ave}

not wholly account for the true physics involved with the melting process. A more complete model would account for removal of energy during the melt removal process, and the effects of latent heat should be included as well. However, this model does provide an approximation of the slipper frictional heating fraction.

4.2 *Single Asperity Mechanical Wear Rates*

As discussed previously, the initial temperature is influential on the mechanical wear rate simulations. Estimations have been made based on the experimental measurements of the third stage slipper from the 2008 HHSTT mission that melt wear accounts for approximately 0 to 20% of the total wear. Using this assumption, an average slipper frictional heating fraction can be determined from Figure 4.5. If melt wear is assumed to represent 20% of the total wear, an average slipper frictional heating fraction would be approximately 0.1265. While the 20% value is only an approximation, the precision of the approximation is not the most important factor. The desired temperature profile only needs to be approximate to calculate the mechanical wear rates effectively.

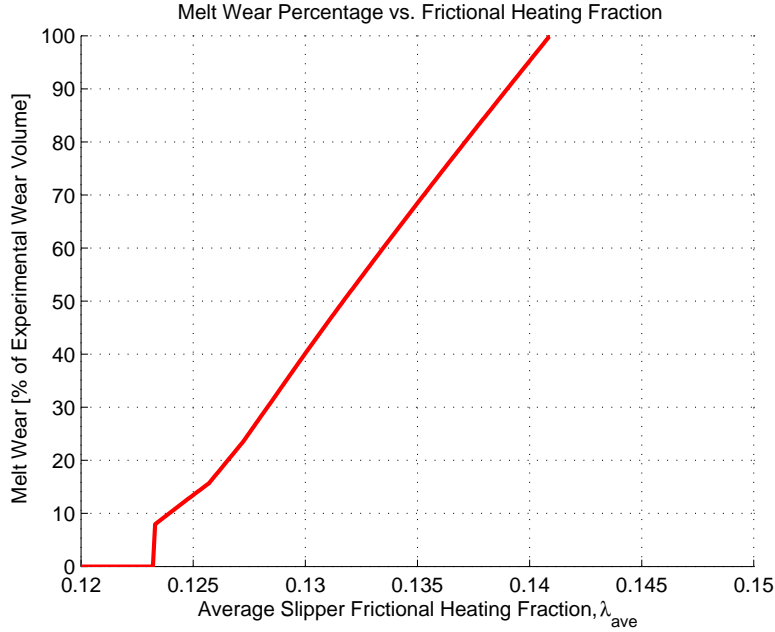


Figure 4.5: Restricted Range Evaluation of Frictional Heating Fraction, λ_{ave}

To generate the temperature profile, the implicit heat transfer solution scheme discussed previously was evaluated with $\lambda_{ave}=0.1265$. The resulting thermal profile is shown in Figure 4.6. The $400 \mu\text{m}$ depth temperature is desired as an input for the CTH simulations, as discussed in Section 3.3.2. However, the thermal simulation does not implement the artificial melt temperature boundary condition, and the temperature is allowed to progress above the melt temperature. Therefore, the surface of the slipper is defined as the point into the depth which is equal to the melt temperature. The temperature at the point $400 \mu\text{m}$ beyond this depth is the defined to be the initial temperature for the CTH simulations. These temperatures were shown in Table 3.4.

Based on these initial temperatures, the CTH simulations were run and the plane strain wear rates were integrated to generate single asperity wear rates, as discussed in Chapter III. Figure 4.8 shows the results of the mechanical wear rate model discussed in Section 3.4, and the numerical values are provided for reference in Appendix D. The black line indicates the results obtained by Hale [16] using the finite element technique, while the other lines indicate results obtained using CTH with differing

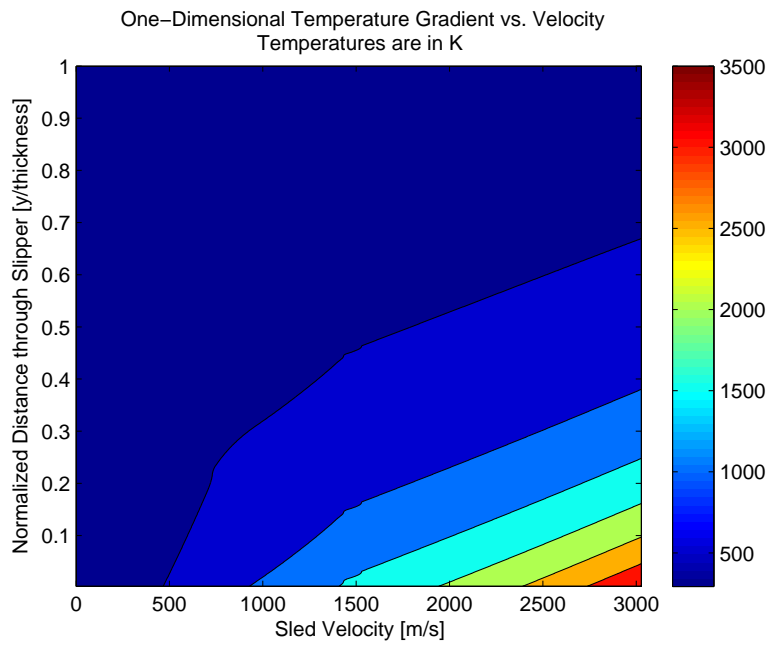


Figure 4.6: One-dimensional Temperature Profile with Respect to Velocity

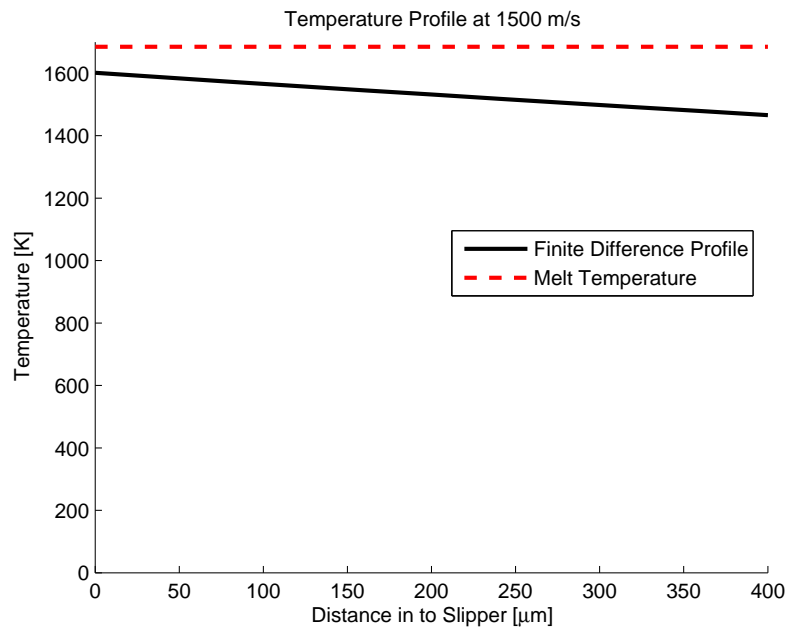


Figure 4.7: Temperature Gradient Near Slipper Surface at 1,500 m/s

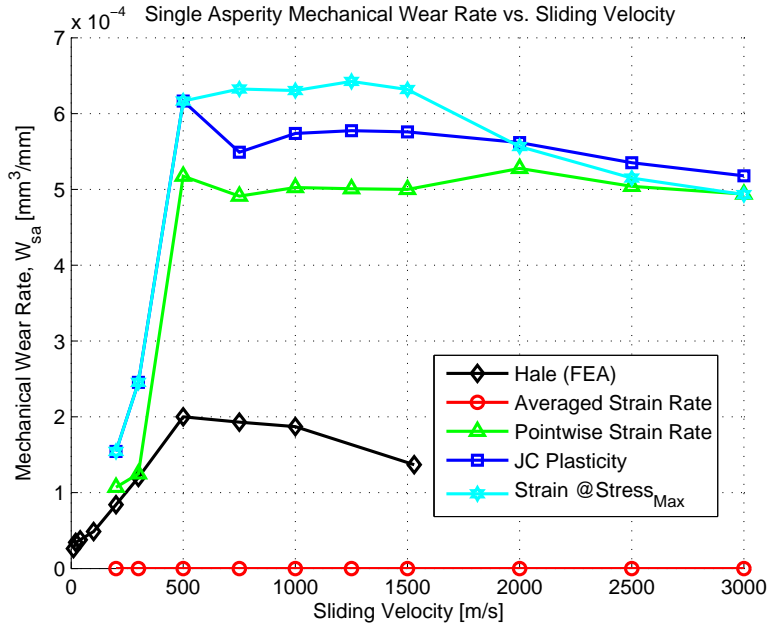


Figure 4.8: Single Asperity Mechanical Wear Rates

failure criteria. The most conspicuous result is that obtained from the failure criteria utilizing the averaged strain rate method described in Section 2.6.1. The critical stress, as defined by this method, is never reached during the CTH simulations, so the wear rates are shown as zero. Obviously, the slipper does not experience zero wear during the sliding event. For this reason, this method is treated as inadequate for the hydrocode simulation technique and is ignored in any subsequent analysis. If the failure criteria limit were decreased, wear rates similar to that seen by Hale are produced. Figure 4.9 shows the progression of damage area compared to an FEA simulation run by Hale versus simulation time for varying levels of critical stress, and other slipper velocities exhibit similar results. This shows that the stresses approach levels close to those defined using the averaged strain rate method, but do not quite exceed the limit. This can be attributed to the treatment of material failure in CTH, where failed material is replaced with void material incapable of carrying stress [13].

The other criteria considered show little deviation from each other and all follow a similar curve. The wear rates increase until they peak around 0.5 - 0.6 mm³/mm when the velocity reaches 500 m/s, where the wear rate levels off and remains essen-

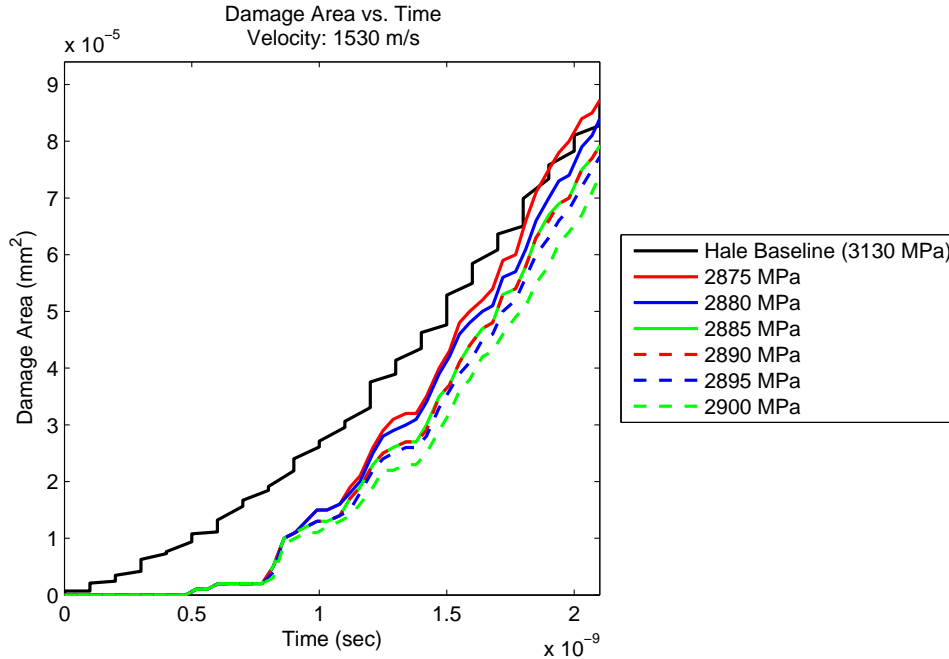


Figure 4.9: Sensitivity to Averaged Strain Rate Criteria, Velocity = 1,530 m/s

tially constant up to 3,000 m/s. While the wear rates do not agree with the results shown by Hale’s research, this is not discouraging because Hale’s total wear model predicted a total wear value that was less than the experimental value.

4.3 Mechanical Wear Criteria Validation

Experimental wear data for the slippers on the forebody sled is non-existent due to the destructive nature of the HHSTT testing scenario. However, slippers from the third stage pusher sled are recoverable, so wear measurements can be made. Hale measured the thickness of one of these slippers to calculate the total wear volume removed. It should be noted that the actual initial thickness of the slipper is not known, but the nominal thickness is defined as 14.7 mm by the HHSTT engineers, so this is the value used to determine volume removed.

The thickness of the worn slipper was measured at several discrete points along its length, and the total wear depth was calculated as the difference between these thicknesses and the nominal thickness. These wear depths were then integrated along

the length to obtain a wear depth per unit width, which was multiplied by the width of the slipper to obtain a total wear volume. The wear volume that Hale calculated was $10,516 \text{ mm}^3$. In order to compare the various failure mechanisms using the third stage pusher sled dynamics data, wear rates at the lower velocities need to be computed. CTH simulations were run for velocities as low as 200 m/s, and Hale's data was used for the slower speeds. The sled reached 200 m/s after traveling a distance of 104.3 m. However, the track is 5,815 meters long, so the finite element derived data at the lower velocities only represents approximately 1.8% of the distance during the sliding event.

Melt wear is excluded from this analysis due to the inability to define the slipper fractional heating fraction coefficient, $\lambda_{slipper}$. The scaling factors accounting for the number of asperities, N , was the same as that used by Hale who calculated a total wear volume of $4,360 \text{ mm}^3$. However, the percentage of contact, d_{pc} , was defined to be 24%, versus 36% used by Hale, for the evaluation of the CTH simulations based on the contact force data for the combined dynamics data set. Figure 4.10 shows the results of this analysis. The dashed red line indicates the experimental wear volume. The experimental wear data only consists of an initial state and an end state, so the progression is shown linearly for the purpose of illustration only. While acknowledging the simplified method to determine the experimental wear volume, this shows the criteria established in this research produce reasonable wear values if melt wear is assumed to account for 10 to 20% of the total wear.

4.4 Total Wear

Figure 4.11 shows the total mechanical wear integrated with respect to the sliding distance for the forebody sled. The results are similar among the various failure mechanisms considered, and they all follow the same general path. The pointwise strain rate method calculated a total wear volume of $8,581 \text{ mm}^3$ while the Johnson-Cook plasticity method and strain at maximum stress method calculated wear volumes of $9,111 \text{ mm}^3$ and $9,150 \text{ mm}^3$, respectively. To calculate total wear removal of

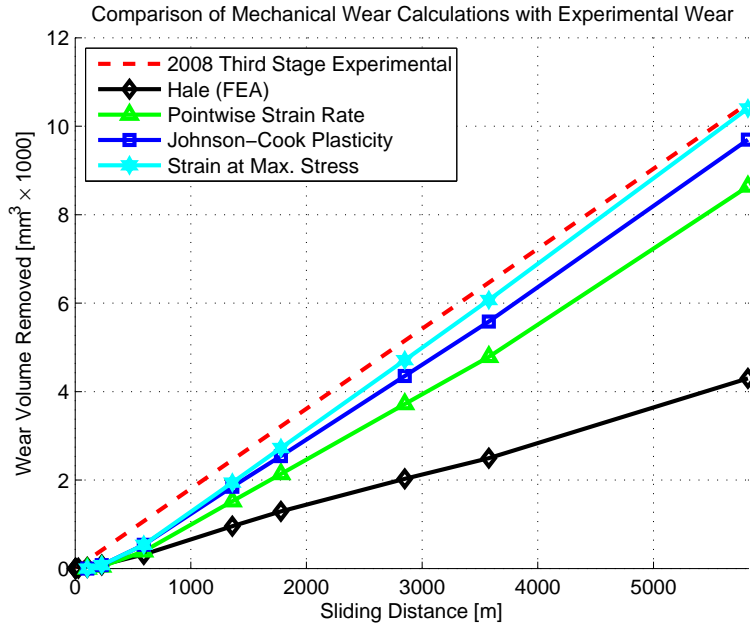


Figure 4.10: Wear Criteria Validation

the forebody slippers would require a melt wear contribution, but this data is not available due to the inability to properly define the amount of thermal heat acquired by the slipper during the sliding event. However, if the melt wear is assumed to contribute between 0 and 50% of the total wear, the results shown in Figure 4.11 can be used to evaluate the total wear for the forebody sled.

Figure 4.12 shows the total wear volume as a function of the percentage total wear attributed to melt wear. The dashed lines show the results for the third stage slipper total wear, and are provided as a reference point. The black dashed line represents the total wear removal calculated by Hale for the 2008 third stage slipper using FEA and the averaged strain rate method of $4,360 \text{ mm}^3$. The red dashed line represents the experimental wear volume measured by Hale on slipper from the third stage of the 2008 HHSTT sled. This experimental volume was $10,516 \text{ mm}^3$. The three curves for the various failure criteria are based on the total volume of wear removal calculated from the mechanical wear rates. The total mechanical wear values for each criteria were divided by the percentage of total wear attributed to mechanical wear,

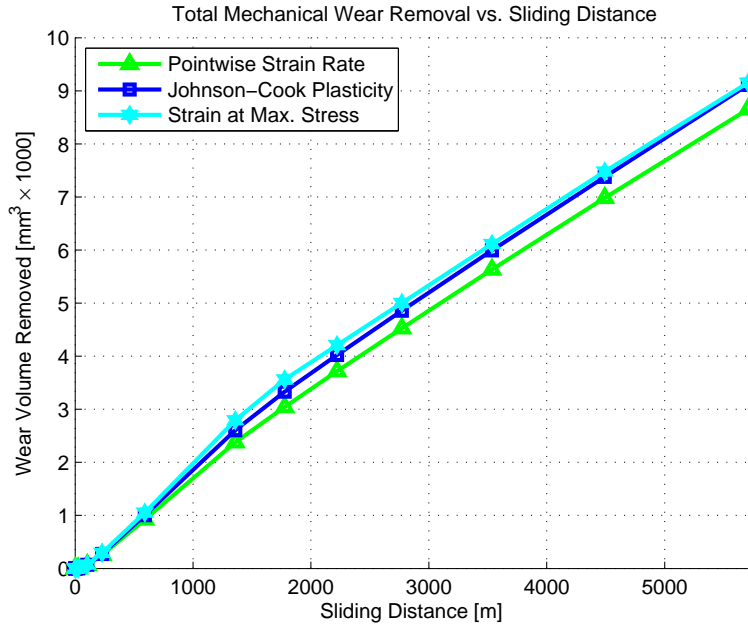


Figure 4.11: Forebody Sled Slipper Mechanical Wear

or in other words, the total mechanical wear values were divided by 100% minus the percentage of total wear attributed to melt wear.

Based on these results, if the melt wear is allowed to contribute between 0 and 50% of the total wear, the pointwise strain rate criterion would produce a total wear volume ranging from 8,581 mm³ to 17,162 mm³, the Johnson-Cook plasticity criterion would produce a total wear volume ranging from 9,111 mm³ to 18,222 mm³, and the strain at maximum stress criterion would produce a total wear volume ranging from 9,150 mm³ to 18,300 mm³. Figure 4.13 shows the same data as Figure 4.12, but presents the total wear in a different context. Rather than plotting total wear volume on the y-axis, the total wear volume is shown as a percentage of the original slipper volume. This shows that the percentage of slipper volume removed varies between 2.83% and 6.03% depending on the percentage of wear attributed to melt and the failure criterion being used. This is compared to 3.47% of slipper material removed based on the 2008 third stage slipper experimental results, and 1.44% calculated by Hale for the 2008 third stage slipper using the FEA method.

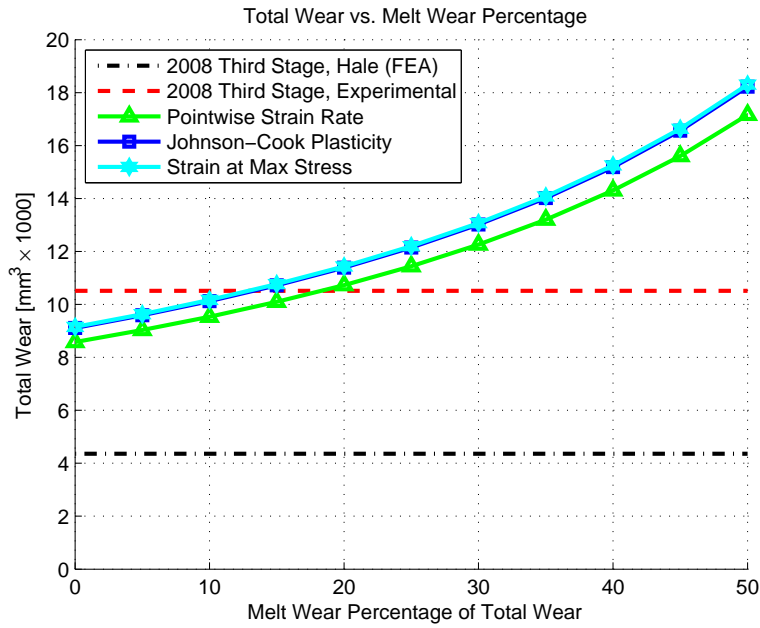


Figure 4.12: Total Forebody Sled Slipper Wear versus Percentage of Total Wear Attributed to Melt Wear

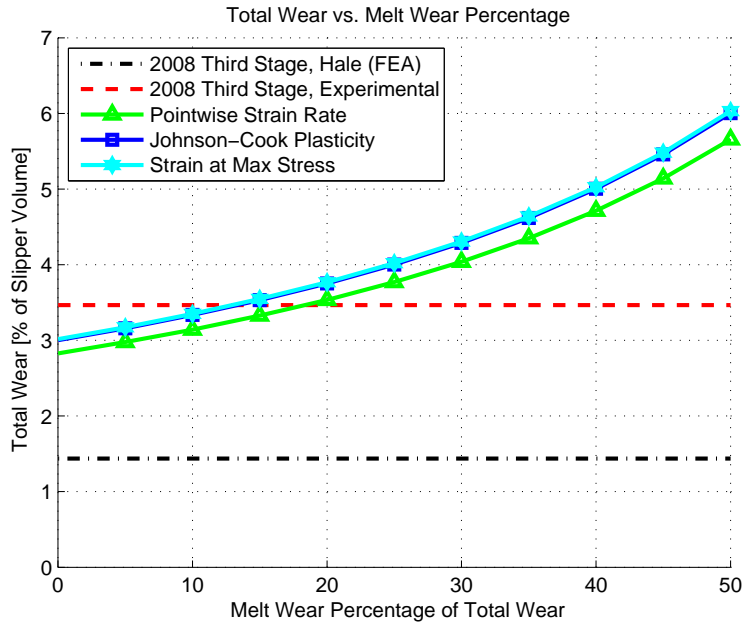


Figure 4.13: Percentage Forebody Sled Slipper Worn versus Percentage of Total Wear Attributed to Melt Wear

V. Summary and Conclusions

This chapter summarizes the results of this research. First, key elements of the literature search and theoretical background will be discussed, along with a short summary of the numerical modeling and results obtained. Some conclusions based on the research work will be provided, and the chapter will conclude with recommendations for future research work.

5.1 Summary of Research

Previous research in the wear field has produced models that are capable of evaluating the phenomenon at slow sliding speeds, and has provided a foundation for this research. Much of the past research studied the effects of mild sliding wear and friction, and the relationship between the coefficient of friction, the applied pressure, and the sliding velocity. These factors were critical for understanding the thermodynamics of the slipper as it slides against the rail. Temperature measurements taken of sliding bodies also illustrated the key mechanisms that result in melt wear. Previous research at AFIT laid the groundwork for modeling mechanical wear using a “single asperity” numerical solution. Metallurgy studies at AFIT have provided valuable insight regarding plasticity effects and the thermal environment of the HHSTT slipper.

Based on this previous research, the wear model for the slipper was separated into mechanical wear and melt wear. The mechanical wear was modeled using an Eulerian-Lagrangian hydrocode to simulate the collision between the slipper and a hemispherical asperity, and the simulations were two-dimensional plane strain in nature. Failure criteria were defined based on the viscoplastic behavior of the slipper material so that the mechanical wear rates from the plane strain simulations could be evaluated. The plane strain simulations provided an evaluation of the wear in a two-dimensional plane; however, the wear event is three-dimensional, so the results of the plane strain simulations were integrated across the width of the asperity to approximate the three-dimensional effect. Sensitivity studies of the slipper initial vertical

velocity and initial temperature were conducted. It was found that the vertical velocity did not have an effect on the wear rate because it makes a small contribution to the overall velocity vector, when considered in the context of the horizontal velocities seen by the HHSTT slippers. Conversely, the initial temperature did exhibit a significant effect on the wear rate. This is due to the nature of the viscoplasticity model used for this research.

The wear rate sensitivity to initial temperature indicated that a thermal profile of the slipper needed to be generated, and this was accomplished by numerically solving the heat conduction equation in one-dimension with two spatial boundary conditions: a flux boundary condition at the slipper-rail interface and a constant temperature boundary condition at the top edge of the slipper. The flux condition was defined using force data produced by the HHSTT to evaluate the frictional heating resulting from sliding. The possibility of defining a one-dimensional gradient as the initial temperature of the simulation was considered. However, due to the micro-level scope of the simulations, the temperature gradient in the region of interest was nearly constant. Rather than add complexity to the model, the temperature at a depth of 400 μm into the slipper was chosen as the initial temperature. The 400 μm depth was based on hardness measurements taken by Hale of a used slipper indicating that the heat affected zone was approximately 400 μm deep.

The fraction of frictional heating absorbed by the slipper was analyzed with respect to melt wear so that an appropriate range of slipper frictional heating fractions could be determined. This was accomplished by evaluating the melt depth if half of the frictional energy was absorbed by the slipper and half by the rail, and this result was expanded to evaluate the melt depth if the fraction of frictional energy entering the slipper varied from 0 to 0.5. This analysis provided a temperature profile for the slipper that was used to define the initial temperature of the slipper material for CTH simulations.

The mechanical wear rates are expressed in terms of volume per distance slid. In order to evaluate the total wear removed, the wear rates needed to be integrated with respect to sliding distance. A simple integration of the single asperity wear rates would be an incomplete assessment, though. The nature of the single asperity simulation requires the assumption that the slipper is in contact with the rail during the entire collision event. However, it is well documented that the slipper does not remain in contact with the rail during a test mission, but actually bounces up and down. Therefore, a scaling factor accounting for the percentage of contact was introduced. An additional scaling factor needed to be introduced to account for multiple asperities on the rail. This was done by correlating wear rates with the model developed by Archard, which was based on experimentation and also accounts for the three-dimensional aspects of the wear phenomena. The results of this study are encouraging. Limited experimental wear data is currently available for the HHSTT slippers at high velocity, but the experimental data that is available is generally in agreement with the results produced by this numerical modeling technique.

5.2 Conclusions

The result of the frictional heating analysis confirmed that using an average fraction of frictional heating value of 0.5 is inappropriate for modeling the sliding thermodynamics of the HHSTT slipper. Using this value produced a melt depth 10 times higher than experimental total wear values. Instead, a reasonable average frictional heating fraction of approximately 0.125 is appropriate if melt wear is assumed to account for 20% of the total slipper wear. Using 0.125 for the slipper frictional heating fraction, a slipper thermal profile was generated to define initial temperatures for mechanical wear simulations.

The mechanical wear simulations produced reasonable results given the experimental wear volume measured from the third stage of the 2008 HHSTT test sled. Evaluating the total mechanical wear for the third stage slipper and comparing with the experimental value showed that the total mechanical wear ranged from 80 to 100%

of the experimental. This indicates that the material failure criteria outlines in Sections 2.6.2-2.6.4 are appropriate for CTH hydrocode simulations. Additionally, the $1\ \mu\text{m}$ by $1\ \mu\text{m}$ mesh used in the CTH simulations has been determined to be adequately refined to capture the slipper behavior when impacting an asperity. If the total wear is evaluated for the forebody slippers, given a typical HHSTT velocity profile for the forebody sled, the total volume removed is calculated to range from 2.83% to 6.03% of the original slipper volume. The range accounts for various failure criteria and the percentage of wear attributed to melt wear. These values are reasonable given that the third stage slipper from the 2008 HHSTT test mission wore 3.47% of its original volume.

5.3 Recommendations for Future Research

While the culmination of this research work, and the work of others, has provided a firm understanding of the mechanical wear phenomenon, the models used to represent the thermal characteristics of the slipper have been simplified to eliminate undesirable variables and reduce the complexity of the problem. The thermal analysis of the slipper bulk temperature has been evaluated assuming that the slipper is in contact with the rail for the duration of the sliding event, and thus, can be treated using simple conduction equations. Higher fidelity thermal models would account for the bouncing aspect of the slipper dynamics by including the effects of convection. Additionally, studies have also shown that the effects of fluid frictional heating can have significant consequence at hypersonic velocities.

In addition to the treatment of the thermodynamics, Johnson and Cook [23] have developed a failure criteria based on fracture mechanics models for metals subjected to high strain rates, temperatures, and pressures. The model is based on the accumulation of strain experienced by a material. This research did not utilize this model due to the accumulative nature of the model because the duration of the single asperity collisions was too short to accumulate any meaningful damage based on the

model definition. However, alternative methods to the single asperity method for evaluating wear could utilize this fracture model effectively.

Appendix A. Heat Transfer Analysis Code

A.1 Heat Transfer Code Description

The Matlab[®] code provided in this appendix is the one used to evaluate melt wear and the slipper thermal profile. Use of this code requires DADS data supplied in a specific format. The data is supplied in four columns where the first column is the simulation time in seconds, the second column is the sled position in meters, the third column is the sled velocity in meters per second, the final column is the slipper contact force in Newtons. These units are imperative because all subsequent calculations are made assuming these units.

The first cell of the code defines key parameters for the simulation including: the simulation time step, the finite difference spatial gradient size, the target velocities being evaluated, and an additional variable called “tempStep” which is used to reduce memory requirements when the temperature profiles are plotted. The code then loads the DADS data and defines the necessary constants. Curve fits for the force data and heat flux are then defined. The actual finite difference equations are then evaluated. Finally, the finite difference results are evaluated and plotted.

A.2 Heat Transfer Matlab[®] Code

```
%% ONE-DIMENSIONAL SLIPPER TEMPERATURE GRADIENT ANALYSIS

clear; clc; close all;

fprintf('Setting Switches...\n')

% Constant to Reduce Memory Allocation for Total Thermal Profile
tempStep = 50;

% Time Step (seconds)
dt = 0.00005;

% Finite Difference Gradient Size (microns)
dy=30e-6;
```

```

% Critical Velocities to Evaluate Temperature Profile
velEval = [10 20 40 100 200 300 500 750 1000 1250 1500 2000 2500 3000];

%% LOAD DATA

fprintf('Loading Data...\n')

%{
Format of data for loading to "dataDADS" variable:

Column 1: Time (seconds)
Column 2: Sled Longitudal Position (meters)
Column 3: Sled Forward Velocity (meters/second)
%}

dataDADS = load('heatXferDADSHybrid.txt');

time = dataDADS(:,1);
cg_horiz = dataDADS(:,2);
vsled_horiz = dataDADS(:,3);

timeOld = time;
time = time(1):dt:time(end);
time = time';

% Position and velocity arrays are interpolated below to account for
% time step differences between forebody sled and pusher sled data
cgOld = cg_horiz;
vsOld = vsled_horiz;

clear cg_horiz;
clear vsled_horiz;
clear force_data;

cg_horiz = zeros(size(time,1),size(time,2));
vsled_horiz = zeros(size(time,1),size(time,2));

cg_horiz(1) = cgOld(1);
vsled_horiz(1) = vsOld(1);

indices = zeros(length(timeOld),1);

index = 1;

```

```

for iter = 1:size(timeOld,1)
    while(1)
        if time(index) >= timeOld(iter)
            cg_horiz(index) = cgOld(iter);
            vsled_horiz(index) = vsOld(iter);
            indices(iter) = index;
            break;
        else
            index = index + 1;
            if index > length(time)
                indices(length(indices)) = length(time);
                break;
            end
        end
    end
end

iter = 1;
for index = 1:(size(time,1)-1)
    if index == indices(iter)
        iter = iter + 1;

        if iter<=length(indices)
            iLo = indices(iter-1);
            iHi = indices(iter);

            cgLo = cg_horiz(iLo);
            cgHi = cg_horiz(iHi);

            vsLo = vsled_horiz(iLo);
            vsHi = vsled_horiz(iHi);
        end
    else
        cg_horiz(index) = cgLo + (cgHi-cgLo)*...
            ((index-iLo)/(iHi-iLo));
        vsled_horiz(index) = vsLo + (vsHi-vsLo)*...
            ((index-iLo)/(iHi-iLo));
    end
end

for index = 1:length(vsled_horiz)
    vsled_horiz(index) = max(0,vsled_horiz(index));
end

```

```

fprintf('\t... DATA LOADED\n\n')

%% CONSTANTS

fprintf('Setting Constants...\n')

Cp_air = 1004;           % J/(kg K) for 298K
nu_air = 15.7e-6;
Cp_He = 5193;           % J/(kg K) for 298K
nu_He = 122.237e-6;

D_HeBag = 1310;         % distance initial position to start of He bag

Tinit = 293;           % initial temperature, K

% slipper specifics
Sw = 4*0.0254;          % slipper width, m
Sl = 8*0.0254;          % slipper length, m
An = Sw*Sl;             % slipper area, m^2 ( = 32 sq in)
thickness = 14.7E-3;    % slipper thickness, m (14.7 mm)
vol = An * thickness;   % slipper "plate" volume, m^3
rho_V300 = 8000;        % density, kg/m^3
mass = rho_V300 * vol;  % single slipper mass, kg
Cp_V300 = 420;          %858 % specific heat, J/(kg K)...at 700K
numslippers = 4;       % number of slippers in the sled
Tmelt = 1685;          % V300 melt temperature

Km = 31;                % thermal conductivity, J/(m s K)
alpha = Km/(rho_V300 * Cp_V300); % thermal diffusivity of VM300, m^2/s

H_VM300 = 2e9;          % Slipper Hardness (Pa)

SlipPartition = 0.50;   % heat percentage going into the slipper

aspRad = 6e-6;
aspArea = pi*aspRad^2;

fprintf('\t... CONSTANTS SET\n\n')

%% DEFINE FORCE CURVE FIT

fprintf('Defining Curve Fit for Force Data...\n')

```



```

A = 1.28640e2;
B = -4.02600e2;
C = 1.68400e3;

force_data = A*time.^2 + B*time + C;

fprintf('\t... FORCE CURVE FIT DEFINED\n\n')

%% CALCULATE COEFFICIENT OF FRICTION USING HALE DISSERTATION EQN 3.1

fprintf('Calculating Coefficient of Friction...\n')

P = force_data/An;
PV = (P*10^-6).*(vsled_horiz*1000);

COF = zeros(length(PV),1);

for index = 1:length(COF)
    if PV(index) < 4.45e8
        COF(index) = 0.2696*exp(-3.409e-7*PV(index))+...
            0.3074*exp(-6.08e-9*PV(index));
    else
        COF(index) = 0.02;
    end
end

fprintf('\t... COEFFICIENT OF FRICTION CALCULATED\n\n')

%% COMPUTE FLASH TEMPERATURE

fprintf('Computing Flash Temperature...\n')

W = P .* aspArea;
deltaTFlash = (COF*((pi*H_VM300)^0.75).*(W).^0.25).*sqrt(vsled_horiz)/...
    (3.25*sqrt(Km*rho_V300*Cp_V300));

fprintf('\t... FLASH TEMPERATURE COMPUTED\n\n')

%% COMPUTE FRICTIONAL HEATING (HEAT FLUX)

fprintf('Calculating Heat Flux...\n')

```

```

d = 1.57315e6;
e = 6.72000e-1;
HeatFlux = d*exp(e*time); % units: Watts/m^2

fprintf('\t... HEAT FLUX CALCULATED\n\n')

%% CALCULATE TEMP PROFILES USING FINITE DIFFERENCE METHOD

fprintf('Generating Temperature Profile...\n')

r=alpha*dt/dy^2; % units: non-dimensional

t=time; % units: sec
N=size(t,1);

y=0:dy:thickness; % units: meters (all lengths in meters)
M=size(y,2);

T(1:M,1)=Tinit; %Temp just over the interface at time t=0 (Ambient)
T(M,1:N)=Tinit; %Temp far away from the interface for all times (Ambient)

Tzero = T(2,1)+ 2*dy*HeatFlux(1)/Km; % units: K

A = zeros(length(y),length(y));
A(1,1) = 1;
A(size(A,1),size(A,2)) = 1;

for index = 2:size(A,1)-1
    A(index,index-1) = -1/dy^2;
    A(index,index) = (2*alpha*dt+dy^2)/(alpha*dt*dy^2);
    A(index,index+1) = -1/dy^2;
end

for j = 2:N %time(t)
    % Define Lower Boundary Temperature Based on Flux
    T(1,j)=T(1,j-1)+r*(T(2,j-1)-2*T(1,j-1)+Tzero);

    % Lower Boundary Temperature Bounded By Melt Temperature
    if T(1,j) > Tmelt
        T(1,j) = Tmelt;
    end

    % Calculate Temperatures at Current Time Step Simultaneously

```

```

    C = T(:,j-1)/(alpha*dt);
    C(1) = T(1,j);
    C(end) = Tinit;

    T(1:length(C),j) = A\C;

    % Add Heat Flux to Lower Boundary
    Tzero=T(2,j)+2*HeatFlux(j)*dy/Km;
end

fprintf('\t... TEMPERATURE PROFILE GENERATED\n\n')

%% EVALUATE TEMPERATURE PROFILES

tempProfiles = zeros(size(T,1),length(velEval));

velIndices = zeros(length(velEval),1);

for index = 1:length(velEval)
    if max(vsled_horiz)>velEval(index)
        iter = 1;
        while(1)
            if vsled_horiz(iter) > velEval(index)
                velIndices(index) = iter;
                tempProfiles(:,index) = T(:,iter);
                break;
            end
            iter = iter + 1;
        end
    end
end

%% PLOTTING

fprintf('Plotting Data...\n')

figNum = 0;

figNum = figNum+1;
figure(figNum)
hold on
plot(vsled_horiz,T(1,:));
plot([vsled_horiz(1) vsled_horiz(end)],[Tmelt Tmelt],...
```

```

        'r--', 'LineWidth', 2)
xlabel('Sled Velocity (m/s)')
ylabel('Temperature (K)')
title({'Slipper Surface Temperature vs. Sled Velocity'})
legend('Surface Temperature',...
        'Melt Temperature',...
        'Location', 'SouthEast')
grid on;
xlim([0 max(vsled_horiz)])

figNum = figNum+1;
figure(figNum)
isoBars = unique([linspace(0,Tinit,1) ...
        linspace(Tinit,Tmelt+100,10)]);
contourf(vsled_horiz(1:tempStep:end),...
        (1:M)/M,T(:,1:tempStep:end),...
        isoBars)
title({'One-Dimensional Temperature Gradient vs. Velocity';...
        'Temperatures are in K'})
xlabel('Sled Velocity (m/s)')
ylabel('Normalized Distance through Slipper (y/thickness)')
caxis([0 100*(ceil((Tmelt+100)/100))])
colormap(jet)
colorbar('Location', 'EastOutside')

figNum = figNum+1;
figure(figNum)
showHeight = 800e-6;
plotIndex = 1;
while(1)
    if y(plotIndex)>showHeight
        break;
    end
    plotIndex = plotIndex + 1;
end
contourf(vsled_horiz(1:tempStep:end),...
        10^6*y(1:plotIndex),...
        T(1:plotIndex,1:tempStep:end),...
        isoBars)
title({'One-Dimensional Temperature Gradient vs. Velocity';...
        'Temperatures are in K'})
xlabel('Sled Velocity (m/s)')
ylabel('Distance from Bottom of Slipper (\mum)')

```

```

caxis([0 100*(ceil((Tmelt+100)/100))])
colormap(jet)
colorbar('Location','EastOutside')

fprintf('\t... DATA PLOTTED\n\n')

fprintf('...PROGRAM COMPLETE...\n\n')

fprintf('Vel (m/s)\tSurface Temp (K)\tHAZ Temp (K)\tFlash Temperature(K)\n')

for index = 1:length(velEval)
    fprintf('%4.0f\t\t%4.0f\t\t\t\t%4.0f\t\t\t\t%4.0f\n',...
        velEval(index),...
        tempProfiles(1,index),...
        tempProfiles(plotIndex,index),...
        deltaTFlash(velIndices(index)))
end

```

Appendix B. CTH Input Process

B.1 CTH Input Summary

Included in this appendix is a sample CTH input file used to evaluate plane strain wear rates. For a given sliding velocity and asperity size, the user must update a variables. First the simulation time, “tstop,” needs to be updated, and the time step variables need to be updated. These variables include: “dt,” “dtfrequency,” and the second terms in “SaveTime,” “PlotTime,” and “HisTime.” Finally, the slipper initial velocity and temperature needs to be updated. The velocity components are defined with units of cm and a vertical velocity in to the rail is a negative value. The temperature is defined in units of electron volts, eV. The conversion from Kelvin to electron volts is as defined in Equation 2.1, where T_{eV} is the temperature in units of electron volts and T_K is the temperature in units of Kelvin.

$$T_{eV} = T_K/11604.5 \quad (2.1)$$

Additionally, the units of pressure and stress are expressed as dynes/cm². This is accounted for in the post processing code provided in Appendix C. However, the implementation of the Johnson-Cook viscoplastic model requires the conversion of a couple material constants. Table 2.1 shows the material constants in units compatible with CTH.

Table 2.1: VascoMax 300 and 1080 Steel Johnson-Cook Coefficients

Coefficient	VascoMax 300	1080 Steel
A (dynes/cm ²)	2.1×10^{10}	0.7×10^{10}
B (dynes/cm ²)	0.124×10^{10}	3.6×10^{10}
C	0.03	0.17
m	0.8	0.25
n	0.3737	0.6

B.2 Example CTH Input File


```

*tbad = 99999999
* Courant condition multiplier
*dtcourant = 0.6
* Acceleration due to gravity = -9.80 m/s^2
ygravity = -980
endcontrol

*****
* mesh input set
*****
* geom=2DR(rectangular x,y)
* geom=2DC(cylindrical x=radius, y=axis)
* geom=3DR(rectangular x,y,z)
* type=e (Eulerian) now the default (CTHv8.1)
* x#=coordinate range for plot
* y#=coordinate range for plot
* dxf=width of first cell in the region
* dxl=width of last cell in the region
* n=number of cells added in this region
* w=total width of this region in centimeters
* r=ratio of adjacent cell widths
*****

* coordinates for 2D rectangular Eulerian mesh
mesh
  block 1 geom=2dr
    x0 = 0.0000
    x1 w = 850e-4 dxf = 1.0e-4 dxl = 1.0e-4
    endx

    y0 = 0.0000
    y1 w = 850e-4 dyf = 1.0e-4 dyl = 1.0e-4
    endy
  endblock
endmesh

*****
* EOS input set
*****
eos
  material1 ses grepxy1      * epoxy rail coating (Cinnamon/Cameron)
  material2 ses iron         * 1080 steel rail
  material3 ses steel_v300   * VascoMax 300 slipper

```



```

material4 mgr platinum      * platinum for simulated sled mass
endeos

*****
* elastic-plastic input set
*****
epdata
* cell yield stress and plastic strain rate data is saved
  vpsave
* compute and save Lagrangian strain tensor components
  lstrain
* volume averaged yield strength normalized by sum of volume fractions
  mix = 3

matep = 1      *Epoxy Glider Coating
  poisson 0.46
  yield 1.0e8

matep = 2      * 1080 Steel rail
  JO USER
  AJO 0.7e10 * A
  BJO 3.6e10 * B
  CJO 0.17 * C
  MJO 0.25 * m
  NJO 0.6 * n
  TJO 0.14391 * Melting temperature
  poisson 0.27

matep = 3      * VascoMax 300 slipper
  JO USER
  AJO = 2.1e10 * A
  BJO = 0.124e10 * B
  CJO = 0.003 * C
  MJO = 0.8 * m
  NJO = 0.3737 * n
  TJO = 0.145202 * Melting temperature
  poisson 0.283

matep = 4 * platinum simulated sled mass
  poisson .2
  yield 10e10
endepdata

```

```

*****
* diatom input set
*****
diatom
  block 1
    package '1080 steel rail'
      material 2
      numsub 100
      temperature = 2.55935e-2 * eV = 74.93F = 297 K
      velocity 0.0, 0.0
      insert box
p1 0 0
  p2 850e-4 200e-4
    endinsert
    delete circle
  center 700e-4 200e-4
  radius 6e-4
    enddelete
    insert circle
  center 700e-4 200e-4
  radius 6e-4
    endinsert
  endpackage

  package 'slipper'
    material 3
    numsub 100
    temperature = 0.044896
    velocity = 750e2, -0.5e2
    insert box
      p1 0.0 200e-4
      p2 694e-4 325e-4
    endinsert
    delete box
p1 692e-4 200e-4
p2 694e-4 202e-4
    enddelete
    delete circle
  center 692e-4 202e-4
  radius 2e-4
    enddelete
    insert circle
  center 692e-4 202e-4

```

```
radius 2e-4
  endinsert
endpackage
```

```
endblock
enddiatom
```

```
*****
```

```
* tracer input set
```

```
*****
```

```
tracer
```

```
      add 0.06755, 0.01905 to 0.07115, 0.01905 n=37
add 0.06755, 0.01915 to 0.07115, 0.01915 n=37
add 0.06755, 0.01925 to 0.07115, 0.01925 n=37
add 0.06755, 0.01935 to 0.07115, 0.01935 n=37
add 0.06755, 0.01945 to 0.07115, 0.01945 n=37
add 0.06755, 0.01955 to 0.07115, 0.01955 n=37
add 0.06755, 0.01965 to 0.07115, 0.01965 n=37
add 0.06755, 0.01975 to 0.07115, 0.01975 n=37
add 0.06755, 0.01985 to 0.07115, 0.01985 n=37
add 0.06755, 0.01995 to 0.07115, 0.01995 n=37
add 0.06755, 0.02005 to 0.07115, 0.02005 n=37
add 0.06755, 0.02015 to 0.07115, 0.02015 n=37
add 0.06755, 0.02025 to 0.07115, 0.02025 n=37
add 0.06755, 0.02035 to 0.07115, 0.02035 n=37
add 0.06755, 0.02045 to 0.07115, 0.02045 n=37
add 0.06755, 0.02055 to 0.07115, 0.02055 n=37
add 0.06755, 0.02065 to 0.07115, 0.02065 n=37
add 0.06755, 0.02075 to 0.07115, 0.02075 n=37
add 0.06755, 0.02085 to 0.07115, 0.02085 n=37
add 0.06755, 0.02095 to 0.07115, 0.02095 n=37
add 0.06755, 0.02105 to 0.07115, 0.02105 n=37
add 0.06755, 0.02115 to 0.07115, 0.02115 n=37
add 0.06755, 0.02125 to 0.07115, 0.02125 n=37
add 0.06755, 0.02135 to 0.07115, 0.02135 n=37
add 0.06755, 0.02145 to 0.07115, 0.02145 n=37
add 0.06755, 0.02155 to 0.07115, 0.02155 n=37
add 0.06755, 0.02165 to 0.07115, 0.02165 n=37
add 0.06755, 0.02175 to 0.07115, 0.02175 n=37
add 0.06755, 0.02185 to 0.07115, 0.02185 n=37
add 0.06755, 0.02195 to 0.07115, 0.02195 n=37
add 0.06755, 0.02205 to 0.07115, 0.02205 n=37
```

```

add 0.06755, 0.02215 to 0.07115, 0.02215 n=37
add 0.06755, 0.02225 to 0.07115, 0.02225 n=37
add 0.06755, 0.02235 to 0.07115, 0.02235 n=37
add 0.06755, 0.02245 to 0.07115, 0.02245 n=37
endtracer

```

```

*****
* convection control input set
*****
Convct          * enable convection of internal energy
  * use slope of internal energy and mass density, discard KE residual
  convection = 1
  * scheme for interface tracker
  interface = smyra
endconvct

```

```

*****
* fracture input set
*****
Fracts          * enable fracture data (dynes/cm^2)
  pressure
  pfrac1 = -1.0e8 * fracture stress or pressure for nth material
  pfrac2 = -2.0e10
  pfrac3 = -7.45e10
  pfrac4 = -1.2e10
  pfmix = -1.20e10 * fracture stress or pressure in a cell with no void present
  pvoid = -1.20e10 * fracture stress or pressure in a cell with a void present
endfracts

```

```

*****
* edits input set
*****

```

```

edit
  exact
  shortta          * short edits based on time
    time = 0.0 , dt = 8.80e-11
  ends
  longt            * long edits based on time
    time = 0.0e0 , dt = 8.80e-11
  endl
  plott            * plot dumps based on time

```

```

    time 0.0e-6 dtfrequency 8.80e-11
  endp
  histt          * tracer history based on time
    time 0.0e-6 dtfrequency 8.80e-11
    htracer all
  endhistt
ende

*****
* boundary condition input set
*****
* 0=symmetry
* 1=sound speed based absorbing
* 2=extrapolated pressure with no mass allowed to enter
* 3=extrapolated pressure but mass is allowed to enter
*****

boundary          * enable boundary condition data
  bhydro          * enable hydrodynamic boundary conditions
    block 1
      bxbot = 1 , bxtop = 1
      bybot = 1 , bytop = 1
    endb
  endh
endb

*heatconduction * enable heat conduction
* MAT1 TABLE = 3 * conductivity tables defined in DEFTABLE list below
* MAT2 TABLE = 1
* MAT3 TABLE = 2
*endh

* DEFTABLE=1 * 1080 STEEL
* T(eV)    k(erg/s/eV/cm)
* 1.4684e-3 4.7700e10
* 1.0377e-2 4.8100e10
* 1.9090e-2 4.5200e10
* 2.7900e-2 4.1300e10
* 3.6711e-2 3.8100e10
* 4.5521e-2 3.5100e10
* 5.4332e-2 3.2700e10
* 6.3142e-2 3.0100e10
* 7.1953e-2 2.4400e10

```

```

* 8.9574e-2 2.6800e10
* 1.1111e-1 3.0100e10
* endd

* DEFTABLE=2 * VascoMax 300 Steel
* T(eV) k(erg/s/eV/cm)
* 3.6711e-3 2.4715e10
* 1.4684e-2 2.7424e10
* 2.9369e-2 2.9794e10
* 3.9158e-2 3.0132e10
* endd

* DEFTABLE=3 * Epoxy
* T(eV) k(erg/s/eV/cm)
* 3.6711e-3 6.5e8
* 1.4684e-2 6.5e8
* 2.9369e-2 6.5e8
* 3.9158e-2 6.5e8
* endd

*vadd * Added velocity to maintain gouging in view
* block = 1
* tadd = 0.0
* xvel = -1.08333e+5
*endvadd

*mindt * minimum allowable time step in mesh
* time = 0.0 dt = 8.80e-11
*endm

maxdt * maximum allowable time step in mesh
time = 0.0 dt = 8.80e-11
endm

spy

PlotTime(0.0, 8.80e-11);
SaveTime(0.0, 8.80e-11);
Save("VOID,VOLM,M,P,XXDEV,YYDEV,XYDEV,VX,VY,T,TK,PM,TM,Q3,YLD,DMG");

ImageFormat(2048,1536);

```

```

UserVariable("VMStress","Von Mises Stress (MPa)");
define VMStress()
{
    variable S, DXX, DYY, DXY, DZZ, S11, S22, S12, S33, P1, P2, P3, VM;

        S = Get("P");
DXX = Get("XXDEV");
DYY = Get("YYDEV");
DXY = Get("XYDEV");

DZZ = (DXX+DYY)*0.283;

S11 = S + DXX;
S22 = S + DYY;
S33 = S + DZZ;
S12 = DXY;

P1 = S11/2 + S22/2 - sqrt((S11*S11-2*S11*S22+4*S12*S12+S22*S22))/2;
P2 = S11/2 + S22/2 + sqrt((S11*S11-2*S11*S22+4*S12*S12+S22*S22))/2;
P3 = S33;

VM = sqrt((P1-P2)^2 + (P2-P3)^2 + (P3-P1)^2);
VM = VM/10; % Convert to Pa
VM = VM/1e6; % Convert to MPa

return VM;
}

UserVariable("TempF","Temperature (deg F)");
define TempF()
{
    variable TeV, TK, TF;

    TeV = Get("T");

    TK = TeV*11604.5;

    TF = (TK*1.8)-459.67;

    return TF;
}

UserVariable("TempK","Temperature (K)");

```

```

define TempK()
{
variable TeV, TK;

TeV = Get("T");

TK = TeV*11604.5;

return TK;
}

UserVariable("DeltaT","Temperature Change (K)");
define DeltaT()
{
variable TeV, TK, T0, deltaT;

TeV = Get("T");

TK = TeV*11604.5;

    T0 = 300;

deltaT = TK - T0;

return deltaT;
}

define main()
{
pprintf(" PLOT: Cycle=%d, Time=%e\n",CYCLE,TIME);
XLimits(400e-4,725e-4);
YLimits(175e-4,300e-4);
Image("Materials");
Window(0,0,0.75,1);
Label(sprintf("Materials at %6.2e seconds", TIME));
Plot2DMats(0.3);
ULabel("Test: (cm)");
Draw2DMesh();           % toggle on/off mesh
MatColors(RED,GREEN,YELLOW,NO_COLOR);
MatNames("Epoxy Coating","1080 Steel Rail","VascoMax 300 Slipper","");
DrawMatLegend("",0.71,0.2,0.99,0.9);
EndImage;
}

```



```

Image("VonMisesStress");
Window(0,0,0.75,1);
ColorMapRange(0,3130);
ColorMapClipping(OFF,ON);
Label(sprintf("von Mises Stress at %6.2e seconds", TIME));
Plot2D("VMStress");
Draw2DMatContour;
DrawColorMap("vonMises Stress (MPa)", 0.7,0.4,0.9,0.9);
EndImage;

Image("PlasticStrainRate");
Window(0,0,0.75,1);
ColorMapRange(1e6,1e9);
ColorMapClipping(OFF,OFF);
Label(sprintf("Plastic Strain Rate at %6.2e seconds", TIME));
Plot2D("PSR");
Draw2DMatContour;
DrawColorMap("Plastic Strain Rate (1/sec)", 0.7,0.4,0.9,0.9);
EndImage;

Image("Materials_small");
Window(0,0,0.75,1);
Label(sprintf("Materials at %6.2e seconds", TIME));
Plot2DMats(0.3);
Label("Test Label: Distance (cm)");
Draw2DMesh(); % toggle on/off mesh
MatColors(RED, GREEN, YELLOW, NO_COLOR);
MatNames("Epoxy Coating", "1080 Steel Rail", "VascoMax 300 Slipper", "");
DrawMatLegend("", 0.71, 0.2, 0.99, 0.9);
EndImage;

Image("Temp");
Window(0,0,0.75,1);
ColorMapRange(0, .12);
ColorMapClipping(OFF, OFF);
Label(sprintf("Temperature at %6.2e seconds", TIME));
%Draw2DMesh();
Plot2D("T");
Draw2DMatContour;
DrawColorMap("Temperature (eV)", 0.7, 0.4, 0.9, 0.9);
EndImage;

Image("DeltaTemp");

```

```

Window(0,0,0.75,1);
ColorMapRange(0,600);
ColorMapClipping(OFF,OFF);
Label(sprintf("Temperature Change from Initial at %6.2e seconds", TIME));
%Draw2DMesh();
Plot2D("DeltaT");
Draw2DMatContour;
DrawColorMap("Temperature Change (K)", 0.7,0.4,0.9,0.9);
EndImage;

}

SaveHis("POSITION,YLD,Q3,PSR,VOLM+3,P,XXDEV,YYDEV,XYDEV");
SaveTracer(ALL);
HisTime(0,8.80e-11);

define spyhis_main()
{
  HisLoad(1,"hscth");
  Label("EFP Velocity (Tracer 1)");
  TPlot("VY.1",1,AUTOSCALE);
}

endspy

```

Appendix C. Post Processing of CTH Data

C.1 CTH Data Extraction

CTH outputs tracer data to a file called 'hscth' in a comma-delimited format. To use this data with the post process code supplied here, the data must be converted to a tab-delimited format using Excel, or some other equivalent software. The 'hscth' file also includes data pertaining to the CTH cycle number and the current step time. This information is not used for the post processing analysis and needs to be removed from the data.

The data set should consist of columns containing data in this order: time, x-position, y-position, z-position, xy-stress deviator, yy-stress deviator, xx-stress deviator, material pressure (hydrostatic stress), volume fraction of the slipper, plastic strain rate, plastic strain of the slipper, and the Johnson-Cook plasticity critical von Mises stress (CTH 'YLD' variable). The input deck supplied in Appendix B already outputs the data in this format, with the addition of the cycle number and time step, which are subsequently removed before using the code. The default data filename for this code is "cthData.txt" but this can be modified.

C.2 Post Processing Matlab[®] Code

```
% CTH DATA POST PROCESS - PLANE STRAIN EVALUATION

clear all; close all; clc

aspRad = 6;

velocity = 622;

tic

% (USER INPUT) POISSON'S RATIO, MESH SIZE, AND CRITICAL MASS FRACTION

nu = 0.283;           % Poisson's ratio of material

meshSize = 1.0e-4*1.0e-4; % Area of a single mesh cell in cm^2
```

```

if velocity < 100
    newDirectory = ['Data/00' num2str(velocity) ...
        'mps/0' num2str(aspRad) 'micron'];
elseif velocity <1000
    newDirectory = ['Data/0' num2str(velocity) ...
        'mps/0' num2str(aspRad) 'micron'];
else
    newDirectory = ['Data/' num2str(velocity) ...
        'mps/0' num2str(aspRad) 'micron'];
end

cd(newDirectory)

disp(' ')

%% IMPORT DATA

dataFile = 'cthData.txt';

data = load(dataFile);

disp('Data Imported...')

%% CATEGORIZE DATA

time = data(:,1);

numCycles = length(time);
numPoints = (size(data,2)-1)/11;

xPoints = zeros(numCycles,numPoints);
yPoints = zeros(numCycles,numPoints);
pressureData = zeros(numCycles,numPoints);
xxdevData = zeros(numCycles,numPoints);
yydevData = zeros(numCycles,numPoints);
xydevData = zeros(numCycles,numPoints);
vfData = zeros(numCycles,numPoints);
srData = zeros(numCycles,numPoints);
strainData = zeros(numCycles,numPoints);
jcpData = zeros(numCycles,numPoints);

xLoc = 2;

```

```

yLoc = 3;
xyLoc = 5;
yyLoc = 6;
xxLoc = 7;
pLoc = 8;
vfLoc = 9;
srLoc = 10;
sLoc = 11;
jcpLoc = 12;

for iter = 1:numPoints
    xPoints(:,iter) = data(:,xLoc);
    yPoints(:,iter) = data(:,yLoc);
    pressureData(:,iter) = data(:,pLoc);
    xxdevData(:,iter) = data(:,xxLoc);
    yydevData(:,iter) = data(:,yyLoc);
    xydevData(:,iter) = data(:,xyLoc);
    vfData(:,iter) = data(:,vfLoc);
    srData(:,iter) = data(:,srLoc);
    strainData(:,iter) = data(:,sLoc);
    jcpData(:,iter) = data(:,jcpLoc);

    xLoc = xLoc + 11;
    yLoc = yLoc + 11;
    xyLoc = xyLoc + 11;
    yyLoc = yyLoc + 11;
    xxLoc = xxLoc + 11;
    pLoc = pLoc + 11;
    vfLoc = vfLoc + 11;
    srLoc = srLoc + 11;
    sLoc = sLoc + 11;
    jcpLoc = jcpLoc + 11;
end

disp('Data Categorized...')

%% CALCULATE DISTANCE SLID

distanceSlid = velocity*time(end)*1000;      % mm

disp('Distance Slid Calculated...')

%% CALCULATE ZZDEV (GIVEN XXDEV, YYDEV, AND POISSON'S RATIO)

```

```

zzdevData = (xxdevData+yydevData)*nu;

disp('ZZ Deviator Calculated...')

%% CONVERT DATA TO Pa

pressureData = pressureData/10;
xxdevData = xxdevData/10;
yydevData = yydevData/10;
xydevData = xydevData/10;
zzdevData = zzdevData/10;
jcpData = jcpData/10;

%% EVALUATE STRAIN RATES DOMAIN

for r = 1:size(srData,1)
    for c = 1:size(srData,2)
        if srData(r,c)<.002
            srData(r,c) = .002;
        end

        if srData(r,c)>10e17
            disp('Strain Rate'),disp(srData(r,c))
            error('Strain Rate Out of Range')
        end
    end
end

%% CALCULATE STRESS TENSOR COMPONENTS
S1 = pressureData + xxdevData;
S2 = pressureData + yydevData;
S3 = pressureData + zzdevData;
S12 = xydevData;

disp('Stress Tensor Components Calculated...')

%% CALCULATE VON MISES STRESS

vmStress = (1/sqrt(2))*sqrt((S1-S2).^2 + (S2-S3).^2 + (S3-S1).^2 + ...
    6*(S12.^2));

disp('von Mises Stress Calculated...')

```

```

%% EVALUATE AVERAGE STRAIN RATE FAILURE AREA

failureASR = zeros(numCycles,numPoints);

failureSumASR = zeros(numCycles,1);

failureCritASR = 3139;

failureCritASR = failureCritASR*10^6;

for row=1:r
    for col=1:c
        if row>1 && failureASR(row-1,col)==1

            failureASR(row,col)=1;

        end

        if vmStress(row,col)>=failureCritASR

            failureASR(row,col)=1;

        end
    end
end

failureASR = failureASR.*vfData;

for iter = 1:length(failureSumASR)
    failureSumASR(iter,1) = sum(failureASR(iter,:));
end

damAreaASR = failureSumASR*meshSize;

WR_ASR = 100*damAreaASR(end)/distanceSlid;

disp('Average Strain Rate Failure Mechanism Evaluated...')

%% EVALUATE POINTWISE STRAIN RATE FAILURE AREA

failurePSR = zeros(numCycles,numPoints);

```

```

failureSumPSR = zeros(numCycles,1);

A = -1.820312149289858e+006;
B = -3.474049725579352e-005;
C = 1.822432851445885e+006;

failureCritPSR = A*(srData.^B) + C;

failureCritPSR = failureCritPSR*10^6;

for row=1:r
    for col=1:c
        if row>1 && failurePSR(row-1,col)==1

            failurePSR(row,col)=1;

        end

        if vmStress(row,col)>=failureCritPSR(row,col)

            failurePSR(row,col)=1;

        end
    end
end

failurePSR = failurePSR.*vfData;

for iter = 1:length(failureSumPSR)
    failureSumPSR(iter,1) = sum(failurePSR(iter,:));
end

damAreaPSR = failureSumPSR*meshSize;

WR_PSR = 100*damAreaPSR(end)/distanceSlid;

disp('Pointwise Strain Rate Failure Mechanism Evaluated...')

% EVALUATE JOHNSON-COOK PLASTICITY FAILURE AREA

failureJCP = zeros(numCycles,numPoints);

failureSumJCP = zeros(numCycles,1);

```



```

for row=1:r
    for col=1:c
        if row>1 && failureJCP(row-1,col)==1

            failureJCP(row,col)=1;

        end

        if vmStress(row,col)>=jcpData(row,col)

            failureJCP(row,col)=1;

        end
    end
end

failureJCP = failureJCP.*vfData;

for iter = 1:length(failureSumJCP)
    failureSumJCP(iter,1) = sum(failureJCP(iter,:));
end

damAreaJCP = failureSumJCP*meshSize;

WR_JCP = 100*damAreaJCP(end)/distanceSlid;

disp('Johnson-Cook Plasticity Failure Mechanism Evaluated...')

%% EVALUATE STRAIN AT MAX STRESS FAILURE AREA

failureSMS = zeros(numCycles,numPoints);

failureSumSMS = zeros(numCycles,1);

A = 2.25900e-2;
B = -5.02900e-2;
C = 5.34400e-3;

failureCritSMS = A*(srData.^B) + C;

for row=1:r
    for col=1:c

```

```

        if row>1 && failureSMS(row-1,col)==1
            failureSMS(row,col)=1;
        end

        if strainData(row,col)>=failureCritSMS(row,col)
            failureSMS(row,col)=1;
        end
    end
end

failureSMS = failureSMS.*vfData;

for iter = 1:length(failureSumSMS)
    failureSumSMS(iter,1) = sum(failureSMS(iter,:));
end

damAreaSMS = failureSumSMS*meshSize;

WR_SMS = 100*damAreaSMS(end)/distanceSlid;

disp('Strain at Max Stress Failure Mechanism Evaluated...')

%% SAVE WEAR RATES TO .txt FILE

if velocity < 100
    fileName = ['WearRates_00' num2str(velocity) ...
                'mps_0' num2str(aspRad) 'micron.txt'];
elseif velocity <1000
    fileName = ['WearRates_0' num2str(velocity) ...
                'mps_0' num2str(aspRad) 'micron.txt'];
else
    fileName = ['WearRates_' num2str(velocity) ...
                'mps_0' num2str(aspRad) 'micron.txt'];
end

fid=fopen(fileName,'wt');
fprintf(fid,'%6.5e\t%6.5e\t%6.5e\t%6.5e\t',...
        WR_ASR,...
        WR_PSR,...

```

```
        WR_JCP,...
        WR_SMS);
fclose(fid);

disp('Failure Data Saved...')

cd ../../../../

%% END PROGRAM

disp('PROGRAM COMPLETE...')

toc
```

Appendix D. Tabulated Wear Rates

The wear rates tabulated in this appendix are the wear rates for the VascoMax 300 slipper as it is accelerating down the track. Included are the wear rates calculated by Hale [16] using the FEA technique and the average strain rate maximum von Mises stress criterion. Hale also calculated the wear rates for sliding velocities of 622 and 1,250 m/s, but these were calculated for a sled that is decelerating. The dynamics data is dramatically different for a decelerating sled than an accelerating sled. Since this research is concerned with a sled that is accelerating for the entire run, those wear rate values have been omitted. They can be obtained from Hale’s Ph.D dissertation.

Table 4.1: Single Asperity Mechanical Wear Rates

Horizontal Velocity (m/s)	Distance Slid (m)	Hale FEA [16] (mm ³ /mm)	Dynamic Strain Rate (mm ³ /mm)	Johnson-Cook Plasticity (mm ³ /mm)	Strain at Max. Stress (mm ³ /mm)
10	0.21	2.630×10^{-5}	—	—	—
20	0.89	3.440×10^{-5}	—	—	—
40	3.75	3.790×10^{-5}	—	—	—
100	25.24	4.880×10^{-5}	—	—	—
200	102.55	8.420×10^{-5}	5.020×10^{-4}	5.298×10^{-4}	5.628×10^{-4}
300	228.35	1.100×10^{-4}	5.148×10^{-4}	5.785×10^{-4}	6.286×10^{-4}
500	591.64	2.000×10^{-4}	7.360×10^{-4}	7.868×10^{-4}	7.959×10^{-4}
750	1357.54	1.930×10^{-4}	5.542×10^{-4}	6.340×10^{-4}	7.477×10^{-4}
1,000	1777.70	1.870×10^{-4}	5.257×10^{-4}	5.405×10^{-4}	4.954×10^{-4}
1,250	2221.62	—	5.039×10^{-4}	5.188×10^{-4}	4.907×10^{-4}
1,500	2771.05	—	4.981×10^{-4}	5.130×10^{-4}	4.944×10^{-4}
1,530	2849.47	1.370×10^{-4}	—	—	—
2,000	3535.00	—	4.877×10^{-4}	4.979×10^{-4}	4.946×10^{-4}
2,500	4491.00	—	4.695×10^{-4}	4.861×10^{-4}	4.741×10^{-4}
3,000	5781.27	—	4.653×10^{-4}	4.843×10^{-4}	4.624×10^{-4}

Bibliography

1. Archard, J. F. “The Temperature of Rubbing Surfaces,” *Wear*, 2(6):438–455, October 1959.
2. Archard, J. F. and W. Hirst. “The Wear of Metals Under Unlubricated Conditions,” *Proceedings of the Royal Society of London. Series A, Mathematical and Physical Sciences*, 236(1206):397–410, 1956.
3. Bayer, R. G. *Wear Analysis for Engineers*. HNB Publishing, New York, 2002.
4. Bayer, R. G. *Mechanical Wear Fundamentals and Testing*. Marcel Dekker, Inc., New York, 2004.
5. Bowden, F. P. and P. H. Thomas. “The Surface Temperature of Sliding Solids,” *Proceedings of the Royal Society of London. Series A, Mathematical and Physical Sciences*, 223(1152):29–40, April 1954.
6. C. E. Anderson, Jr. “An Overview of the Theory of Hydrocodes,” *International Journal of Impact Engineering*, 5:33–59, 1987.
7. Cameron, G. J. *An Evaluation of High Velocity Wear, AFIT/GAE/ENY/07-M06*. Master’s Thesis, Air Force Institute of Technology, Wright-Patterson AFB, OH, 2007.
8. Chmiel, A. J. *Finite Element Simulation Methods for Dry Sliding Wear, AFIT/GAE/ENY/08-M03*. Master’s Thesis, Air Force Institute of Technology, Wright-Patterson AFB, OH, 2008.
9. Cinnamon, J. D. *Analysis and Simulation of Hypervelocity Gouging Impacts AFIT/DS/ENY/06-01*. Ph.D. Dissertation, Air Force Institute of Technology, Wright-Patterson AFB, OH, 2006.
10. Cinnamon, J. D., A. N. Palazotto, and Z. Keenan. “Material Characterization and Development of a Constitutive Relationship for Hypervelocity Impact of 1080

- Steel and VascoMax 300,” *International Journal of Impact Engineering*, 33(1-12):180–189, December 2006.
11. Cinnamon, J. D., A. N. Palazotto, and A. G. Szmerekovsky. “Further Refinement and Validation of Material Models for Hypervelocity Gouging Impacts,” *AIAA Journal*, 46(2):317–327, 2008.
 12. Crawford, D. A. *CTH Course Notes*. Sandia National Laboratories, Albuquerque, New Mexico, August 2008.
 13. E. Jr., Hertel, J. Bell, M. Elrick, A. Farnsworth, G. Kerley, J. McGlaun, S. Petney, S. Silling, P. Taylor, and L. Yarrington. “CTH: A Software Family for Multi-Dimensional Shock Physics Analysis,” *Shock Waves*, 1(3):377–382, September 1994.
 14. E. S. Jr., Hertel and G. I. Kerley. *CTH Reference Manual: The Equation of State Package*. Sandia National Laboratories, Albuquerque, New Mexico, April 1998.
 15. Farrell, R. M. and T. S. Eyre. “The Relationship Between Load and Sliding Distance in the Initiation of Mild Wear in Steels,” *Wear*, 15(5):359–372, May 1970.
 16. Hale, C. S. *Consideration of Wear Rates at High Velocity AFIT/DS/ENY/10-08*. Ph.D. dissertation, Air Force Institute of Technology, Wright-Patterson AFB, OH, 2009.
 17. Hale, C. S., A. N. Palazotto, and W. P. Baker. “Consideration of Wear at High Velocities.” *Proceedings of the 50th AIAA/ASME/ASCE/AHS/ASC Structures, Structural Dynamics and Materials Conference*. AIAA, Palm Springs, California, 4-7 May 2009.
 18. Hale, C. S., A. N. Palazotto, A. J. Chmiel, and G. J. Cameron. “Consideration of Wear at High Velocities.” *Proceedings of the 49th AIAA/ASME/ASCE/AHS/ASC Structures, Structural Dynamics and Materials Conference*. AIAA, Schaumburg, Illinois, 7-10 April 2008.

19. Hooser, M. D. "Simulation of a 10,000 Foot per Second Ground Vehicle." *Proceedings of the 21st AIAA Advanced Measurement Technology and Ground Testing Conference*. AIAA, Denver, Colorado, 19-22 June 2000.
20. Hooser, M. D. and A. Schwing. "Validation of Dynamic Simulation Techniques at the Holloman High Speed Test Track." *Proceedings of the 38th AIAA Aerospace Sciences Meeting and Exhibit*. AIAA, Reno, Nevada, 10-13 January 2000.
21. Incropera, F. P. and D. P. DeWitt. *Fundamentals of Heat and Mass Transfer*. John Wiley & Sons, New York, 1990.
22. Johnson, G. R. and W. H. Cook. "A Constitutive Model and Data for Metals Subjected to Large Strains, High Strain Rates and High Temperatures," *Proceedings of the 7th International Symposium on Ballistics: Hague, Netherlands*, April 1983.
23. Johnson, G. R. and W. H. Cook. "Fracture Characteristics of Three Metals Subjected to Various Strains, Strain Rates, Temperatures, and Pressures," *Engineering Fracture Mechanics*, 21(1):31-48, 1985.
24. Korkegi, R. H. and R. A. Briggs. "The Hypersonic Slipper Bearing - A Test Track Problem," *Journal of Spacecraft & Rockets*, 6(2):210-212, 1969.
25. Kreith, F. and M. S. Bohn. *Principles of Heat Transfer*. Brookes/Cole, Pacific Grove, CA, 2001.
26. Lim, S. C. and M. F. Ashby. "Wear-Mechanism Maps," *Acta Metallurgica*, 35(1):1-24, January 1987.
27. McGlaun, J. M. and S. L. Thompson. "CTH: A Three-Dimensional Shock Wave Physics Code," *International Journal of Impact Engineering*, 10(1-4):351-360, 1989.
28. Meyers, M. A. *Dynamic Behavior of Materials*. John Wiley & Sons, New York, 1994.

29. Montgomery, R. S. "Friction and Wear at High Sliding Speeds," *Wear*, 36(3):275–298, March 1976.
30. Rabinowicz, E. *Friction and Wear of Metals*. John Wiley & Sons, New York, 1995.
31. Saka, N., A. M. Elieche, and N. P. Suh. "Wear of Metals at High Sliding Speeds," *Wear*, 44(1):109–125, August 1977.
32. Stachowiak, G. W. *Wear - Materials, Mechanisms and Practice*. Tribology in Practice Series. John Wiley & Sons, Chichester, England, 2005.
33. Szmerekovsky, A. G. *The Physical Understanding of the Use of Coatings to Mitigate Hypervelocity Gouging Considering Real-Test Sled Dimensions AFIT/DS/ENY/04-06*. Ph.D. dissertation, Air Force Institute of Technology, Wright-Patterson AFB, OH, 2004.
34. Szmerekovsky, A. G., A. N. Palazotto, and J. D. Cinnamon. "An Improved Study of Temperature Changes During Hypervelocity Sliding High Energy Impact." *Proceedings of the 47th AIAA/ASME/ASCE/AHS/ASC Structures, Structural Dynamics and Materials Conference*. AIAA, Newport, Rhode Island, 1-4 May 2006.
35. Zukas, J. A. *Introduction to Hydrocodes*, volume 49. Elsevier, New York, 2004.

REPORT DOCUMENTATION PAGE

Form Approved
OMB No. 0704-0188

The public reporting burden for this collection of information is estimated to average 1 hour per response, including the time for reviewing instructions, searching existing data sources, gathering and maintaining the data needed, and completing and reviewing the collection of information. Send comments regarding this burden estimate or any other aspect of this collection of information, including suggestions for reducing this burden to Department of Defense, Washington Headquarters Services, Directorate for Information Operations and Reports (0704-0188), 1215 Jefferson Davis Highway, Suite 1204, Arlington, VA 22202-4302. Respondents should be aware that notwithstanding any other provision of law, no person shall be subject to any penalty for failing to comply with a collection of information if it does not display a currently valid OMB control number. **PLEASE DO NOT RETURN YOUR FORM TO THE ABOVE ADDRESS.**

1. REPORT DATE (DD-MM-YYYY) 25-03-2010		2. REPORT TYPE Master's Thesis		3. DATES COVERED (From — To) Sept 2008 — Mar 2010	
4. TITLE AND SUBTITLE Consideration of Wear Rates at High Velocities				5a. CONTRACT NUMBER	
				5b. GRANT NUMBER	
				5c. PROGRAM ELEMENT NUMBER	
6. AUTHOR(S) Stephen P. Meador				5d. PROJECT NUMBER	
				5e. TASK NUMBER	
				5f. WORK UNIT NUMBER	
7. PERFORMING ORGANIZATION NAME(S) AND ADDRESS(ES) Air Force Institute of Technology Graduate School of Engineering and Management (AFIT/EN) 2950 Hobson Way Wright-Patterson AFB OH 45433-7765				8. PERFORMING ORGANIZATION REPORT NUMBER AFIT/GAE/ENY/10-M16	
9. SPONSORING / MONITORING AGENCY NAME(S) AND ADDRESS(ES) Air Force Office of Scientific Research Attn: Maj Michelle Ewy 4015 Wilson Blvd, Rm 713 Arlington, VA 22203-1954 (703) 696-7297 michelle.ewy@afosr.af.mil				10. SPONSOR/MONITOR'S ACRONYM(S) AFOSR/NA	
12. DISTRIBUTION / AVAILABILITY STATEMENT APPROVED FOR PUBLIC RELEASE; DISTRIBUTION UNLIMITED				11. SPONSOR/MONITOR'S REPORT NUMBER(S)	
13. SUPPLEMENTARY NOTES					
14. ABSTRACT The goal of this research is to study sliding contact wear of test sled slippers at high velocities. Experimentation representative of the slippers is infeasible, so numerical studies are used. An Eulerian-Lagrangian hydrocode called CTH is used to study mechanical wear. Failure criteria have been established to evaluate the stresses and strains resulting from the hydrocode simulation of a single asperity collision. The results from the hydrocode simulations are scaled to account for slipper bounce and multiple asperities, and these results produce total wear values that are approximately 90% of total experimental wear. Slipper thermodynamics have also been evaluated. The fraction of frictional heating energy entering the slipper has been evaluated, and an average value of approximately 0.125 has been determined. Total wear for a slipper reaching 3,000 m/s and following a typical slipper velocity profile has been evaluated to range from 3 to 6% of the total slipper volume.					
15. SUBJECT TERMS high velocity wear rate, VascoMax 300, Holloman High Speed Test Track (HHSTT), CTH, hydrocode, melt					
16. SECURITY CLASSIFICATION OF:			17. LIMITATION OF ABSTRACT UU	18. NUMBER OF PAGES 136	19a. NAME OF RESPONSIBLE PERSON Dr. Anthony N. Palazotto
a. REPORT U	b. ABSTRACT U	c. THIS PAGE U			19b. TELEPHONE NUMBER (include area code) (937) 255-3636, ext 4599